APTAMER FUNCTIONALIZED ELECTROACTIVE POLYMERS FOR DETECTION OF BIOMOLECULES

by

Kelli Kay Burke, B.S.

A thesis submitted to the Graduate Council of
Texas State University in partial fulfillment
of the requirements for the degree of
Master of Science
with a Major in Chemistry
December 2020

Committee Members:

Jennifer Irvin, Co-Chair

Tania Betancourt, Co-Chair

Chad Booth

FAIR USE AND AUTHOR'S PERMISSION STATEMENT

Fair Use

Duplication Permission

DEDICATION

This thesis is dedicated to my parents, Angie and Michael Burke, and to my grandparents, Wesley and Barbara Pair, whose love, encouragement, and generosity made this academic endeavor possible.

ACKNOWLEDGEMENTS

Firstly, I would like to thank Dr. Jennifer Irvin for her endless support and guidance I have received while working in her lab. I am profoundly grateful for the opportunity I have had to work in a lab under such an inspiring chemist.

I would also like to thank the other members of my committee, Dr. Tania Betancourt and Dr. Chad Booth. Dr. Betancourt's expertise in biomolecules has proven crucial to this research. Dr. Betancourt has also provided several significant resources used in this research including her water purification system, UV-Vis spectrophotometer, fluorescence microscope, laminar flow hood, and reagents. Enrolling and participating in Dr. Booth's undergraduate organic chemistry class along with his graduate polymers class has grown and reinforced my knowledge in organic and polymer chemistry.

I would like to thank the entire Irvin research group for their endless support and input. I would like to specifically thank Damilola Runsewe, who is working on a similar project for his dissertation. Many hours were spent in lab or in meeting discussing and collaborating on our projects to improve experimental procedures or results. I would like to thank Marisa Snapp-Leo, who has since graduated and left the Irvin research group, for training me on all of the electrochemical equipment used and for her friendship and support. I would also like to thank Mariana Acosta for her constant support, friendship, and for presence and assistance in lab.

I would also like to acknowledge the members of Dr. Betancourt's research group, who have helped me to better understand working with biomolecules and have

assisted me with the use of the resources in Dr. Betancourt's lab. I would like to specifically thank Nakya Mesa-Diaz from Dr. Betancourt's group who began working with and preparing the aptamer to be used for my research.

I would like to thank Dr. Shiva Rastogi for providing his expertise, assistance, and resources during the monomer synthesis portion of this thesis. Dr. Rastogi was crucial for the set-up, work up, and analysis of several different reactions performed during this thesis. I would also like to thank Dr. William Brittain for the resources he has provided to me including his fume hoods used during several synthetic reactions and purification columns, and his goniometer for contact angle measurements.

Lastly, I would like to thank my family and my partner for their never-ending love and support. Without them, this work would not have been possible.

TABLE OF CONTENTS

Page

LIST OF TABLES

Table **Page**

LIST OF FIGURES

Figure **Page**

LIST OF ABBREVIATIONS

Abbreviation	Description
ACN	Acetonitrile
AMP	Adenosine Monophosphate
ATP	Adenosine Triphosphate
ATR	Attenuated Total Reflectance
BS^3	Bissulfosuccinimidyl Suberate
BSA	Bovine Serum Albumin
CE	Counter Electrode
CuAAC	Cu(I) Catalyzed Alkyne-Azide Cycloaddition
CV	Cyclic Voltammetry
DCM	Dichloromethane
DIPEA	Diisopropylethylamine
DMAP	4-Dimethylaminopyridine
DMF	Dimethylformamide
DMSO	Dimethylsulfoxide
DNA	Deoxyribonucleic acid
DPV	Differential Pulse Voltammetry
EAP	Electroactive Polymer
$E_{a,p}$	Polymer Oxidation
$E_{c,p}$	Polymer Reduction

EDC	1-Ethyl-3-(3-dimethylaminopropyl)carbodiimide
EDOT	Ethylenedioxythiophene
EDTA	Ethylenediaminetetraacetic Acid
E_g	Band Gap
$E_{on,m}$	Onset of Monomer Oxidation
$E_{p,m}$	Peak of Monomer Oxidation
EtOAc	Ethyl Acetate
EtOH	Ethanol
FAM	Fluorescein Amidite
Fbr	Fibrinogen
FTIR	Fourier Transform Infrared
GC-MS	Gas Chromatogram-Mass Spectrometry
GFP	Green Fluorescent Protein
HCV	Hepatitis C Virus
IgG	Immunoglobulin
IR	Infrared
ITO	Indium Tin Oxide
LYZ	Lysozyme
MP	Melting Point
MUC1	Mucin 1

n-Doped	Negatively Doped
NHS	N-Hydroxysuccinimide
NMR	Nuclear Magnetic Resonance
NOESY	Nuclear Overhauser Effect Spectroscopy
p-Doped	Positively Doped
PAN	Polyacrylonitrile
PBS	Phosphate Buffer Saline
PCR	Polymerase Chain Reaction
PDGF	Platlet-Derived Growth Factor
PEDOT	Poly(3,4-ethylenedioxythiophene)
ProDOT	3,4-Propylenedioxythiophene
pTsOH	*para*-Toluenesulfonic Acid
RE	Reference Electrode
RNA	Ribonucleic Acid
SCE	Standard Calomel Electrode
SELEX	Systematic Evolution of Ligands by Exponential Enrichment
SHE	Standard Hydrogen Electrode
SRD	Scan Rate Dependence
SWV	Square Wave Voltammetry
TBAP	Tetrabutylammonium Perchlorate

tBDMSCl	*tert*-Butyldimethylsilyl Chloride
TBTA	Tris(benzyltriazolylmethyl)amine
tBuOH	*tert*-Butylalcohol
TEAA	Tetraethylammonium Acetate
$TEABF_4$	Tetraethylammonium Tetrafluoroborate
ThAm	Thienyl Amide
Th-COOH	2-Thiophenecarboxylic Acid
THF	Tetrahydrofuran
TLC	Thin Layer Chromatography
Tris	Tris(hydroxymethyl)aminomethane
UV-Vis	Ultraviolet-Visible
VEGF	Vascular Endothelial Growth Factor
WE	Working Electrode

ABSTRACT

3,4-Propylenedioxythiophene (ProDOT) based monomers were synthesized and polymerized via electrochemical polymerization. The electrochemical properties of the resulting polymer films were studied in organic and aqueous solutions using cyclic voltammetry (CV). The polymer films were then functionalized with an adenosine-specific aptamer via click chemistry. Aptamer functionalization was confirmed by fluorescence microscope imaging and by CV. Aptamer functionalized polymer films were used to electrochemically detect adenosine at different concentrations to evaluate the analytical sensing ability of the fabricated biosensor.

1. INTRODUCTION

1.1 Electroactive Polymers

Electroactive polymers, or EAPs, are polymers that can experience changes in properties such as color,[1] permeability,[2] volume,[3] conductivity,[4] and more based on the oxidation state of the polymer. Because of their easily modifiable properties, EAPs have a wide range of potential applications including electrochemical capacitors,[5] electrochromics,[6] electrochemical biosensors,[7] actuators,[8] and much more.

EAPs were first synthesized and observed in 1977 by Shirakawa, MacDiarmid, and Heeger.[9] Their studies showed that doping the semiconducting polymer polyacetylene with halogen substituents increased the overall conductivity of the polymer by a factor of millions. The resulting conductivity of the doped polymer was comparable to that of many metals, coining the phrase “synthetic metals”, used to describe EAPs. Their work in conducting polymers resulted in these scientists winning the Nobel Prize in the year 2000.[10] Interest in EAPs and their potential applications has grown exponentially ever since. For the purpose of this thesis, EAPs will be used as electrodes for the development of biosensors.

1.2 Common EAPs

The exceptional conducting properties of EAPs are due to the π-bond conjugation of the polymeric system, which allows for the π electrons to delocalize and move freely throughout the polymer. Since the discovery of doped polyacetylene, many different EAPs have been synthesized and studied, including the conjugated polyheterocycles, such as polythiophene, poly(3,4-ethylenedioxythiophene), and polypyrrole.

Polyheterocycles are unique in that their complex structures allow for structural modification of the polymer. Functionalizing the EAP with different moieties can result in tunable, desirable properties of the polymer.[11] Electron rich heteroatoms such as sulfur, nitrogen, and oxygen contribute to the electron density and the conductivity of the polymeric system. Figure 1 illustrates some of the structures of common EAPs.

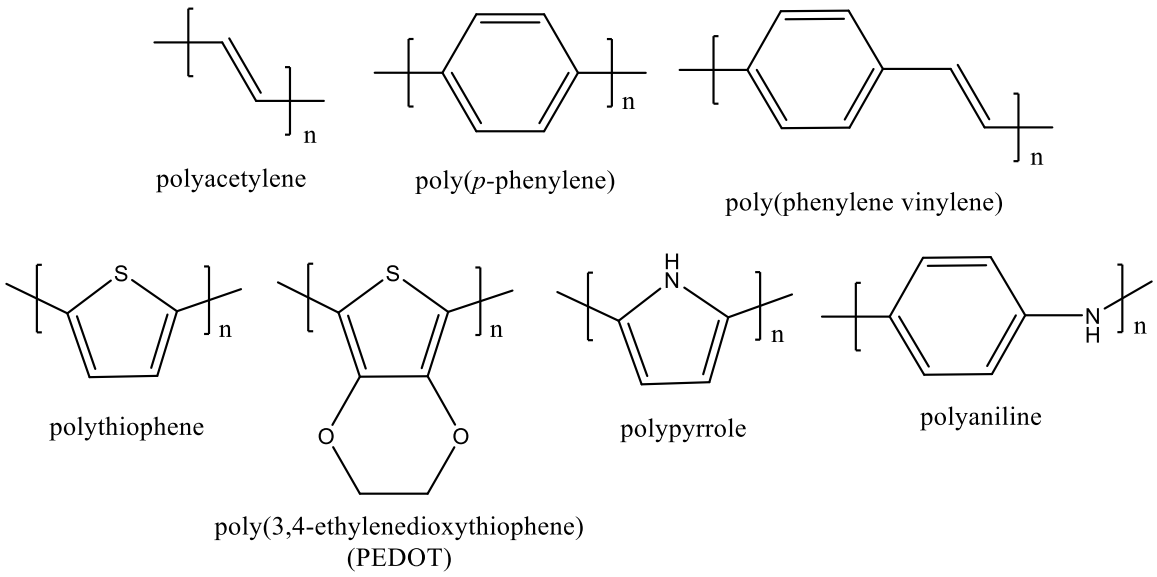

Figure 1: Common EAPs and their names

1.3 Oxidative Polymerization Mechanism

Chemical and electrochemical oxidative polymerization reactions are the most widely used methods of synthesizing EAPs.[12] Oxidative polymerization is a process in which one monomer molecule loses an electron via oxidation of the monomer, forming a radical cationic monomer species that is stabilized through resonance. This radical-cation can then couple with another radical-cation species to form a dicationic dimer. The dication is then reduced to form a neutral dimer. The neutral dimer can then be oxidized, creating a radical-cationic species and repeating this oxidation polymerization process.[13]

This oxidative polymerization mechanism is illustrated in Figure 2 using the polymerization of thiophene as an example. Oxidative polymerization reactions can occur through chemical means by using an oxidizing agent, and through electrochemical means by applying a voltage to an electrolyte solution containing monomer.

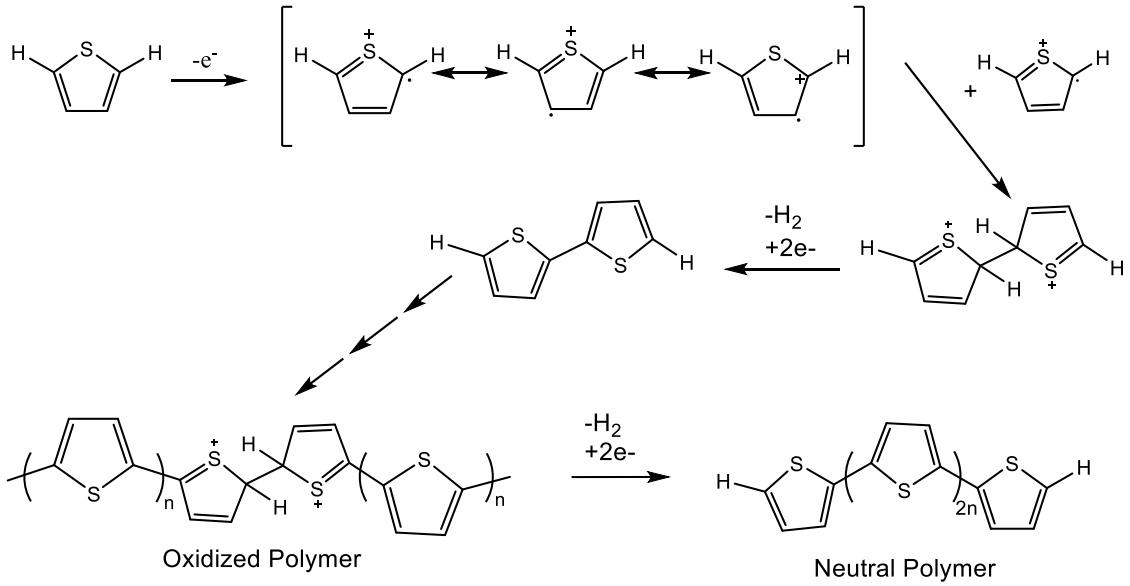

Figure 2: Oxidative polymerization mechanism of polythiophene.

1.4 Conduction Mechanism in EAPs

The most accepted mechanism for the conduction in conjugated heterocycles like polythiophene and polypyrrole is illustrated in Figure 3. In this mechanism, a one-electron oxidation of the neutral polymer occurs to produce a radical cation species called a polaron. The polymeric ring system stabilizes the radical cation through resonance delocalization. The polaronic species can then undergo a second one-electron oxidation to form a bipolaronic species containing two cations. A separation of 3-5 rings is energetically favorable to stabilize and avoid interactions between the two cations in the bipolaronic system.[14] These oxidation and reduction reactions between neutral, polaronic, and bipolaronic species are typically reversible and can occur through chemical and

electrochemical means.[15]

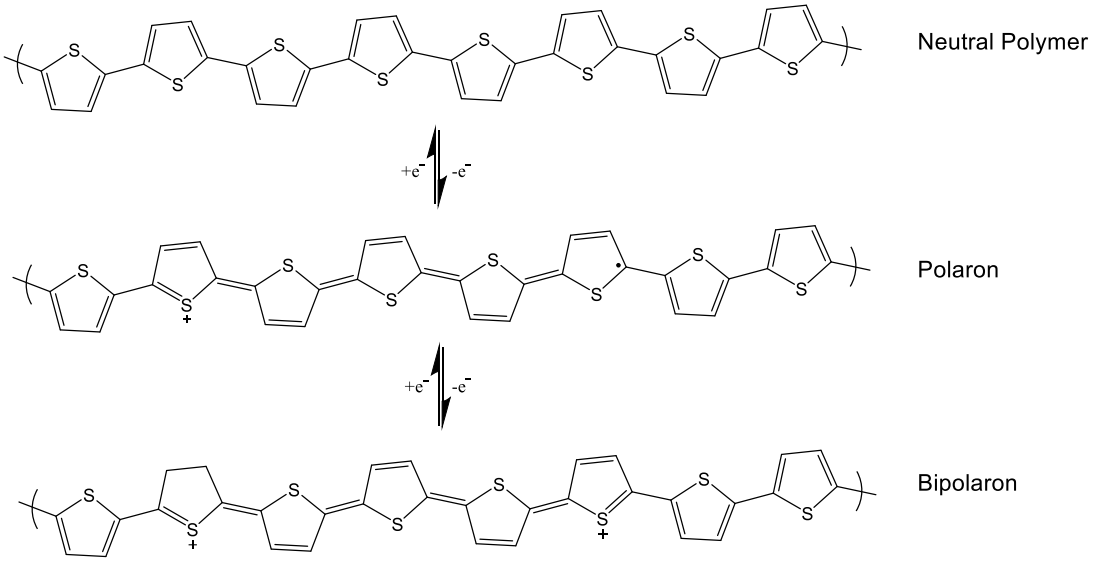

Figure 3: Different oxidation states of polythiophene.[15]

1.5 Band Gap Theory

The electronic structure of a material determines whether the material will have conductive or insulative properties. Band gap, E_g, is a term that is used to describe the energy gap between the valence band and the conduction band of a polymeric system.[16] When an electron has enough energy to be promoted into the conduction band of the system, the material becomes conductive. As the energy gap between the valence and conduction bands become smaller, less energy is needed to promote an electron from the valence band into the conduction band. Increased conjugation in a polymeric system has shown to lower the band gap and increase the conductivity of the system.[17] Figure 4 illustrates the change in band gap associated with the increase of conjugation of a system.

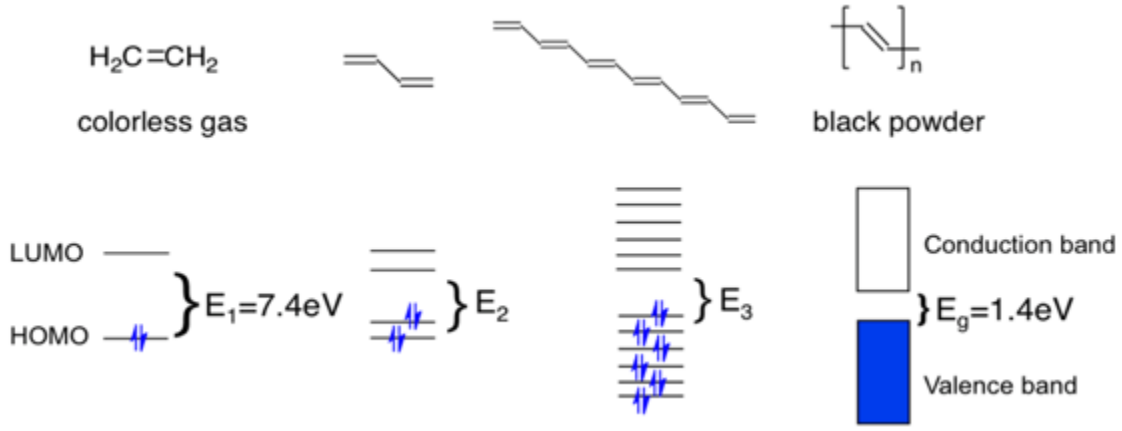

Figure 4: An increase in conjugation of the system results in the decrease of the band gap. Used with permission.[15]

A fixed amount of energy is needed to promote an electron from the valence band to the conduction band of the polymer; this is the E_g of the polymer, which is determined from the onset of the π to π* transition in the UV-Vis (ultraviolet-visible) spectrum of the neutral EAP. While UV-Vis spectra are normally plotted as absorbance versus wavelength in nm, band gaps are reported in eV using a conversion (Equation 1)[18] from wavelength of light absorbed by the oxidized polymer in nm to the band gap in eV.

$$Energy\ (eV) = \frac{1240}{\lambda\ (nm)} \qquad \text{Equation 1}$$

Oxidized polymers absorb higher wavelengths of light than the corresponding neutral polymers, which relates to a smaller band gap value. When a polymer is oxidized, intermediate energy levels between the valence and conduction bands form, making for a smaller band gap and less energy needed to promote electrons into the conduction band.[19]

1.6 Doping of EAPs

Doping EAPs is a process that involves oxidation and reduction reactions of the neutral, insulating polymer into the charged and conductive forms of the polymer. The

positive, or p-doped state of the polymer is produced by the oxidation of the neutral polymer. The p-doped polymer can then be reneutralized by a reversible reduction reaction. The negative, or n-doped state of the polymer is produced by the reduction of the neutral polymer. These oxidation and reduction reactions are reversible, making it possible for the polymeric system to switch between the three oxidation states (neutral, p-doped, and n-doped). Figure 5 illustrates the reversible switching between oxidation states of the polymer. The EAP can exhibit changes in physical and chemical properties depending on the oxidation state of the polymer.

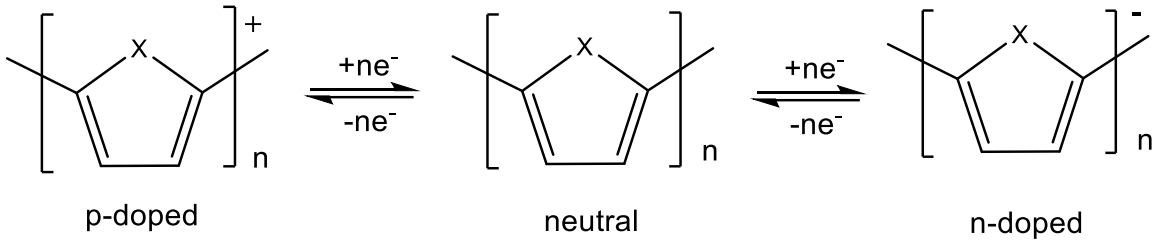

Figure 5: Doping process of an EAP through reversible oxidation/reduction reactions. X refers to a heteroatom in the cyclic system, typically S, O, or NH.

1.7 Use of Conductive Polymers in Biosensors

A biosensor is an integrated device that provides analytical information about a test sample and utilizes a biological recognition element and an electrical, thermal, or optical transduction method.[20] In the case of EAP based biosensors, the EAP is functionalized with a biological molecule such as an antibody, enzyme, oligonucleotide or aptamer that shows a high affinity and specificity for the target analyte.[21,22] The target analyte interacts with the functionalized EAP, and the electrochemical properties of the EAP change in response. The change in electrochemical properties can be detected in several different ways.[21,22,23]

Significant work has been done in the development of electrochemical biosensors

based on oligonucleotides.[24] As an example, Galán *et al.* reported a method for synthesis of a label-free electrochemical DNA sensor based on "click" modified PEDOT electrodes.[25] Azido-EDOT was electrochemically polymerized onto a gold electrode. Acetylene-terminated DNA probes specific for the Hepatitis C virus (HCV) were immobilized onto the azido-PEDOT electrodes by means of copper(I) catalyzed Huisgen 1,3-dipolar cycloaddition, or "click" chemistry. Several solutions with different concentrations of the complementary target sequence of the DNA-modified electrode were used to determine the analytical performance of the sensor. Non-complementary DNA sequences were used to determine the selectivity of the sensor. Differential pulse voltammetry (DPV) measurements were taken to determine the effectiveness of DNA immobilization and performance metrics of the sensor. Electrochemical methods for DPV experiments are described in greater detail in section 3.1.1 of this thesis. Figure 6 shows the differential pulse voltammogram of azido-PEDOT that had been incubated with acetylene-free DNA (red dots), a DNA-free solution (black squares), and the acetylene-functionalized DNA probe (blue triangles).

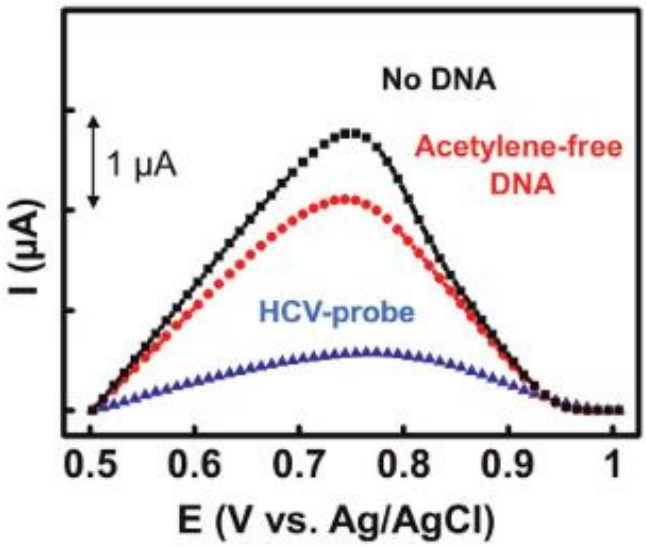

Figure 6: Differential pulse voltammograms of azido-PEDOT incubated with HCV DNA probe, acetylene-free DNA, and a DNA-free solution. Reprinted with permission from Biosensors and Bioelectronics, Vol 74, Teresa Galán, Beatriz Prieto-Simón, Margarita Alvira, Ramón Eritja, Günther Götz, Peter Bäuerle, Josep Samitier, "Label-Free Electrochemical DNA Sensor Using "Click"-Functionalized PEDOT Electrodes", pg 751-756, Copyright (2015), with permission from Elsevier.[25]

The electroactivity of the polymer film after incubation with the HCV probe is significantly lower than that of the polymers incubated with acetylene-free DNA and DNA-free solutions. This decrease in electroactivity is due to the formation of bonds with the HCV probe, creating an insulating layer on top of the polymeric film, impeding the ability of the polymer film to perform ion exchange with the electrolyte solution.

Figure 7 shows DPV measurements of HCV modified PEDOT electrodes that have been exposed to solutions containing the HCV target, non-complementary DNA sequence (Nc1), a mixture of non-complementary sequences (Nc1+ Nc2) and HCV target, and a DNA-free solution. Electrodes that were exposed to solutions containing the HCV target showed a sharp and reproducible decrease in electroactivity when compared to electrodes that were incubated with a DNA-free solution and with non-complementary DNA sequences. This decrease in electroactivity is due to the change in the environment

of the electroactive polymer when the HCV probe hybridizes with its target molecule. Results from these experiments have proven this to be an effective method for synthesizing a sensitive and selective electrochemical HCV sensor made from modified electroactive polymer films.

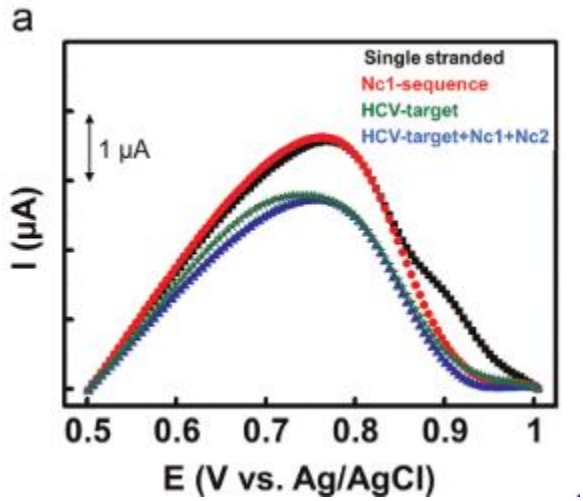

Figure 7: Differential pulse voltammograms of HCV modified PEDOT electrodes when incubated with solutions containing the HCV target, non-complementary DNA sequence (Nc1), a mixture of non-complementary sequences (Nc1+Nc2) and HCV target, and a DNA-free solution (single stranded). Reprinted with permission from Biosensors and Bioelectronics, Vol 74, Teresa Galán, Beatriz Prieto-Simón, Margarita Alvira, Ramón Eritja, Günther Götz, Peter Bäuerle, Josep Samitier, "Label-Free Electrochemical DNA Sensor Using "Click"-Functionalized PEDOT Electrodes", pg 751-756, Copyright (2015), with permission from Elsevier.[25]

For the purpose of this thesis, a biosensor will be developed with the use of an aptamer functionalized conductive polymer.

1.8 Use of Aptamers in Biosensors

Aptamers are small sequences of nucleotides (typically 20-60 nucleotides in length) that display high affinity and selectivity for their target molecules including amino acids, proteins, cancer cells, and many other organic and inorganic molecules.[26] In 1990, a procedure was developed by Tuerk and Gold to identify aptamers for specific

target molecules.[27] The procedure for identifying aptamers was called "Systematic Evolution of Ligands by Exponential Enrichment", or SELEX. The identification process of SELEX works by introducing a pool of randomized RNA strands to a target molecule. RNAs that do not bind to the target molecule are removed from the pool of RNA. The RNA sequences that bind to the target molecule are then amplified into double stranded DNA. This double stranded DNA is then transcribed into RNA strands that make up the new pool of RNAs for a new round of binding to the target molecule. As this process continues, there is an exponential increase in the best binding RNA ligand for the target molecule until that RNA sequence dominates the population of sequences. Later that same year, Ellington and Szostak used the same method to identify RNA sequences that specifically bind to a variety of organic dyes.[28] These papers are some of the first publications on the use and production of aptamers. The SELEX technology has been expanded to the development of DNA aptamers as well.[27]

Compared to other biorecognition molecules such as antibodies and enzymes, aptamers offer high thermal stability, are easily modifiable, are relatively inexpensive to synthesize, and have high binding affinities to their target molecules.[29] These properties make them great candidates for the development of biosensors.

Once an aptamer is exposed to its target molecule, the aptamer will change its conformation. This change in conformation can occur in several different ways depending on the size of the target molecule and the aptamer. The aptamer will conform to the most thermodynamically favored conformation with its target molecule. Figure 8 illustrates a change in conformation of an aptamer in response to recognition and binding to a small molecular weight target.

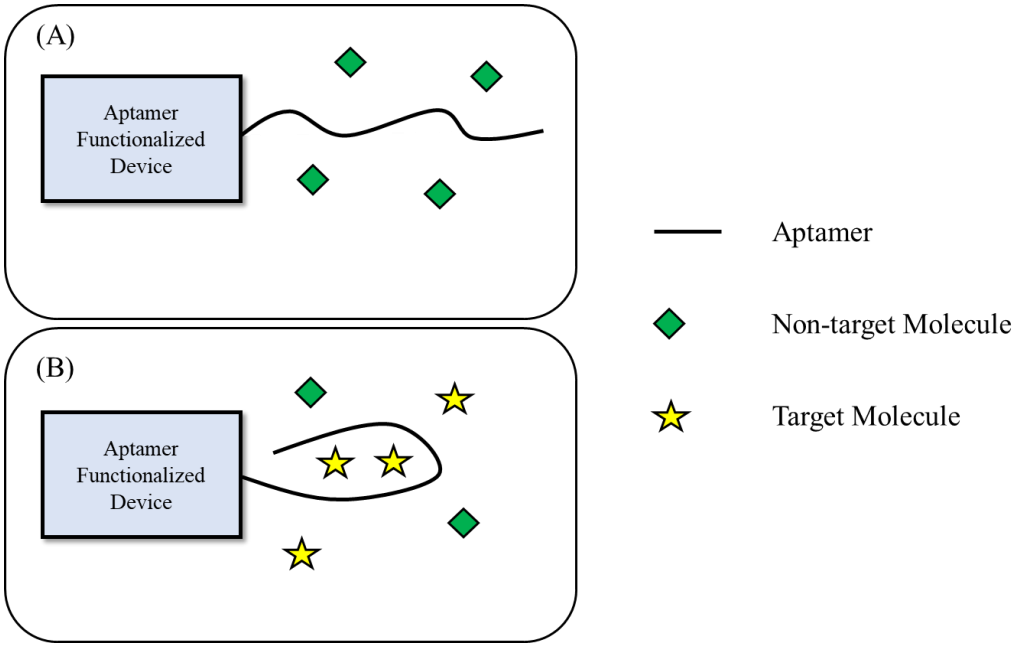

Figure 8: The behavior of an aptamer functionalized device when (A) it is not in the presence of a target molecule, and (B) when it is in the presence of a small molecular weight target molecule.

The aptamer and target molecule can interact in several different ways including through ionic bonding, hydrogen bonding, London dispersion forces, electrostatic interactions, steric interactions, and other non-covalent interactions. The way in which the aptamer and the target molecule interact depends on the chemical structures of both the aptamer and target molecule. The binding of the aptamer to its target can be detected spectroscopically or electrochemically, including through the use of an EAP as an electrode for electrochemical interrogation. Microfluidic devices,[30] gold nanoparticles,[31] hydrogels,[32] and many other devices have been functionalized with aptamers and used to detect the presence of cancer cells in a blood sample.[33] Aptamers have also been employed as biorecognition molecules for the development of biosensors. The following are examples of such aptamer-enabled biosensors.

Le Floch *et al.* reported two different electrochemical methods for the detection of

the human α-thrombin enzyme using the ferrocene-bearing cationic form of polythiophene that had been functionalized with the corresponding aptamer.[34] In the first method of electrochemical detection ,the direct method described in Figure 9, samples of differing thrombin concentrations were deposited on a gold electrode grafted with the thrombin aptamer and allowed to react for 30 minutes.

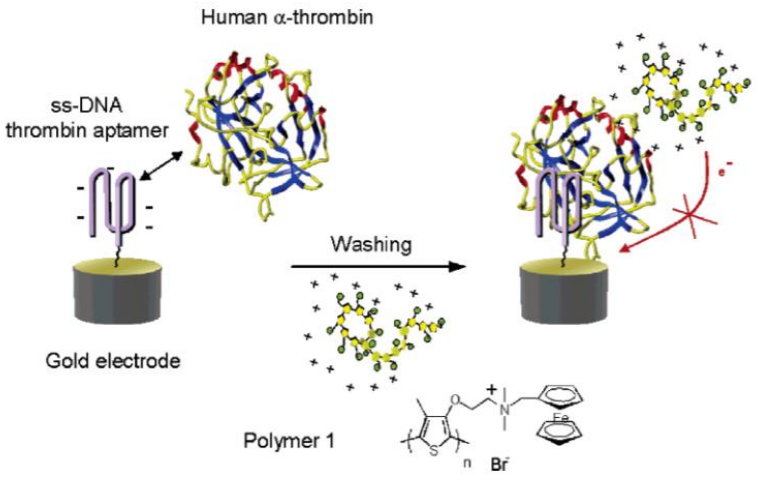

Figure 9: Schematic description of direct electrochemical detection methods. Reprinted with permission from Le Floch, F.; A. Ho, H.; Leclerc, M. Label-Free Electrochemical Detection of Protein Based on a Ferrocene-Bearing Cationic Polythiophene and Aptamer. *Anal. Chem.* 2006, *78* (13), 4727–4731. Copyright (2006) American Chemical Society.[34]

The electrodes were then rinsed with water and dipped in a solution containing the cationic form of polythiophene for 1 minute. The electrodes were then rinsed with water and electrochemically analyzed using square-wave voltammetry (SWV). SWV is a form of voltammetry that combines the square wave and staircase potential and applies this potential to an electrode. For this method, if thrombin molecules and the aptamer bind, no electrochemical signal is expected because thrombin would block the cationic, electroactive polythiophene from electrostatically binding to the negatively charged electrode surface. If thrombin does not interact with the electrode, an electrochemical signal is expected to be present.[34] Figure 10 shows the square wave voltammograms

obtained with a non-specific oligonucleotide sequence versus a human α-thrombin-specific aptamer sequence. As expected, the electrochemical response from the human α-thrombin-specific aptamer is significantly lower than that of the non-specific nucleic acid.

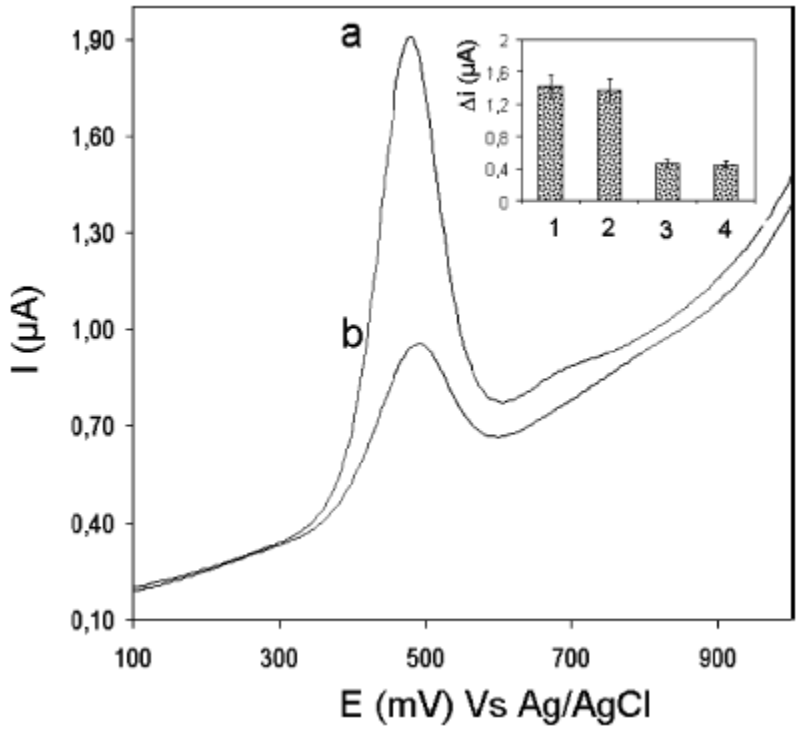

Figure 10: Square wave voltammogram of (a) a non-specific nucleic acid strand (control) versus (b) a specific human α-thrombin-specificaptamer. Figure inlay shows the electrochemical response of the human α-thrombin specific aptamer to solutions containing (1) no analyte, (2) bovine serum albumin (BSA), (3) thrombin, and (4) BSA + thrombin. Reprinted with permission from Le Floch, F.; A. Ho, H.; Leclerc, M. Label-Free Electrochemical Detection of Protein Based on a Ferrocene-Bearing Cationic Polythiophene and Aptamer. *Anal. Chem.* 2006, *78* (13), 4727–4731. Copyright (2006) American Chemical Society.[34]

For the second method of electrochemical detection (indirect method), an excess of human α-thrombin aptamer was added to a solution containing a known concentration of thrombin and allowed to bind to the thrombin. A nuclease enzyme was then introduced, causing all the aptamers not bound to thrombin to undergo hydrolysis. Enzyme activity was then terminated with a solution of ethylenediaminetetraacetic acid

(EDTA). The solution was then heated to 95° C to break the thrombin-aptamer bonds. The released aptamers were then electrochemically detected using gold electrodes grafted with a complementary sequence of nucleic acids after further exposure to ferrocene-bearing cationic polythiophene.[34] Figure 11 shows the Square wave voltammograms obtained after electrochemical detection of human thrombin at five different concentrations. As expected, with higher concentrations of human α-thrombin, more thrombin-specific aptamer can bind to the analyte, and a larger signal is produced from the increased amount of thrombin-specific aptamer detected electrochemically.

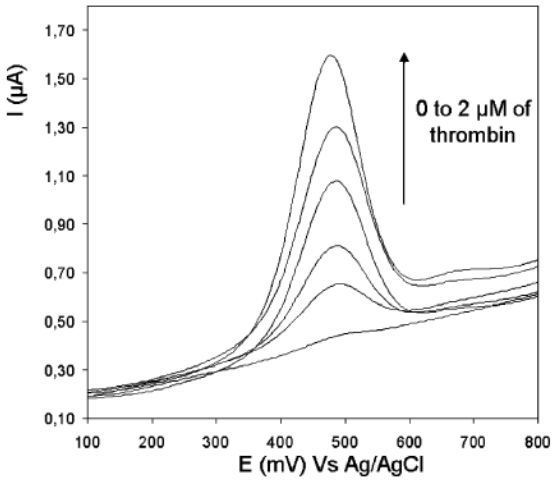

Figure 11: Square wave voltammograms for 0 M, 125 nM, 250 nM, 500 nM, 1 µM, and 2 µM thrombin solutions. Reprinted with permission from Le Floch, F.; A. Ho, H.; Leclerc, M. Label-Free Electrochemical Detection of Protein Based on a Ferrocene-Bearing Cationic Polythiophene and Aptamer. *Anal. Chem.* 2006, *78* (13), 4727–4731. Copyright (2006) American Chemical Society.[34]

Results from this research have shown that the α-thrombin enzyme can be electrochemically detected at concentrations as low as 75 fmol for the second, indirect method of electrochemical detection. This research shows the promise of EAPs as possible electrochemical detection materials.

In 2014, Taleat *et al.* successfully developed a biosensing device for the human

MUC1 cancer biomarker made by fabricating a sandwich assay on conductive polymer film of poly *o*-aminobenzoic acid.[35] *o*-Aminobenzoic acid was electrochemically polymerized onto a graphite-based screen printed electrode, and the terminal carboxylic acid groups of the polymer were converted into N-hydroxysuccinimide esters to immobilize MUC1 monoclonal mouse antibody onto the conductive polymer device. Next, the electrodes were incubated in a solution containing the MUC1 protein at various concentrations. The MUC1 protein binds to the antibodies on the EAP device. After incubation with the MUC1 solution, the electrode was incubated in a solution containing MUC1 specific aptamer. After incubation with aptamer solution, the electrodes were incubated in a solution containing methylene blue indicator. Methylene blue interacts with the guanine bases in the aptamer sequence of the MUC1 aptamer. Because of its electroactivity, binding of methylene blue to the sandwich assembly results in electrochemical signal changes that are indicative of binding of the anti-MUC1 aptamer to the MUC1 antigen immobilized onto the electrode surface via anti-MUC1 antibodies. Figure 12 illustrates the fabrication of these devices.

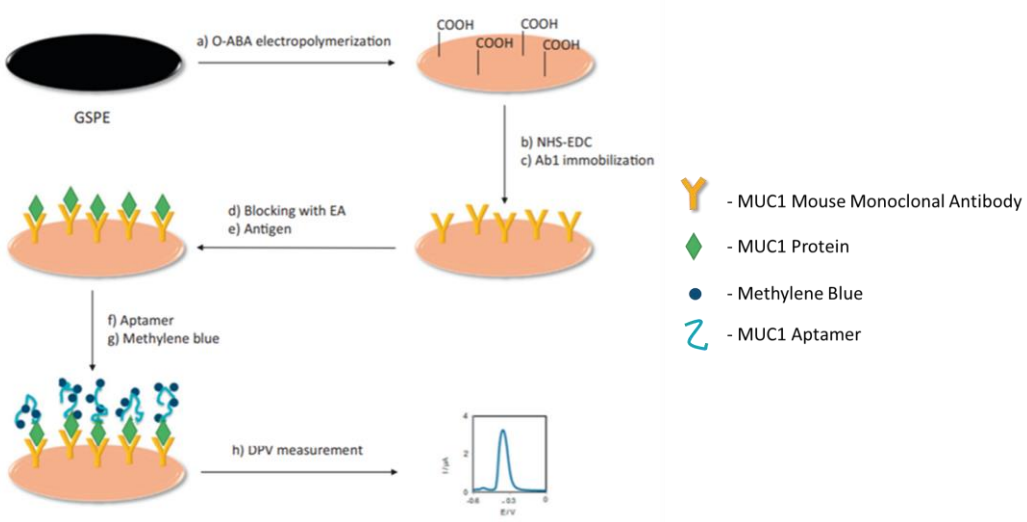

Figure 12: Process of developing a sandwich assay biosensing device for the MUC1 protein on a polymer film made from *o*-aminobenzoic acid. Reprinted from Journal of Electroanalytical Chemistry, 717-718, Taleat, Z.; Cristea, C.; Marrazza, G.; Mazloum-Ardakani, M.; Săndulescu, R., Electrochemical Immunoassay Based on Aptamer-Protein Interaction and Functionalized Polymer for Cancer Biomarker Detection, 119-124, Copyright (2014), with permission from Elsevier.[35]

Cyclic voltammetry (CV) experiments were conducted to evaluate the effectiveness of the biosensors. Figure 13 shows CVs obtained from these devices that were immersed in solutions of differing concentrations of MUC1 proteins. The redox peaks in the CVs correspond to the redox potentials of the methylene blue attached to the bound aptamers. The figure shows CV cycles a, b, c, d, and e which refers to devices that were incubated in a solution with 0, 3, 5, 7 or 10 ppb of MUC1 protein. The current response of the biosensor increases as the concentration of MUC1 in the sample increases. This result is expected because when MUC1 protein presence is increased, the amount of binding aptamer is also increased along with the methylene blue that binds to the guanine bases in the aptamer.

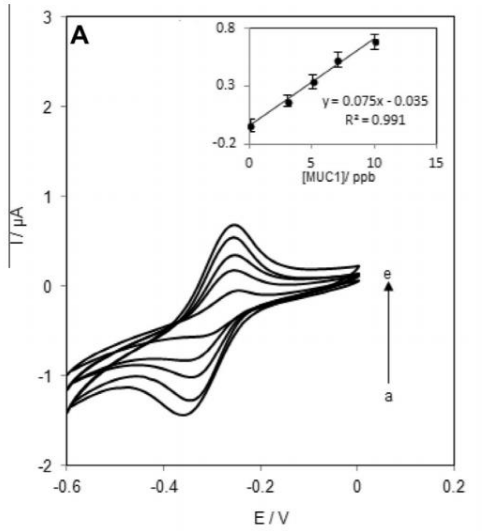

Figure 13: CVs obtained from devices that were incubated in solutions containing no MUC1 protein, 3 ppb MUC1, 5 ppb MUC1, 7 ppb MUC1, and 10 ppb MUC1. As the concentration of MUC1 in solution increases, so does the redox potential of methylene blue on the device, indicating more MUC1 aptamer binding. Inset is a linear plot of current response as a function of MUC1 concentration. Reprinted from Journal of Electroanalytical Chemistry, 717-718, Taleat, Z.; Cristea, C.; Marrazza, G.; Mazloum-Ardakani, M.; Săndulescu, R., Electrochemical Immunoassay Based on Aptamer-Protein Interaction and Functionalized Polymer for Cancer Biomarker Detection, 119-124, Copyright (2014), with permission from Elsevier.[35]

In 2018, Shafaat *et al*. successfully developed a conducting polymer based aptamer-enabled biosensor (aptasensor) for detection of the protein cytochrome C.[36] During apoptosis, or programmed cell death, cytochrome C is released from the mitochondria into the cytosol of a cell. This release of cytochrome C leads to apoptotic cell death. A cytochrome C biosensor could be used as a method for early detection of apoptosis. To fabricate the biosensor, a solution containing 10 mM pyrrole, 1 mM sodium dodecyl sulfate, and 10 µM cytochrome C aptamer was used during an electrochemical polymerization process. During electrochemical polymerization, cytochrome C aptamers were entrapped and immobilized in the polypyrrole films that were grown onto a screen-printed electrode. After immobilization of the cytochrome C aptamer into the polypyrrole film, solutions containing different concentrations of cytochrome C were applied to the

electrode surface.

Figure 14 shows a Nyquist plot comparing the charge transfer resistance differences between polypyrrole films in the absence of aptamer, in the presence of aptamer, and after a protein-aptamer binding event with a solution containing 1 nM cytochrome C. These plots were obtained in a solution containing 10 mM $[Fe(CN)_6]^{3-/4-}$ and 0.1 M KCl. The curve labeled "a" relates to a polypyrrole film synthesized on an electrode in the absence of the cytochrome C aptamer, the curve labeled "b" relates to a polypyrrole film synthesized in the presence of the cytochrome C aptamer, and the plot labeled "c" relates to a polypyrrole film synthesized in the presence of cytochrome C aptamer after an aptamer-protein binding event. The large increase in charge transfer resistance for the polymer film grown in the presence of cytochrome C aptamer (b) is due to the presence of the negatively charged aptamer repelling the $[Fe(CN)_6]^{-3/-4}$ anions in solution, making more difficult for the redox reaction to occur. This results in the increase of charge transfer resistance, confirming the presence of cytochrome C aptamers entrapped in the polymer film. The large decrease in charge transfer resistance of a polymer film grown in the presence of cytochrome C after an aptamer-protein binding (c) is due to the surplus of positively charged cytochrome C molecules that attract the $[Fe(CN)_6]^{-3/-4}$ anions and decrease the resistance for charge transfer to occur. This decrease in charge transfer resistance confirms the binding of the cytochrome C protein to the aptamers entrapped in the polymer film.

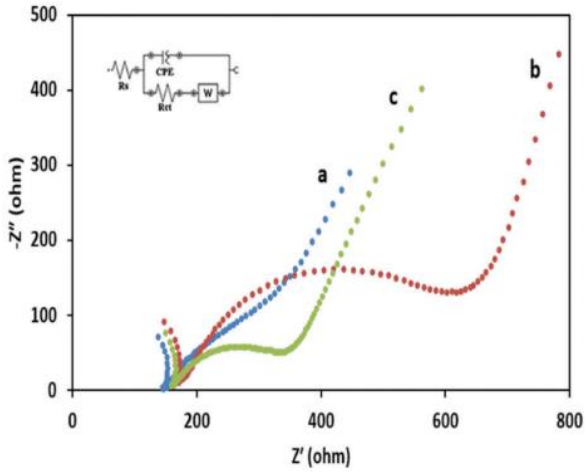

Figure 14: A Nyquist plot comparing the charge transfer resistance of polypyrrole films (a) in the absence of cytochrome C aptamer (b) in the presence of cytochrome C aptamer, (c) and after a protein-aptamer binding event. Reproduced from Ref. 32 with permission from the Centre National de la Recherche Scientifique (CNRS) and The Royal Society of Chemistry.[36]

To test the selectivity of the cytochrome C aptasensor, the aptasensor was exposed to solutions containing the proteins lysozyme (LYZ), albumin (BSA), immunoglobulin (IgG), and fibrinogen (Fbr). Figure 15 shows the change in charge transfer resistance of the aptasensor in the presence of solutions containing these different proteins. There is a significant change in charge transfer resistance only in the presence of the cytochrome C protein, this confirms the specific binding of cytochrome C to the aptasensor.

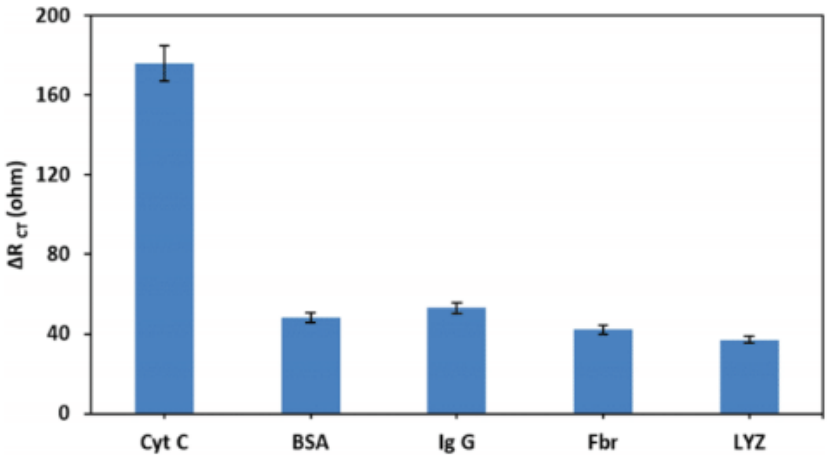

Figure 15: A plot comparing the change in charge transfer resistance of the cytochrome C aptasensor in the presence of cytochrome C (Cyt C), BSA, IgG, and Fbr. The significant increase in change of charge transfer resistance for the aptasensor in the presence of Cyt C confirms the selectivity of the aptasensor for Cyt C over other proteins Reproduced from Ref. 32 with permission from the Centre National de la Recherche Scientifique (CNRS) and The Royal Society of Chemistry.[36]

To test the analytical capabilities of the aptasensor, the aptasensor was exposed to solutions with different concentrations of cytochrome C. Figure 16 shows the change in charge transfer resistance for these electrodes. The charge transfer resistance decreases as the concentration of cytochrome C increases linearly on the range of 10 pM-1nM.

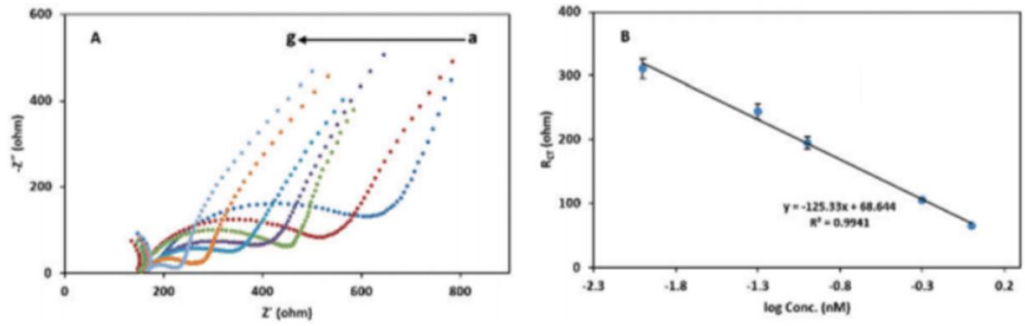

Figure 16: (A) Nyquist plots comparing charge transfer resistance for aptasensors exposed to solutions containing 0 nM (a), 0.005 nM (b), 0.01 nM (c), 0.05 nM (d), 0.1 nM (e), 0.5 nM (f), and 1 nM (g) of Cyt C. (B) the calibration curve plotting the resistance, R_{CT}, of the aptasensor vs the log concentration of Cyt C. The charge transfer resistance decreases linearly for the concentration range of 10 pM-1 nM. Reproduced from Ref. 32 with permission from the Centre National de la Recherche Scientifique (CNRS) and The Royal Society of Chemistry.[36]

Shafaat *et al.* was able to fabricate a conducting polymer based aptasensor that is

specific to the cytochrome C protein and can be used to quantify cytochrome C in solution on a linear range from 10 pM-1nM.

1.9 Motivation for This Thesis

Many modern diseases can be diagnosed by the detection of biomarkers that are specific to a given disease. These biomarkers are called disease-related biomarkers. Many forms of cancer, cardiovascular diseases, infections, immune system disorders, and even genetic disorders can be diagnosed by detection of their specific biomarkers. Many modern methods for detecting these diseases can be expensive and highly invasive. Using an aptamer-functionalized EAP may be a viable and cost-effective method for the detection of these disease-related biomarkers.

1.10 Thesis of This Work

Functionalized ProDOT polymer films are expected to be excellent EAPs to use for the fabrication of an EAP-based, electrochemical biosensor because of their relatively low oxidation potentials and electrochemical stability. Alkyne and azide substituents on a ProDOT-based compound would provide a substrate onto which aptamer functionalization is possible through aqueous click chemistry reactions. Aptamer functionalized PProDOT films should provide a simple, inexpensive, and rapid method for the electrochemical detection of disease related biomolecules.

2. MONOMER SYNTHESIS

2.1 Introduction to Monomer Synthesis

The goal of this monomer synthesis is to develop a monomer that is electron rich and stable during electrochemical experiments, has predictable electrochemistry, can be easily functionalized with different functional groups, and is a well understood compound.

Figure 17 below shows the chemical structure of 3, 4-propylenedioxythiophene (ProDOT). ProDOT is a symmetric molecule that has been studied for many years and whose electrochemistry is well understood.[37] The symmetry of the ProDOT structure allows for the synthesis of a regiosymmetric polymer. Regiosymmetric polymers show a higher degree of crystallinity than corresponding regiorandom polymers.[38] High crystallinity in a polymer results in a higher charge carrier mobility.[39]

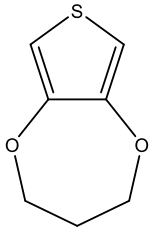

3,4-Propylenedioxythiophene
(ProDOT)

Figure 17: Chemical structure of ProDOT

Reeves *et al.* reports the synthesis of a ProDOT-based monomer functionalized with bromine substituents.[40] Figure 18 shows a simple reaction scheme with the ProDOT($CH_2Br)_2$ that could be synthesized from the procedures of Reeves *et al.* to make a ProDOT-based monomer with any desired nucleophile as a substituent. For all of these

reasons, a monomer based on 3,4-propylenedioxythiophene shows promise for our purposes of creating a polymer film that is electrochemically stable and can be easily functionalized with a biomolecule.

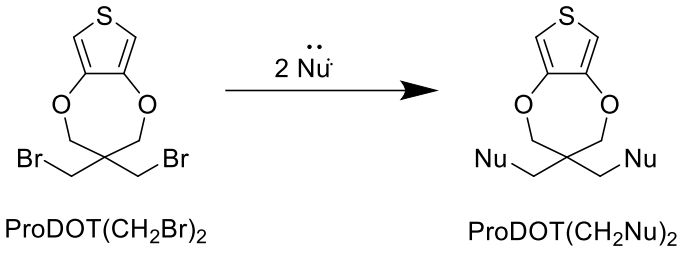

Figure 18: Simple reaction scheme for synthesizing a ProDOT-based monomer from ProDOT($CH_2Br)_2$. A method for synthesizing ProDOT($CH_2Br)_2$ was reported by Reeves *et al.*[40]

In our work, "click chemistry" will be used to attach an aptamer to a conducting polymer. "Click chemistry" refers to a class of reactions that "...must be modular, wide in scope, give very high yields, generate only inoffensive byproducts that can be removed by nonchromatographic methods, and be stereospecific (but not necessarily enantioselective). The required process characteristics include simple reaction conditions (ideally, the process should be insensitive to oxygen and water), readily available starting materials and reagents, the use of no solvent or a solvent that is benign (such as water) or easily removed, and simple product isolation. Purification, if required, must be by nonchromatographic methods, such as crystallization or distillation, and the product must be stable under physiological conditions".[41] One such reaction is Huisgen's 1,3-dipolar cycloaddition, which takes place between a molecule containing an azide group and a molecule containing an alkyne group, resulting in formation of a 1,2,3-triazole ring. Functionalizing a ProDOT monomer with either an alkyne or azide group would be possible following the schematics shown in Figure 18.

There are several reasons as to why an alkyne functionalized ProDOT based

monomer is desired over an azide functionalized ProDOT monomer. Firstly, alkynes are relatively stable compounds that would present an opportunity to form interesting branched conductive molecules through conjugation. Another reason for synthesizing an alkyne functionalized monomer is that more azide functionalized biomolecules are commercially available for coupling when compared to the amount of alkyne functionalized biomolecules available. Lastly, functionalizing a ProDOT monomer with an alkyne group would also produce a novel monomer for electrochemical polymerization. It is because of these reasons that the synthesis of an alkyne functionalized ProDOT based monomer was the first synthetic approach pursued.

2.2 Experimental

2.2.1 Materials

All reagents and solvents for monomer synthesis were used as received from their suppliers. *Tert*-butyldimethylsilyl chloride (*t*BDMSCl), diethyl ether, $CDCl_3$, sodium azide, 4-dimethylaminopyridine (DMAP), and an 18% sodium acetylide slurry in xylene were purchased from Sigma-Aldrich. *p*-Toluenesulfonic acid (*p*TsOH), dichloromethane (DCM), and pyridine were purchased from Acros Organic. Toluene was purchased from Fisher Scientific. 2,2-bis(bromomethyl)-1,3-propanediol was purchased from Tokyo Chemical Industry. 3,4 dimethoxythiophene was purchased from Ark Pharm, Inc. Ethyl acetate (EtOAc) was purchased from VWR. Hexanes were purchased from Avantor Performance Materials. Dimethylformamide (DMF) was purchased from EMD Millipore and silica gel was purchased from Malinckrodt Baker, Inc. Celite ™ (diatomaceous earth, diatomaceous silica) was purchased from Fisher Scientific. Ultrapure deionized water

was obtained from a Millipore Direct Q system (18.2 MΩ).

2.2.2 Instruments

All ^{1}H nuclear magnetic resonance (NMR) and ^{13}C NMR spectroscopy were carried out using a Bruker Avance 400 MHz NMR Spectrometer. Infrared (IR) spectra were obtained using a Bruker Tensor II Fourier-Transform Infrared (FTIR) Spectrometer. Gas chromatography- mass spectrometry (GC-MS) data were obtained using an Agilent 6890N Network GC System equipped with an Agilent 5973 Network Mass Selective Detector.

2.2.3 Synthesis

2.2.3.1 Synthesis of ProDOT($CH_2Br)_2$ via Transetherification of 3,4-Dimethoxythiophene

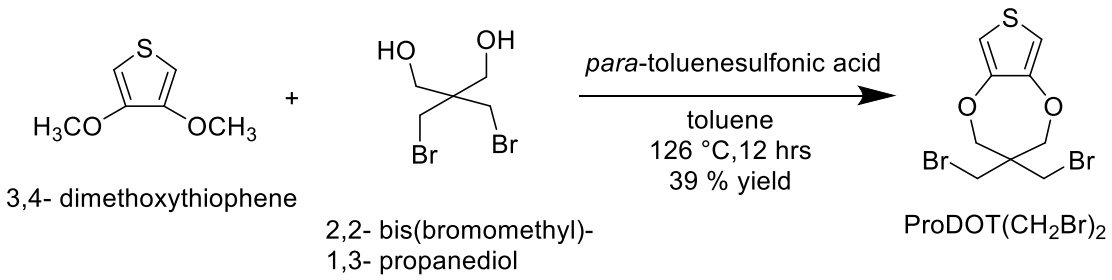

Figure 19: Synthesis of ProDOT($CH_2Br)_2$ via transetherification of 3,4-dimethoxythiophene

ProDOT($CH_2Br)_2$ was prepared via the transetherification of 3,4-dimethoxythiophene with 2,2-bis(bromomethyl)-1,3-propanediol following the procedures of Reeves *et al*.[40] A three neck round bottom flask was equipped with a

Soxhlet extractor, a cellulose thimble filled with 4 Å molecular sieves, a high efficiency condenser, and a stir bar. 3,4-Dimethoxythiophene (3g, 20.7 mmol) was placed under an argon blanket and dissolved in toluene (135 mL). Once the 3,4-dimethoxythiophene was dissolved, 1.1 mole equivalents of solid 2,2-bis(bromomethyl)-1,3-propanediol (5.96g, 22.77 mmol) and 0.1 mole equivalents of *p*TsOH (0.39g, 2.07 mmol) catalyst were added. The reaction mixture was heated at 126° C for 12 hours. The reaction mixture was then washed three times with ultrapure water (100mL each time), dried over $MgSO_4$, and filtered. Solvent was then removed from the organic layer under reduced pressure. Purification of the crude ProDOT$(CH_2Br)_2$ was accomplished using column chromatography with a stationary phase of silica gel and a solvent system of 1:9 ethyl acetate:hexanes. The removal of solvent under reduced pressure produced a white solid productthat was stored at 4ºC under argon. MP: 66-68°C (lit: 66-68°C). Yield: 2.84g, 39.9% (lit: 5.2g, 73%).[40] ^{1}H NMR (400MHz, $CDCl_3$): δ 6.49 (s, 2H), 4.10 (s, 4H), 3.61 (s, 4H); lit: (300MHz, $CDCl_3$): δ 6.49 (s, 2H), 4.10 (s, 4H), 3.61 (s, 4H) ppm.[40]

2.2.3.2 Attempted Synthesis of ProDOT-$(CH_2CCH)_2$ via S_N2 Reaction

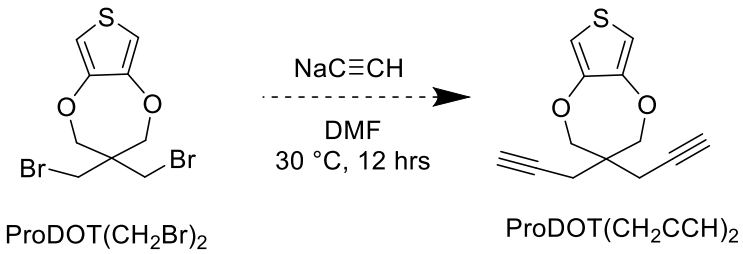

Figure 20: Unsuccessful synthesis scheme of the S_N2 reaction to produce ProDOT$(CH_2CCH)_2$ from ProDOT$(CH_2Br)_2$

Multiple attempts were made to synthesize ProDOT$(CH_2CCH)_2$ through an S_N2

reaction. The procedures of Rutledge were followed.[42] In the first attempt, 3 molar equivalents of sodium acetylide were used. Sodium acetylide slurry in xylene (3.4 mmol sodium acetylide, 163.81 mg sodium acetylide, 910.07 mg sodium acetylide in xylene slurry) was dissolved in 15 mL DMF in a round bottom flask and blanketed with nitrogen. ProDOT($CH_2Br)_2$ (386.4 mg, 1.1 mmol) was dissolved in 15 mL DMF in a separate round bottom flask and added to the sodium acetylide in DMF mixture after fully dissolving. The solution stirred for 12 hours at room temperature. After 12 hours, the reaction solution was extracted with an equal volume of ethyl acetate, washed twice with an equal volume of water, then washed twice with an equal volume of saturated brine solution. The organic layer was then filtered through Celite™ , and solvent was removed under reduced pressure. ^{1}H NMR of the crude product was acquired in $CDCl_3$. ^{1}H NMR (400 MHz, $CDCl_3$): δ 6.58 (s, 1H), 6.54 (s, 1H), 3.79 (s, 2H) ppm.

Crude product was further purified via column chromatography using a mobile phase solvent system of 1:20 ethyl acetate: hexane and a stationary phase of silica gel. Two separate compounds were isolated from the column eluent fractions and analyzed using ^{1}H NMR with $CDCl_3$ as the NMR solvent. Top spot/ first eluent: ^{1}H NMR (400 MHz, $CDCl_3$): δ 6.58 (s, 1H), 6.54 (s, 1H), 3.78 (s, 2H) ppm. Bottom spot/ second eluent: ^{1}H NMR (400 MHz, $CDCl_3$): δ 6.58 (s, 1H), 6.54 (s, 1H), 3.78 (s, 2H) ppm.

In the second attempt to synthesize ProDOT($CH_2CCH)_2$, ProDOT($CH_2Br)_2$ (141.4 mg, 0.41 mmol) was dissolved in 5 mL of dry DMF in a three-neck round bottom flask fitted with gas inlet adapter, condenser, and bubbler. In a separate flask, 3.3 molar equivalents of a sodium acetylide slurry (65.304 mg sodium acetylide, 1.36 mmol sodium acetylide, 362.8 mg slurry) were dissolved in 5 mL dry DMF. Once fully dissolved, 1mL

of the ProDOT($CH_2Br)_2$ in DMF solution was added every 5 minutes to the sodium acetylide in DMF solution. The reaction mixture was blanketed in nitrogen and left to react for 12 hours at room temperature. After 12 hours, the reaction mixture was extracted with an equal volume of ethyl acetate, washed twice with an equal volume of water, and then washed twice with an equal volume of saturated brine solution. The organic layer was then filtered through celite, and the solvent was removed under reduced pressure. ^{1}H NMR of the crude product was taken in $CDCl_3$. ^{1}H NMR (400 MHz, $CDCl_3$): δ 2.31 (s) ppm.

In a third attempt to synthesize ProDOT($CH_2CCH)_2$, a different method of purification was used. ProDOT($CH_2Br)_2$ (68.7 mg, 0.2 mmol) was dissolved in 3 mL dry DMF while 3.4 molar equivalents of sodium acetylide in a xylene slurry (32.688 mg sodium acetylide, 0.68 mmol sodium acetylide, 181.6 mg slurry) were dissolved in 3 mL dry DMF in a separate round bottom flask. The ProDOT($CH_2Br)_2$ in DMF solution was added to the sodium acetylide in DMF solution, and the reaction solution was blanketed in nitrogen and allowed to react for 12 hours at room temperature. After 12 hours, the reaction mixture was extracted with an equal volume of ethyl acetate, washed twice with an equal volume of water, then washed with an equal volume of saturated brine solution. The organic layer was then cooled for 2 hours at -85° C and dried under vacuum for 24 hours at room temperature. ^{1}H NMR of the crude product was taken in $CDCl_3$. ^{1}H NMR (400 MHz, $CDCl_3$): δ 6.58 (s), 6.54 (s), 4.11 (s), 3.61 (s) ppm.

2.2.3.3 Attempted Synthesis of ProDOT($CH_2CCH)_2$ via Protecting Group Chemistry I

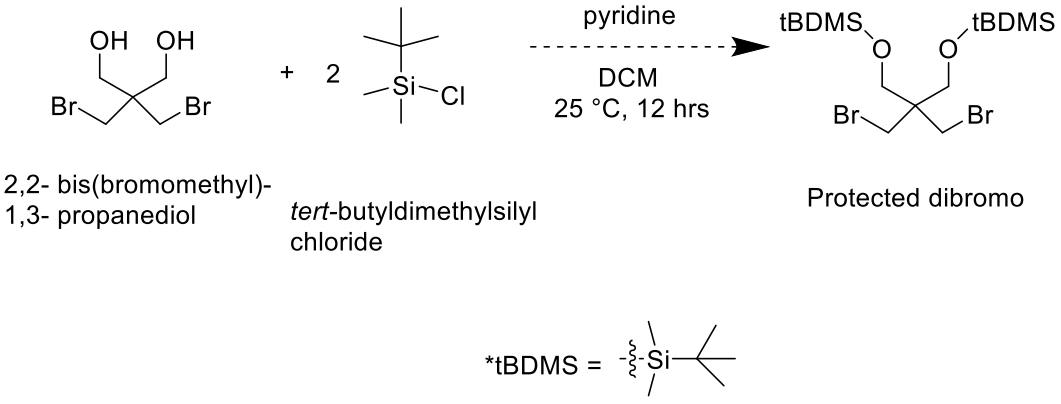

Figure 21: Unsuccessful protection of 2,2-bis(bromomethyl)-1,3-propanediol using *tert*-butyldimethylsilyl chloride

For the first attempt at synthesizing the protected diol, the procedures of Sunazuka *et al.* were followed.[43] A round bottom flask was equipped with a stir bar and gas inlet attached to a bubbler . This flask was then filled with nitrogen gas. 2,2-Bis(bromomethyl)-1,3-propanediol (262 mg, 1mmol) was dissolved in 25 mL DCM and placed into the round bottom flask. 3 Molar equivalents of *t*BDMSCl (0.45216g, 3mmol) and 0.2 molar equivalents of pyridine (0.01582g, 0.2mmol) were added to the reaction flask. The reaction mixture was stirred at room temperature (25° C) for 12 hours. The resulting reaction mixture was washed three times with water (25mL each time) and once with a brine solution (25mL). The organic layer was then dried over $MgSO_4$ and filtered. Solvent was removed under reduced pressure to obtain a yellow oil. ^{1}H NMR of the crude oil was taken in $CDCl_3$. ^{1}H NMR (400 MHz, $CDCl_3$): δ 3.77 (s, 4H), 3.56 (s, 4H), 2.17 (s), 0.90 (s, 9H), 0.07 (s, 6H) ppm.

2.2.3.3 Synthesis of ProDOT($CH_2CCH)_2$ via Protecting Group Chemistry II

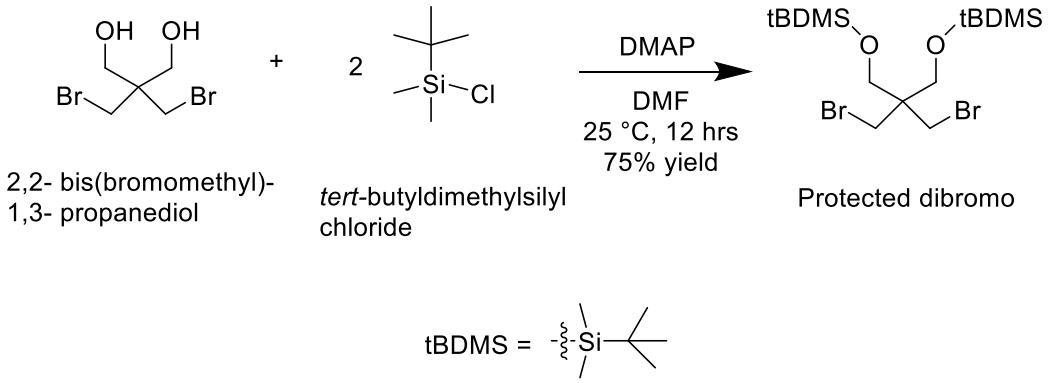

Figure 22: Successful protection of 2,2-bis(bromomethyl)-1,3-propanediol using *tert*-butyldimethylsilyl chloride

The protected diol was prepared following the procedures of Chaudhary *et al.*[44] A round bottom flask was equipped with astir bar and purged with nitrogen . 2,2-Bis(bromomethyl)-1,3-propanediol (2 g, 7.63mmol) was added to the flask and dissolved in 100 mL DMF. 3 Molar equivalents of *t*BDMSCl (3.45 g, 22.9 mmol) along with 0.2 molar equivalents of DMAP (0.18653 g, 1.52 mmol) were added to the reaction flask. The reaction was stirred at room temperature (25° C) for 12 hours. After 12 hours, the reaction mixture was removed from stirring, and diethyl ether (100mL) was added. The reaction mixture was then washed three times with water (100mL each time) and once with a brine solution (100mL). The organic layer was then dried over $MgSO_4$ and filtered. Solvent was removed from the filtrate under reduced pressure. The resulting purified protected diol product was a clear oil. Yield: 2.831g, 75.11%. ^{1}H NMR: (400 MHz, $CDCl_3$): δ 3.56 (s, 4H), 3.45 (s, 4H), 0.90 (s, 18H), 0.07 (s) ppm. ^{13}C NMR: (400 MHz, $CDCl_3$): δ 61.56, 45.93, 34.99, 29.88, 18.38, 1.16 ppm.

2.2.3.4 Attempted Synthesis of Protected Dialkyne via S_N2 Reaction

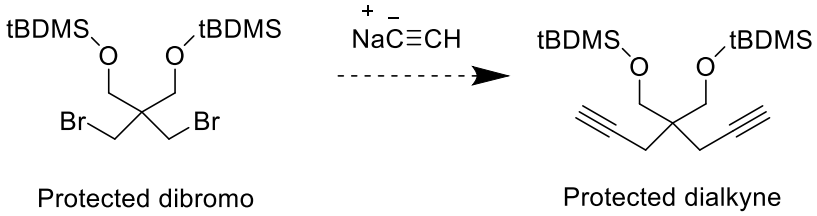

Figure 23: Failed synthesis scheme of protected dialkyne through S_N2 reaction of the protected dibromo.

Several different methods were used when attempting to synthesize the protected dialkyne product from the protected dibromo compound through S_N2 chemistry. In the first attempt to synthesize the protected dialkyne, protected dibromo compound (109mg, 0.022 mmol) was dissolved in DMF (5mL), and 3 equivalents of sodium acetylide (0.667 mmol sodium acetylide, 32 mg sodium acetylide, 178 mg slurry) were added to the reaction flask. The reaction mixture was stirred at room temperature under nitrogen overnight, then the crude mixture was slowly poured over an equal volume of ice water to quench excess sodium acetylide. The mixture was extracted with an equal volume of EtOAc, washed with an equal volume of water, then washed with an equal volume of 1M HCl solution. Solvent was then removed under reduced pressure. A ^{1}H NMR spectrum of the crude product was taken in $CDCl_3$. $_1$H NMR (400 MHz, $CDCl_3$): δ 2.95 (s, 4H), 2.03 (s, 3H), 0.85 (s, 3H) ppm.

Two different methods using only 2 molar equivalents of sodium acetylide were used to synthesize the protected dialkyne from the protected dibromo compound, each method using a different solvent. The protected dibromo compound (52 mg, 0.106 mmol) and 2 molar equivalents of sodium acetylide slurry (56 mg slurry, 10.08 mmol sodium acetylide, 0.212 mmol sodium acetylide) were added to 5 mL of either THF or DMF and

stirred at room temperature, under nitrogen for 12 hours to react. The crude products were slowly poured over an equal volume of ice water to quench excess sodium acetylide. Both crude products were then extracted with an equal volume of ethyl acetate, washed with a equal volume of water, then washed with an equal volume of 1M HCl solution. ^{1}H NMR spectra in $CDCl_3$ were acquired for both crude products. Reaction in THF: ^{1}H NMR (400 MHz, $CDCl_3$): δ 3.56 (s, 4H), 3.45 (s, 4H), 0.89 (s, 18H), 0.07 (s, 12H) ppm. Reaction in DMF: ^{1}H NMR (400 MHz, $CDCl_3$): δ 3.56 (s, 4H), 3.44 (s, 4H), 2.41 (s, 1H), 0.91 (s, 30H), 0.07 (s, 12H) ppm.

The reaction in DMF was repeated at a larger scale to make purification of crude product possible. The protected diol (170 mg, 0.347 mmol) and sodium acetylide slurry (185 mg of slurry, containing 33.3 mg, 0.694 mmol sodium acetylide) were dissolved in DMF (5mL). The reaction mixture was stirred for 12 hours at room temperature under nitrogen. The crude product was isolated following the same procedures as stated above.

Purification of crude protected dialkyne was attempted using a gradient of mobile phase solvent systems for column chromatography, first 200 mL hexane, then 400 mL 1% EtOAc in hexane, then finally 200 mL 2% EtOAc in hexane. The fractions collected were combined and solvent removed under reduced pressure. ^{1}H NMR of the purified protected dialkyne product was taken in $CDCl_3$. ^{1}H NMR (400 MHz, $CDCl_3$): δ 2.42 (s, 1H), 0.91 (s, 20H), 0.08 (s, 12H) ppm.

2.2.3.5 ProDOT(CH_2N_3)$_2$ Synthesis by S_N2 Reaction

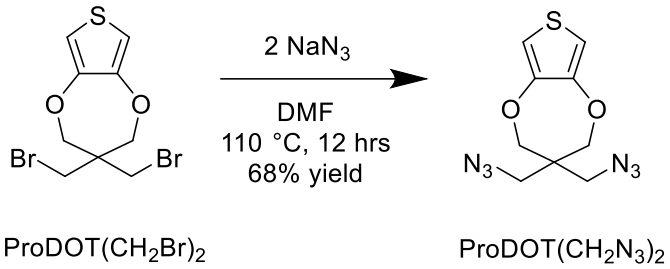

Figure 24: Synthesis scheme of the S_N2 reaction to produce ProDOT(CH_2N_3)$_2$ from ProDOT(CH_2Br)$_2$.

ProDOT(CH_2N_3)$_2$ was prepared via S_N2 reaction following the procedures of Godeau *et al.*[45] A three neck round bottom flask was equipped with a high efficiency condenser, a stir bar, and two vacuum adaptors. ProDOT(CH_2Br)$_2$ (0.5613g, 1.51 mmol) was added to the round bottom flask and dissolved in DMF (50 mL). The solution was blanketed with argon. 10 Molar equivalents of NaN_3 (0.9813 g, 15.1 mmol) were then added to the reaction flask. The reaction was heated at 110° C for 12 hours. Because DMF has a high boiling point, it can be difficult to remove from a crude product even under reduced pressure. DMF is miscible in water and can be removed from the organic layer of a reaction mixture by adding another organic solvent which is not miscible in water to the reaction mixture, then washing the resulting reaction mixture with an aqueous solution. To remove DMF from the crude reaction mixture, diethyl ether (100 mL) was added to the reaction mixture, the reaction mixture was then washed twice with a saturated NH_4Cl solution (25 mL each time) and once with brine solution (25 mL). The crude product was contained in the organic layer composed of diethyl ether while the DMF was contained in the aqueous layer. The organic layer was then separated from the aqueous layer, dried over $MgSO_4$, and filtered. Solvent was removed from the filtrate under reduced pressure. Purification of the crude ProDOT(CH_2N_3)$_2$ was accomplished

using column chromatography with a stationary phase of silica gel and a solvent system of 1:9 ethyl acetate in hexanes. Solvent was removed under reduced pressure producing a white solid product. The white product was stored in the fridge under argon. Yield: 0.273 g, 67.7% (lit: 0.950 g, 90%)[45] ^{1}H NMR (400MHz, $CDCl_3$): δ 6.50 (s, 2H), 3.92 (s, 4H), 3.52 (s, 4H). (lit:^{1}H NMR($CDCl_3$): δ6.49 (s, 2H), 3.91 (s, 2H), 3.52 (s, 2H), 1.58 (s, 4H)).[45]

2.3 Results and Discussion

2.3.1 Synthesis of ProDOT($CH_2Br)_2$ via Transetherification of 3,4-Dimethoxythiophene

Figure 25 shows the labeled ^{1}H NMR spectrum of the purified ProDOT($CH_2Br)_2$ product. All expected peaks and appropriate integration values are present for the chemical structure of ProDOT($CH_2Br)_2$.

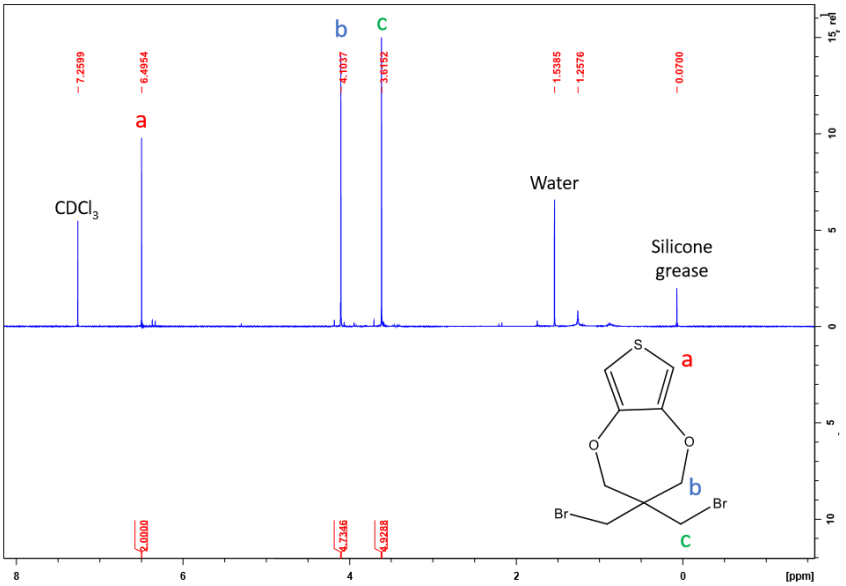

Figure 25: Labeled ^{1}H NMR spectrum of ProDOT($CH_2Br)_2$.

2.3.2 Attempted Synthesis of ProDOT($CH_2CCH)_2$ by S_N2 Reaction

The crude product from the small-scale reaction using 3 equivalents sodium acetylide was a brown, viscous oil. The ^{1}H NMR spectrum of the product (Figure 26) shows several peaks corresponding to the solvent, DMF. Peaks corresponding to the protons next to the oxygen on the seven membered ring (labeled b) and the protons next to the alkyne group (labeled c) were not present in the ^{1}H NMR spectrum. Protons at the position labeled b are expected to appear at approximately 4.10 ppm, and the protons at the position labeled c are expected to appear at approximately 2.50 ppm. Protons at the b position could be obscured by the presence of a large solvent peak, while protons at the position labeled c do not seem to be present on the molecule. The two aromatic proton peaks at 6.54 and 6.57 ppm may result from two species with similar structure, these species could be mono-reacted, fully-reacted, or non-reacted starting material. Integration of the aromatic and alkynyl protons is consistent with the desired chemical structure, but crucial peaks corresponding to protons on the ProDOT backbone structure are missing. Thin layer chromatography (TLC) of the crude product showed multiple spots that could be separated by column chromatography.

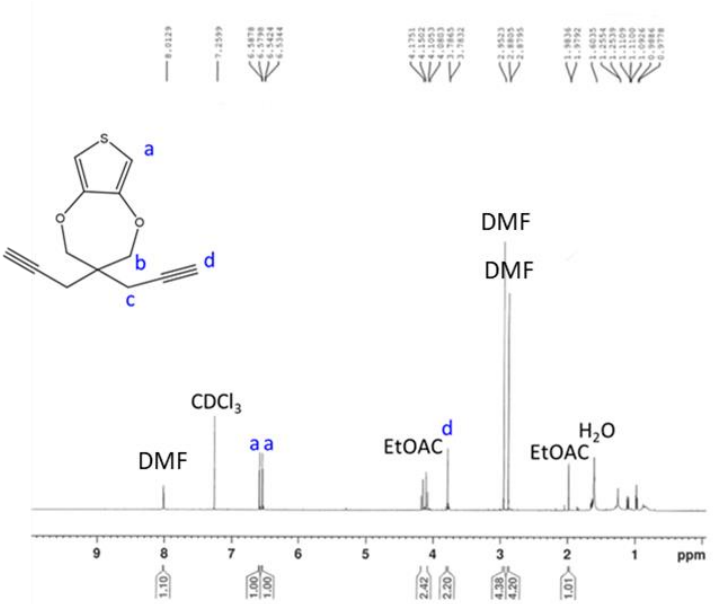

Figure 26: Labeled ^{1}H NMR of crude product from S_N2 reaction using 3 equivalents sodium acetylide.

^{1}H NMR of the two separate fractions collected from the column after purification indicate the lack of a ProDOT structure in the product (Figures 27 and 28). Neither the first fraction nor second fraction show proton peaks that contribute to the CH_2 group on 7-member oxygen containing ring system of ProDOT or of the CH_2 group neighboring the alkynyl substituent (labeled proton groups b and c for both Figure 27 and Figure 28 below). Sodium acetylide is a strong nucleophile and could have attacked the electrophilic methylene carbons adjacent to the oxygens contained in the 7 membered-ring of ProDOT, causing a ring opening reaction with ProDOT. Synthesis of ProDOT($CH_2CCH)_2$ by S_N2 reaction with 3 equivalents sodium acetylide was thus determined to be unsuccessful.

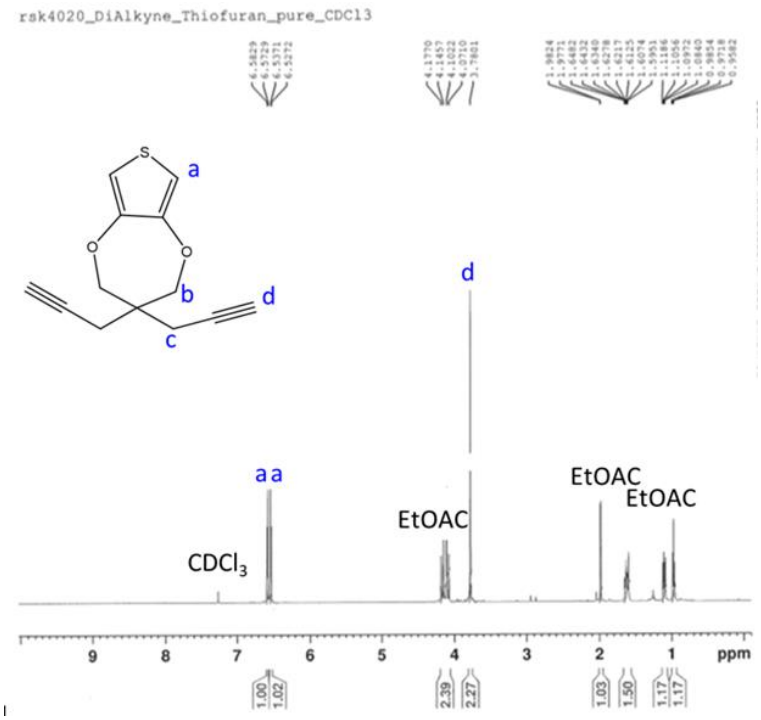

Figure 27: Labeled ^{1}H NMR of the first fraction to elute from the column during the purification process of the crude ProDOT($CH_2CCH)_2$ product.

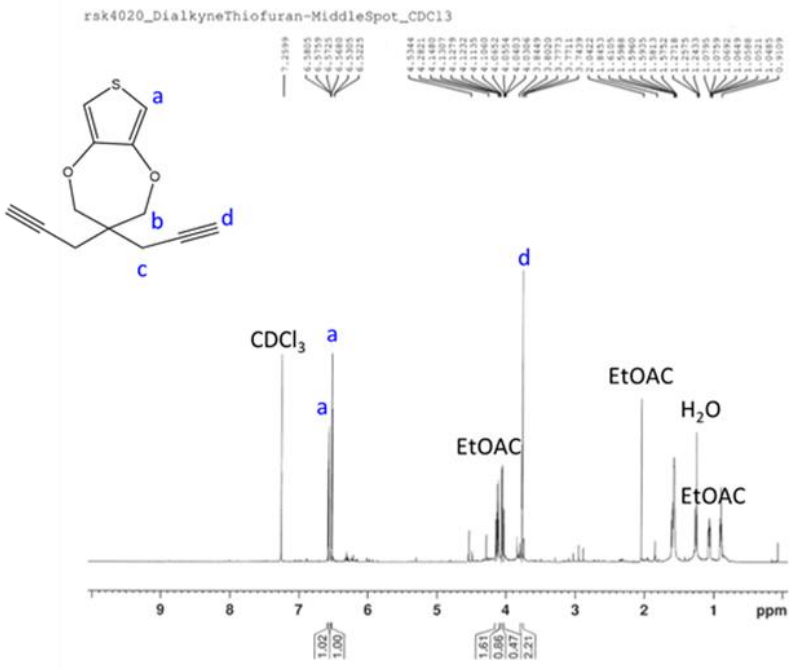

Figure 28: Labeled ^{1}H NMR of the second fraction to elute from the column during the purification process of the crude ProDOT($CH_2CCH)_2$ product.

For the reaction involving 3.3 equivalents sodium acetylide, ^{1}H NMR of the crude product (Figure 29) showed that most proton peaks could be attributed to the presence of DMF in the sample. The aromatic proton peak that is indicative of the thiophene ring present on ProDOT, which usually appears at approximately 6.60 ppm, was absent as well as proton peaks corresponding to the protons labeled b and c, which were expected to appear at approximately 4.10 and 2.50 ppm, respectively. This indicates the total absence of the ProDOT structure in the product. The only product peaks present correspond to alkynyl protons, indicating that the sodium acetylide in solution reacted with something else. Sodium acetylide may have participated in a side reaction with the DMF solvent and was then the only species recovered during the work up of the crude reaction mixture. Sodium acetylide is a strong nucleophile and has potential to react with the DMF solvent. As seen from earlier ^{1}H NMR spectra, it is possible that sodium acetylide could react with the oxygens contained in the structure of ProDOT and cause a ring opening reaction. These ring opening reactions could result in the destruction of the desired product and could affect the ability to recover components of the crude product that correspond to the ProDOT structure of the starting material. Synthesis of ProDOT($CH_2CCH)_2$ by S_N2 reaction with 3.3 equivalents sodium acetylide was thus also determined to be unsuccessful.

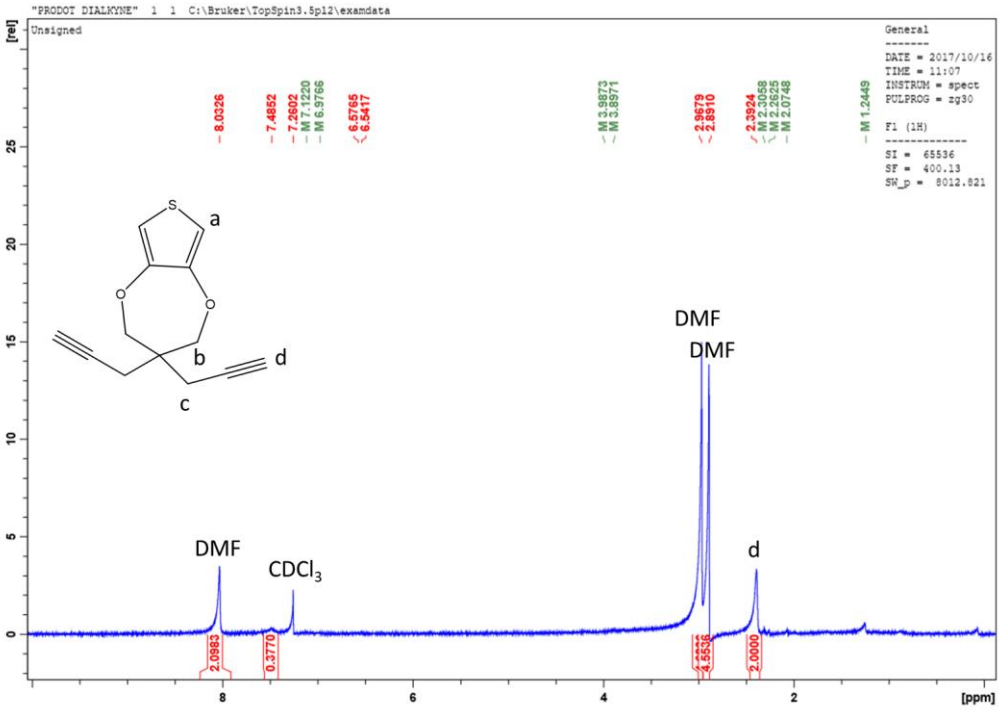

Figure 29: ^{1}H NMR of crude ProDOT($CH_2CCH)_2$ product from S_N2 reaction using 3.3 equivalents sodium acetylide.

For the reaction involving 3.4 molar equivalent of sodium acetylide, ^{1}H NMR of the crude product shows peaks that relate to the starting material (Figure 30). Several peaks show up in the aromatic region just above 6 ppm, referring aromatic protons on several different species that are similar in structure, this could be mono-reacted, fully-reacted, or non-reacted starting material. An alkynyl proton peak is expected at approximately 3.70 ppm; this peak may be present or may be obscured by the peak labeled c. The peaks present that correspond to protons in the starting material are much larger than the peaks that may correspond to an alkynyl functionalized species, one could conclude that most of the product was unreacted starting material. Separation and purification of crude product through TLC methods were unsuccessful.

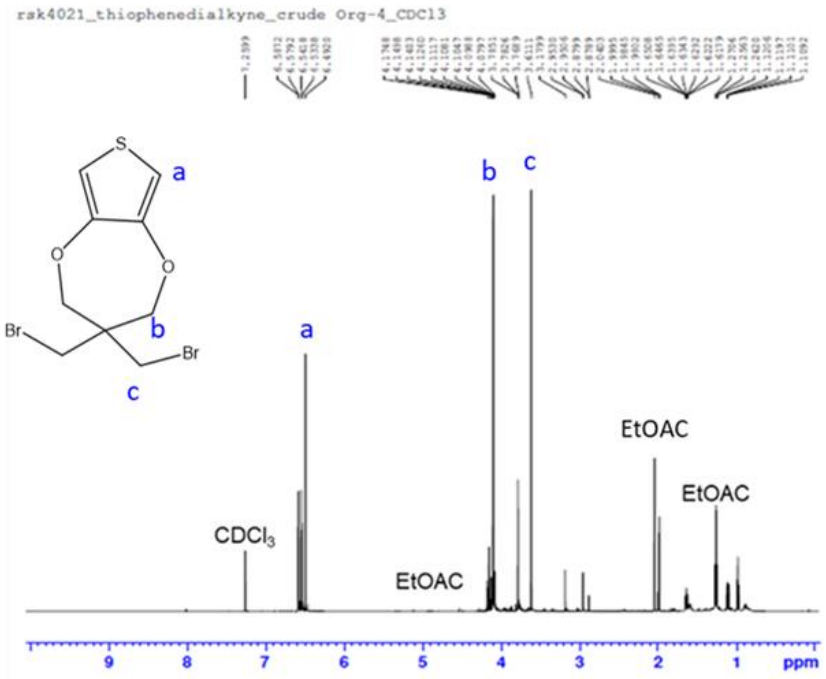

Figure 30: ^{1}H NMR of crude product from attempted synthesis of ProDOT($CH_2CCH)_2$ by S_N2 reaction with 3.4 equivalents sodium acetylide.

All attempts to synthesize ProDOT($CH_2CCH)_2$ via S_N2 reaction and purification methods were unsuccessful. For this reason, a different approach utilizing protecting group chemistry was pursued as it appeared to be a promising strategy for converting the bromine substituents in our 2,2-bis(bromomethyl)-1,3-propanediol into alkyne substituents, creating a starting material with alkyne groups to use during our transetherification reaction. The next section describes this work.

2.3.3 Attempted Synthesis of ProDOT($CH_2CCH)_2$ via Protecting Group Chemistry I

^{1}H NMR of the crude product (Figure 31) revealed that all peaks present were from the starting material, indicating that this method of synthesis was unsuccessful.

Although pyridine and other amines could catalyze this reaction, no catalyst is as efficient as DMAP for the silylation of alcohols.[44] Protection reactions like these are also much slower in solvents other than DMF.[46] Smaller peaks near the identified peaks could correspond to some reacted starting material, though this reaction was not very efficient with the given reaction circumstances.

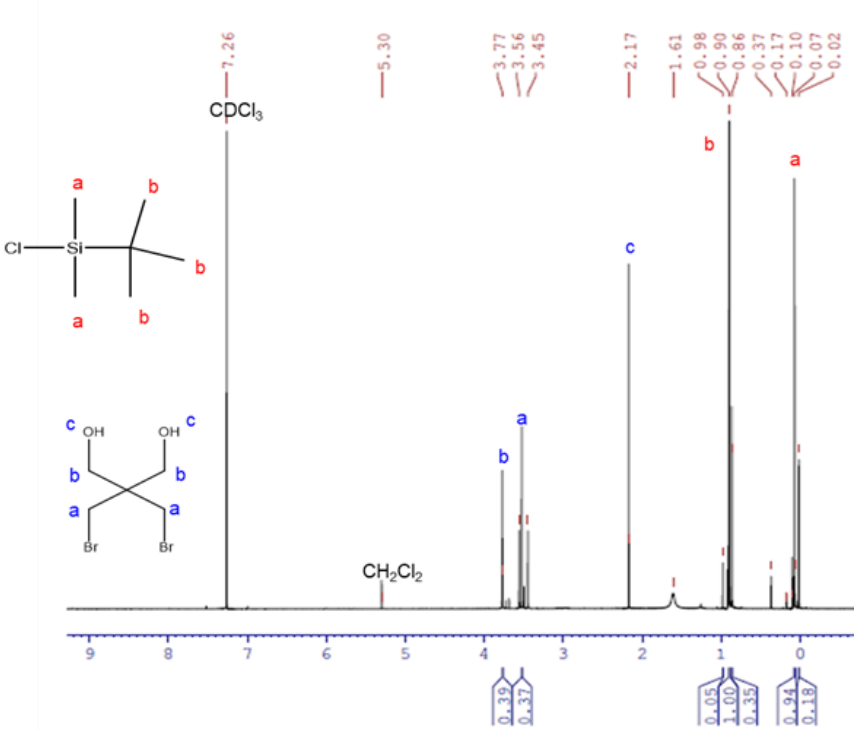

Figure 31: Labeled ^{1}H NMR of crude product from attempted protection reaction of 2,2-bis(bromomethyl)-1,3-propane diol.

2.3.4 Synthesis of ProDOT($CH_2CCH)_2$ via Protecting Group Chemistry II

^{1}H NMR and ^{13}C NMR peaks as well as integration from the ^{1}H NMR spectrum correspond to the desired protected dibromo compound. Figure 32 shows the labeled ^{1}H NMR spectrum, and Figure 33 shows the labeled ^{13}C NMR spectrum of the protected dibromo compound.

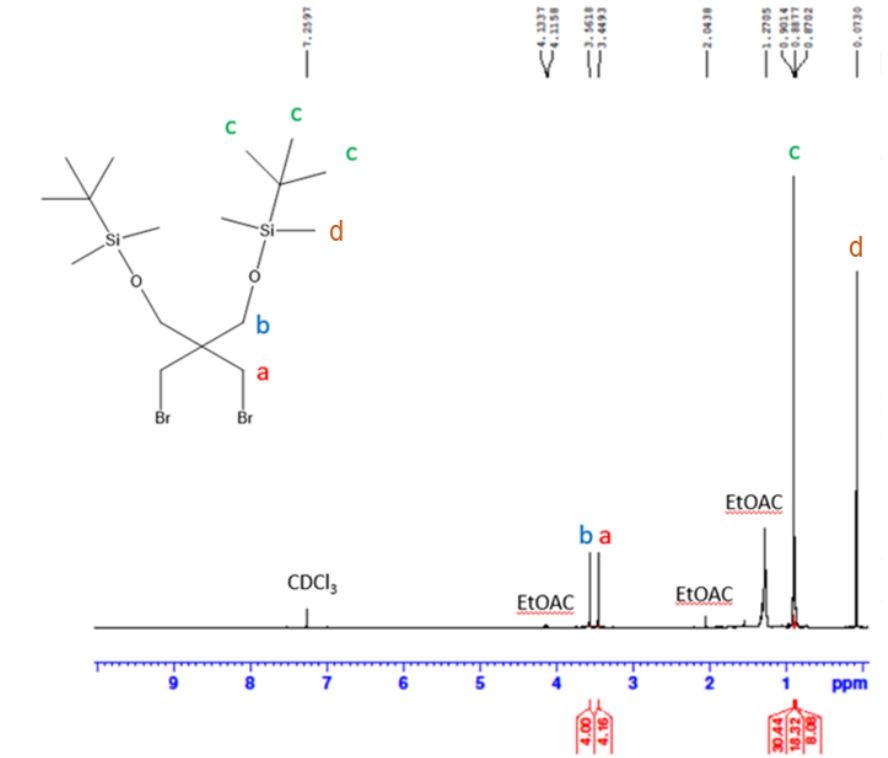

Figure 32: Labeled ^{1}H NMR of protected dibromo compound.

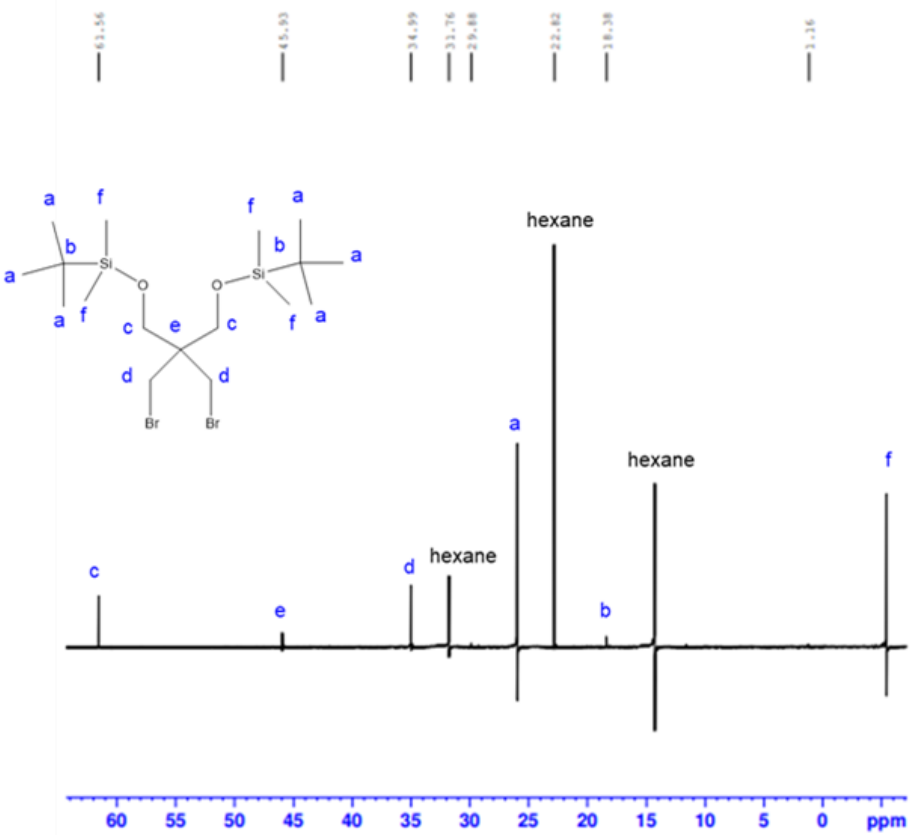

Figure 33: Labeled ^{13}C NMR of protected dibromo compound.

2.3.4 Attempted Synthesis of Protected Dialkyne through S_N2 Reaction

For the reaction involving 3 equivalents of sodium acetylide in DMF, ^{1}H NMR of the crude product showed deprotection of the compound (Figure 34). Peaks that could correspond to alkynyl protons are heavily skewed by DMF solvent peaks and could affect integration values for the ^{1}H NMR spectrum. Peaks that correspond to protons on the silane-based protecting group are present at 0.90 ppm, but integration of the peaks are not consistent with the desired structure. The ^{1}H NMR suggests that acetylide ions are replacing or removing a significant amount of silane protecting groups from the protected dibromo compound. At 3 equivalents of sodium acetylide, the acetylide ion is too nucleophilic to only replace the bromine substituents on the protected dibromo compound.

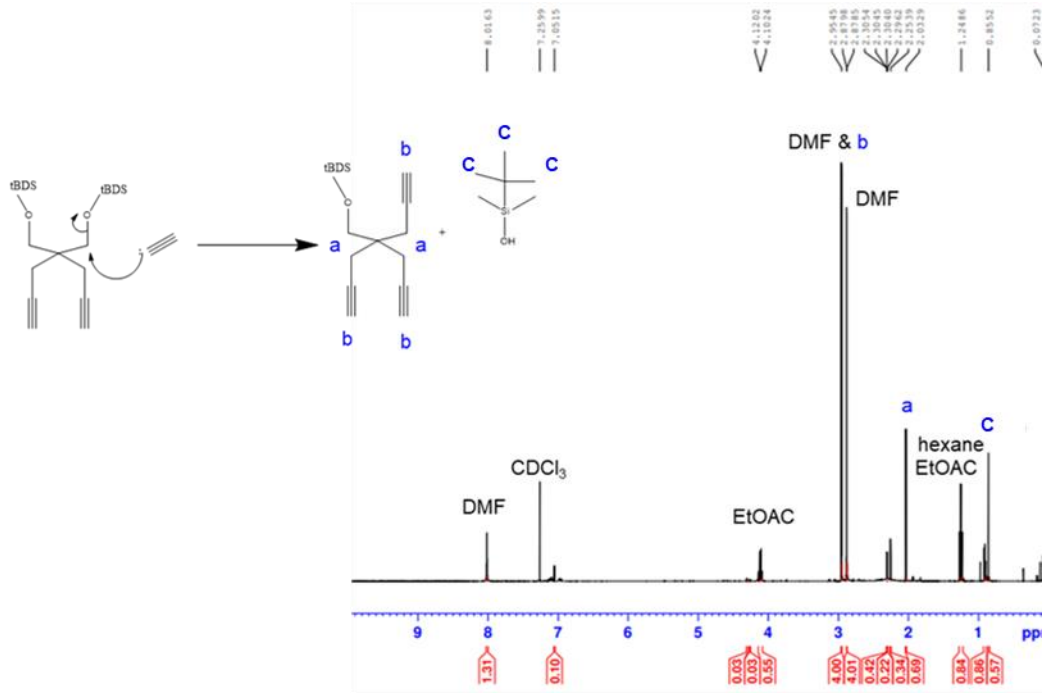

Figure 34: Labeled ^{1}H NMR spectrum of the crude product from the attempted synthesis of a protected dialkyne by S_N2 chemistry using 3 equivalents of sodium acetylide in DMF.

Because 3 equivalents of sodium acetylide caused undesirable side reactions, the

amount of sodium acetylide used was reduced to 2 equivalents. For the reaction involving 2 equivalents sodium acetylide in THF, the ^{1}H NMR of the crude product (Figure 35) did not show a peak indicating an alkynyl proton (expected at approximately 3 ppm), only proton peaks corresponding to unreacted starting material. THF is less polar than DMF and may not have been polar enough to facilitate this S_N2 reaction.

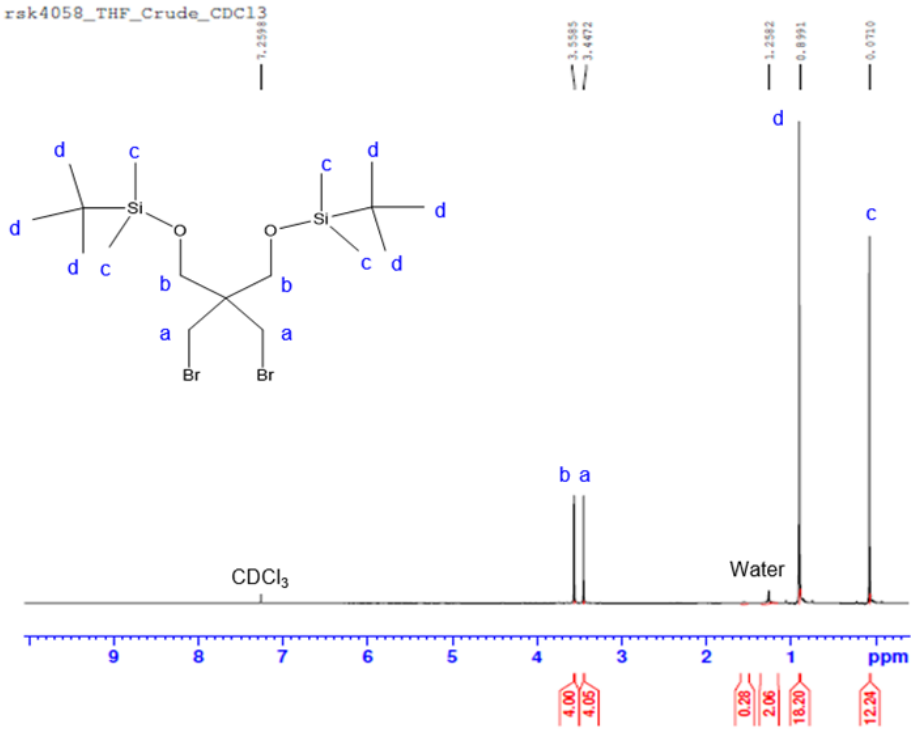

Figure 35: Labeled ^{1}H NMR spectrum of the crude product obtained from the attempted synthesis of a protected dialkyne by S_N2 chemistry using 2 equivalents sodium acetylide in THF; only starting material was obtained.

For the reaction involving 2 equivalents sodium acetylide in DMF, ^{1}H NMR of the crude product (Figure 36) shows a peak in the 1-2.5 ppm range that could correspond to an alkynyl proton peak, although integration of the peak corresponding to an alkynyl proton does not have an integration value consistent with the protected dialkyne structure, this could mean a small amount of acetylide impurity in the product or a very low conversion rate to the protected dialkyne compound. The scale of the reaction was

increased so that purification of the product could be possible.

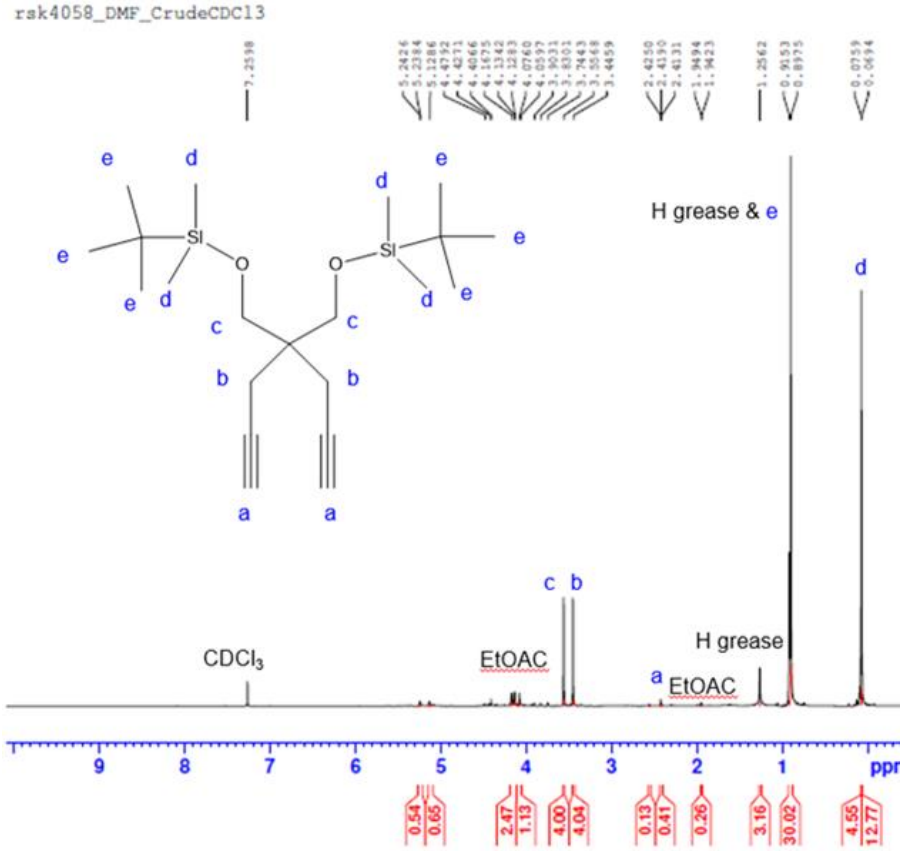

Figure 36: Labeled ^{1}H NMR of the crude product from the attempted synthesis of a protected dialkyne by S_N2 chemistry using 2 equivalents sodium acetylide in DMF.

The ^{1}H NMR spectrum of purified protected dialkyne product (Figure 37) shows the presence of alkynyl protons as well as protons corresponding to the protecting group, but does not show peaks that correspond to the protons neighboring the oxygen and the alkynyl group on the compound (labeled b and c on the structure of the protected dialkyne on Figure 37). Based on the species that was recovered during the purification process of the crude product, it appears that the nucleophilic attack of the acetylide ion deprotected the diol and resulted in direct attachment to the protecting group. .

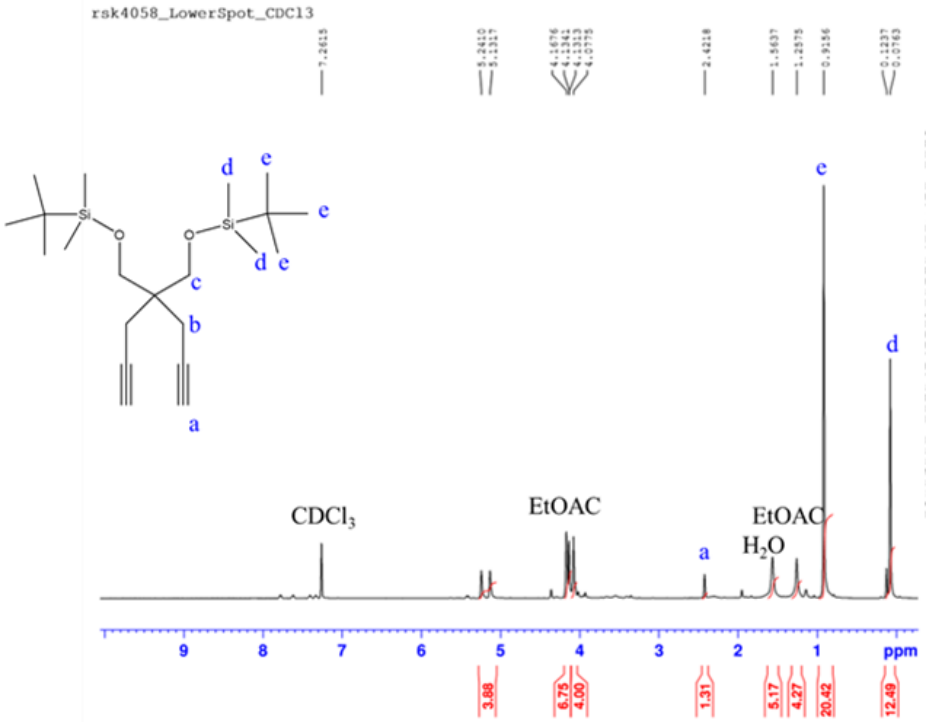

Figure 37: Labeled ^{1}H NMR spectrum of the purified protected dialkyne product obtained from using 2 equivalents sodium acetylide in DMF.

GC-MS was then used to further analyze the components of the purified protected dialkyne product. Figure 38 shows the GC-MS spectrum obtained and some possible fragments from the protected dialkyne structure. The GC-MS spectrum did not show fragmentation patterns expected from the protected dialkyne compound and could not be deciphered, therefore synthesis and purification of protected dialkyne was determined to be unsuccessful.

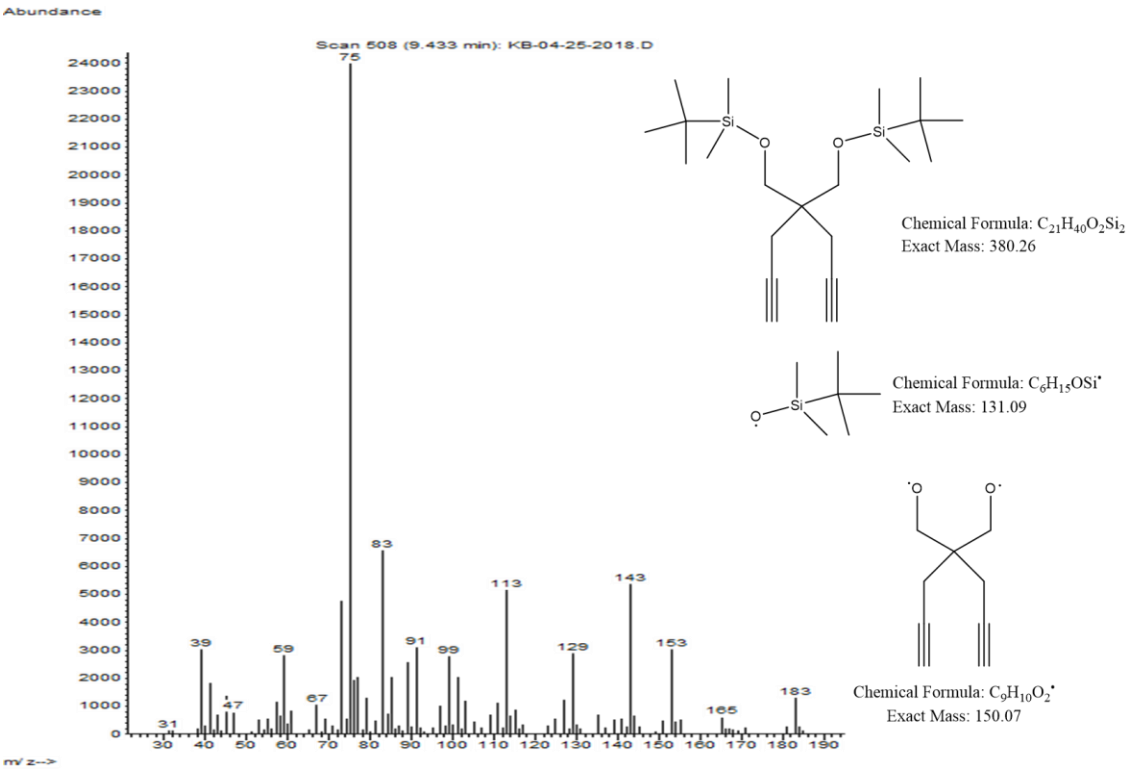

Figure 38: GC-MS spectrum of the purified protected dialkyne product obtained from the S_N2 reaction using 2 equivalents sodium acetylide in DMF including some expected fragments of the protected dialkyne compound.

2.3.5 ProDOT(CH_2N_3)$_2$ Synthesis by S_N2 Reaction

The ^{1}H NMR spectrum of the ProDOT(CH_2N_3)$_2$ product is consistent with the desired structure. Figure 39 shows the labeled ^{1}H NMR of ProDOT(CH_2N_3)$_2$ product.

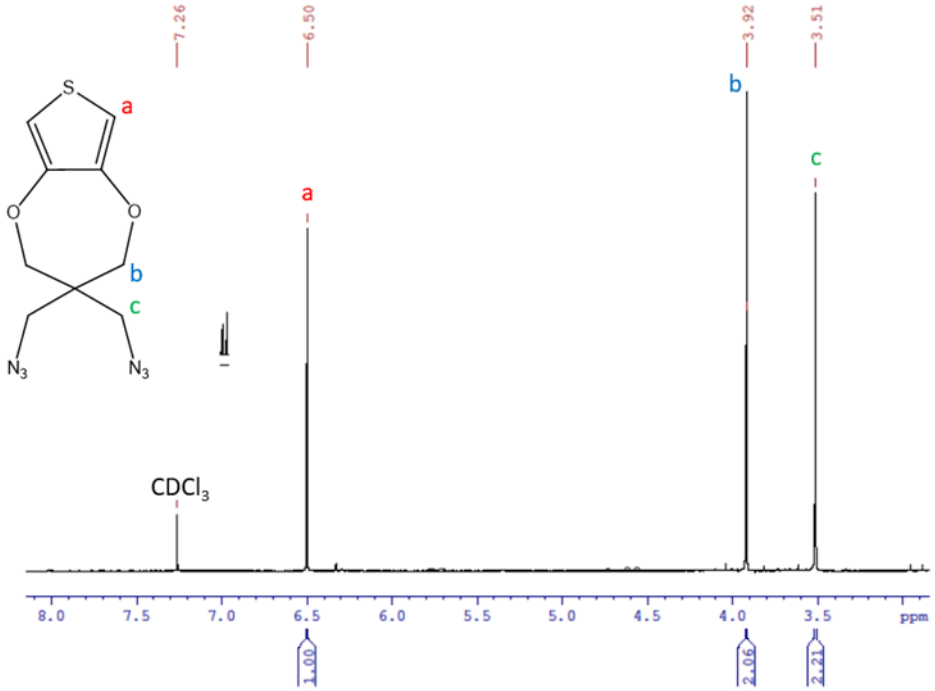

Figure 39: Labeled ^{1}H NMR of ProDOT(CH_2N_3)$_2$.

The reported literature values for the ^{1}H NMR are inconsistent with the structure of ProDOT(CH_2N_3)$_3$.[45] Their reported ^{1}H NMR spectrum values suggest that there are four different hydrogen types on the molecule when only three different hydrogen types exist.

Because of the similarity in ^{1}H NMR spectra between ProDOT(CH_2Br)$_2$ (Figure 25) and ProDOT(CH_2N_3)$_2$ (Figure 39), IR spectra (Figure 40) were taken comparing ProDOT(CH_2Br)$_2$ starting material to the purified ProDOT(CH_2N_3)$_2$ product. Figure 40 shows the IR spectrum of ProDOT(CH_2N_3)$_2$ compared to that of ProDOT(CH_2Br)$_2$, there is a strong peak at around 2100 cm^{-1} that is indicative of the -N=N=N stretching of the azido group. This peak is absent in the IR spectrum of ProDOT(CH_2Br)$_2$. Synthesis and characterization of ProDOT(CH_2N_3)$_2$ was successful.

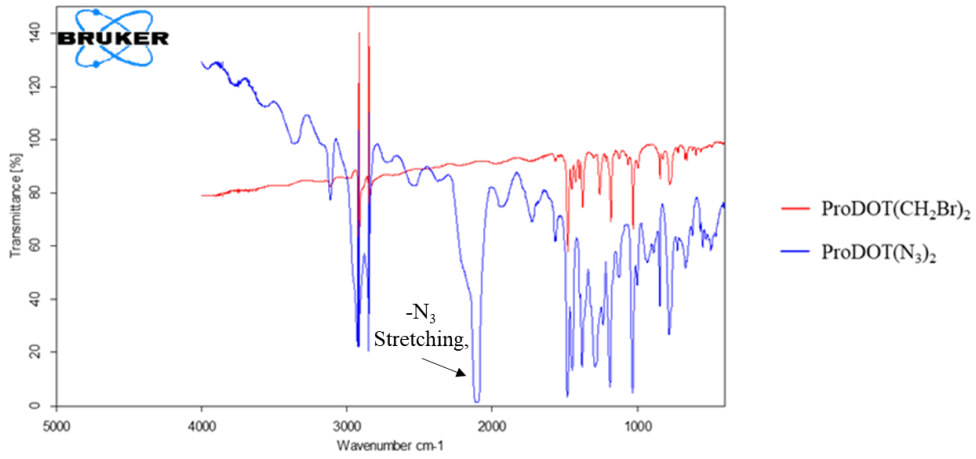

Figure 40: Comparison of ProDOT($CH_2Br)_2$ and ProDOT($CH_2N_3)_2$ IR spectra.

3. ELECTROCHEMISTRY

3.1 Introduction

3.1.1 Introduction to Electrochemistry and Cyclic Voltammetry

Electrochemical polymerization is a process in which a potential is applied to a monomer-containing electrolyte solution. The application of the potential results in the removal of electrons from the monomer, initiating the oxidative polymerization process described in Figure 2 in the introduction section of this thesis. The resulting polymer precipitates as a thin film on a conductive electrode. A system consisting of a working electrode, counter electrode, and reference electrode is commonly used for the polymerization process.[47] The working electrode is a conductive surface where polymer deposition occurs, the counter electrode is made of a conductive material and serves as an electron source/sink, and a redox reaction of known oxidation and reduction potentials occurs at the reference electrode. A potentiostat is used to control the difference in potentials between the working and counter electrodes. Potential measurements are taken relative to the reference electrode.[48] Figure 41 illustrates the three-electrode system described above for electrochemical polymerization.

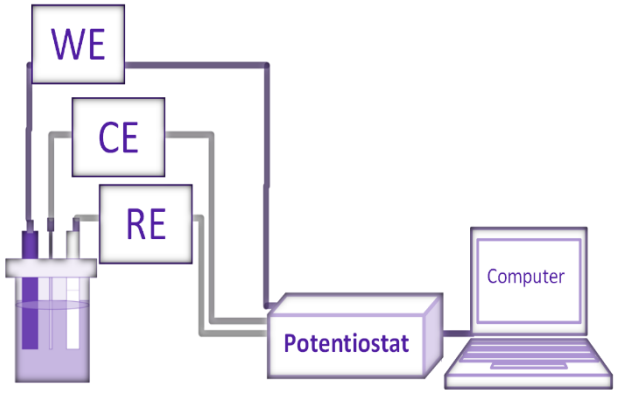

Figure 41: Illustration of a three-electrode system containing a working electrode (WE), counter electrode (CE), and reference electrode (RE).[49] Reprinted with permission from Jacob Frazer.

The process of electrochemical polymerization provides more information about the EAP than the chemical oxidative process. Polymer film deposition can be monitored using cyclic voltammetry (CV), a process in which a potentiostat is used to apply a voltage to a monomer-containing electrolyte solution, first starting at the lowest voltage value of that range and increasing stepwise to the highest voltage value of the range. A negative sweep is then performed, starting at the highest voltage value and decreasing stepwise to the lowest voltage value. The positive (anodic) and negative (cathodic) sweeps combined make up an entire CV cycle.[50] Each cycle deposits another layer of polymer onto the conductive electrode, creating a thicker film with increasing number of cycles. The potentiostat measures the current response at the conductive electrode as the applied voltage changes. From the voltammogram, the oxidation potential of the monomer along with the oxidation and reduction potentials of the polymer can be identified. Figure 42 shows the cyclic voltammogram for the oxidative polymerization of 3,4-ethylenedioxythiophene (EDOT). The voltage range used for the polymerization of EDOT was -0.88 V to 1.65 V. During the first cycle of the voltammogram, no oxidation

is seen until the onset of monomer oxidation ($E_{on,m}$) at 1.13V, with the peak oxidation of the monomer ($E_{p,m}$) occurring at 1.55V. Once the monomer is oxidized, deposition of the polymer onto the conductive electrode occurs. On the negative voltage sweep, polymer reduction ($E_{c,p}$) is observed at approximately -0.16V. On the second cycle, a new oxidation ($E_{a,p}$) peak corresponding to polymer oxidation appears at approximately 0.20V. Monomer oxidation continues and deposits more polymer onto the working electrode with each cycle, which in turn increases the current response for the oxidation and reduction of the polymer.

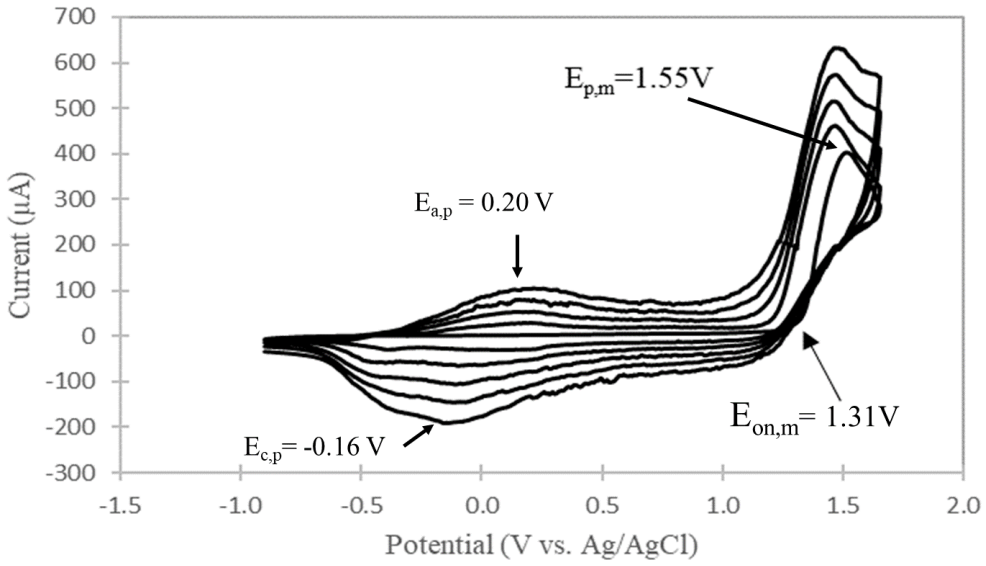

Figure 42: Cyclic voltammogram of the electrochemical polymerization of a 0.01M EDOT solution in 0.1M TBAP in acetonitrile (ACN).*

* This voltammogram was obtained by myself and Crystalrose Quintero.

After polymerization, CV experiments are performed in monomer-free electrolyte solution to further study the EAP film. Because the EAP film is irreversibly oxidized and immobilized onto a working electrode, the theory for surface immobilized redox centers (Equation 2)[51] is used to describe the electrochemistry of the polymeric system.

$$i_p = \frac{n^2 F^2 \Gamma^2 v}{4RT} \qquad \text{Equation 2}$$

In equation 2, i_p is the current response of the polymer, n is the number of transferred electrons, F is Faraday's constant, Γ is the amount of reactant initially present at the surface of the electrode, v is the scan rate, R is the gas constant, and T is the temperature. According to Equation 2, the current response of the polymer film is linearly related to the scan rate of the CV experiment when the film is well adhered onto the surface of the working electrode.

Scan rate dependence (SRD) CV experiments are conducted on the polymer film at several different scan rate values to ensure that the film is well adhered to the working electrode. The voltage range of the CV is reduced to only include the oxidation and reduction peaks of the polymer film. Figure 43 shows an overlay of CVs of PEDOT at several different scan rates. Current response at both the oxidation and reduction potentials of the polymer film is plotted versus the scan rate of the CV experiment in Figure 44. A linear relationship between the current response of the polymer film and the scan rate is apparent for both oxidation and reduction (Figure 44), suggesting that the PEDOT film is electroactive and well adhered to the surface of the working electrode.

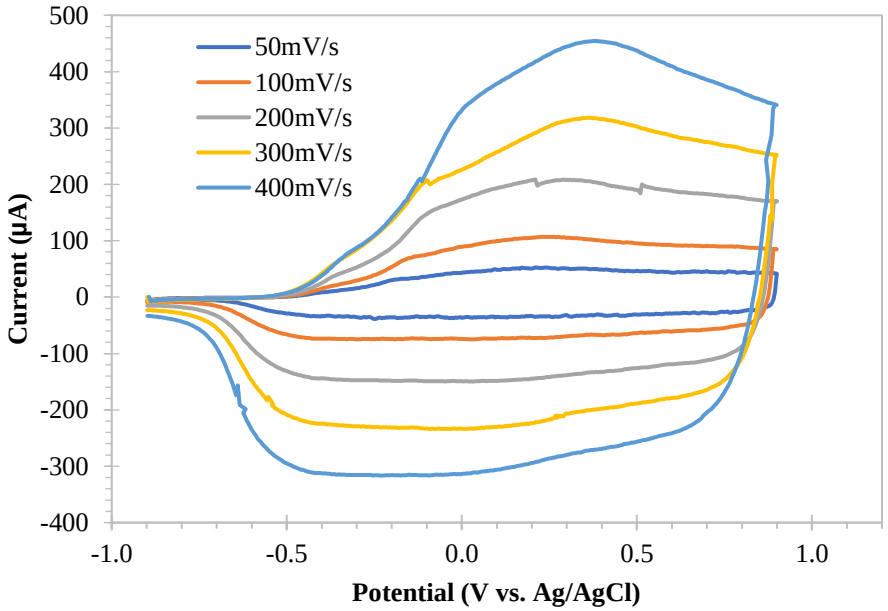

Figure 43: CV of PEDOT at 50, 100, 200, 300, and 400 mV/s in 0.1M TBAP in CH_3CN.*

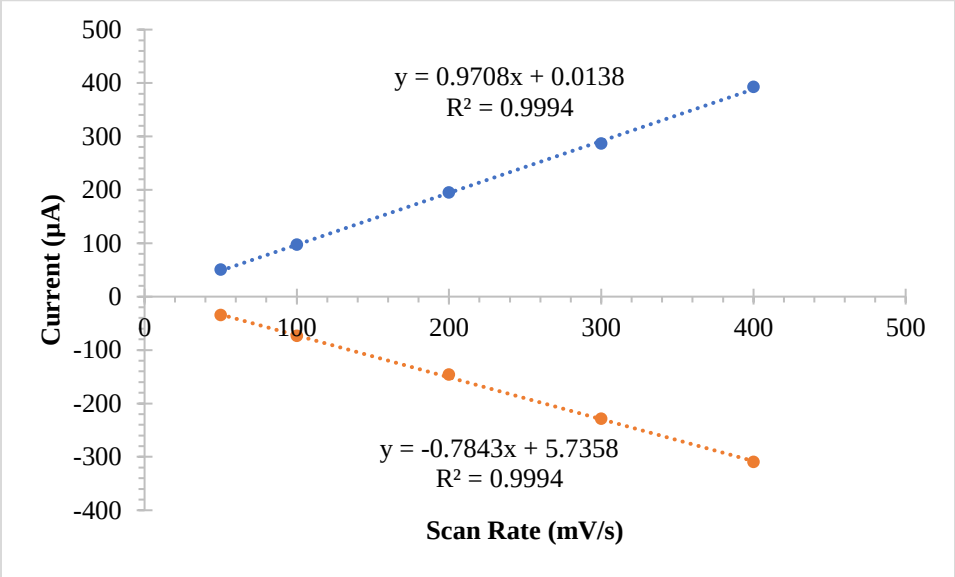

Figure 44: SRD plot of PEDOT.†

* Figure 47 was created based on data obtained from myself and Crystalrose Quintero.
† Figure 48 was created based on data obtained from myself and Crystalrose Quintero.

Several different electrochemical methods can be used to oxidatively polymerize a monomer and have the potential to tell more about a polymer than traditional cyclic voltammetry. Chronocoulometry is another electrochemical method for growing a polymer film. This technique involves applying a constant voltage to a monomer-containing electrolyte solution over a fixed time to promote the oxidation of the monomer, resulting in the oxidative polymerization of the monomer onto the working electrode. The voltage applied to the solution must be a value larger than or equal to the voltage of the onset of monomer oxidation ($E_{on,m}$). With this technique, the current response will increase with time as the polymer film is deposited on the electrode.[52] This method of electrochemical polymerization can be useful when higher voltages could potentially damage or destroy components of polymerization solutions, or when the reduced polymer is soluble in the electrolyte solution.

DPV is an electrochemical method in which a staircase waveform potential that pulses between each step is applied to an electrolyte solution. This electrochemical method can be useful when constant applied potential could damage or destroy components of polymerization solutions. Figure 45 illustrates this pattern of voltage application.

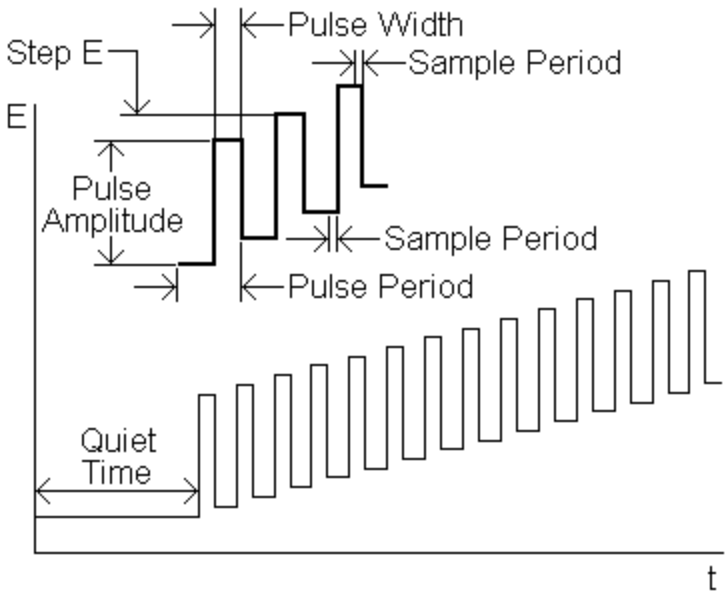

Figure 45: Voltage pattern applied during DPV experiments.[53]

3.1.2 Introduction to Electrode Surface Modification

In some cases, it is necessary to modify the surface of an electrode to promote adhesion of a polymer film or a monolayer of a certain molecule to the electrode surface. In the case of Ahuja *et al.,* surface modification of ITO-coated conductive slides was necessary to fabricate a uric acid biosensor.[54] Ahuja states that physical adsorption of a biomolecule to an electrode surface cannot resist the forces of stirring and washing of the electrode substrate and that the bio-incompatible substrate can interfere with the biocompatibility of the biomolecule. Surface modification of the electrode with a monolayer of organic molecules that can be coupled to the biomolecule would create a much more resistant layer of biomolecules on the surface of the electrode.

To monitor the concentration of uric acid in a sample, Ahuja proposes that one could electrochemically monitor the oxidation and reduction potentials of H_2O_2 in solution. H_2O_2 is produced from the oxidative breakdown of uric acid into allantoin by

the uricase enzyme. Figure 46 below shows the scheme for the enzymatic breakdown of uric acid.

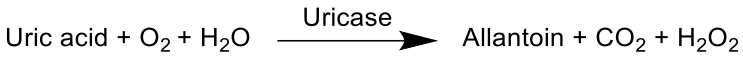

Figure 46: Enzymatic breakdown of uric acid to form allantoin.

An ITO glass electrode modified with the uricase enzyme could prove to be useful for the electrochemical detection of uric acid in solution. A monolayer of organic molecules on the surface of the ITO glass was needed to couple with uricase and to create a more resistant layer of uricase on the surface of the electrode. Figure 47 shows the ITO surface modification process used by Ahuja.

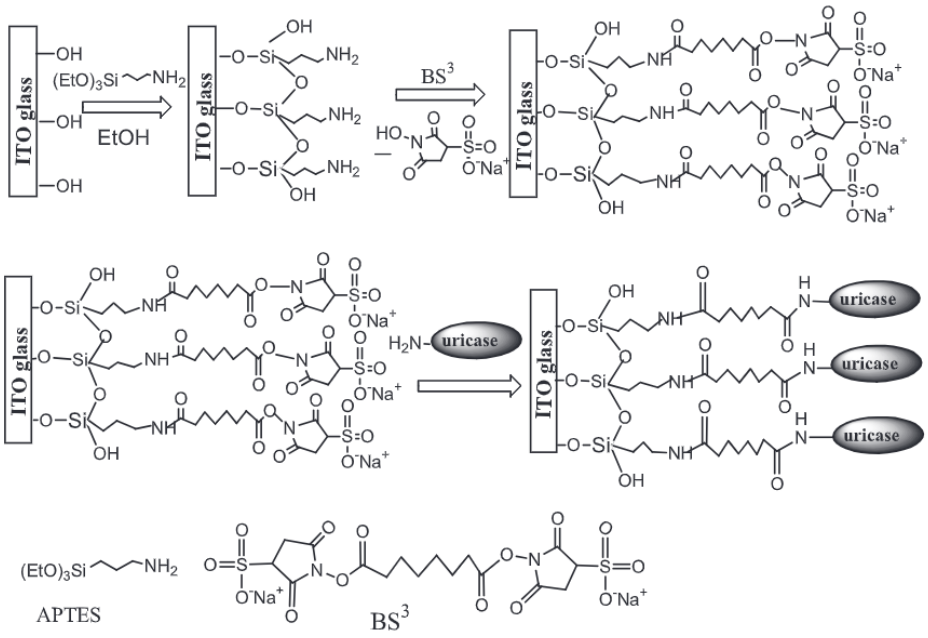

Figure 47: ITO glass surface modification process to fabricate an electrochemical uric acid biosensor. Reprinted from This Solid Films, 519, Tarushee Ahuja, Rajesh, Devendra Kumar, Vinod Kumar Tanwar, Vikash Sharma, Nahar Singh, Ashok M. Biradar, An amperometric uric based biosensor based on Bis[sulfosuccinimidyl] suberate crosslinker /3-aminopropyltriethoxysilane surface modified ITO glass electrode, 1128-1134, Copyright (2010), with permission from Elsevier.[54]

Ahuja first incubated an ITO slide in a 2% (3-aminopropyl)triethoxy (APTES) in

EtOH solution to form Ti-O-Si linkages between the ITO glass and APTES molecules. After successful modification with APTES, the slide was then incubated in a solution containing 5 mM bis[sulfosuccinimidyl]suberate (BS^3) in a sodium acetate buffer solution to form amide bonds between BS^3 and APTES. The final step of ITO modification involved the incubation of the BS^3 modified slide in a PBS solution containing the uricase enzyme. From this reaction, another amide bond was formed between the uricase enzyme and the BS^3 immobilized on the surface of the electrode. Ahuja confirmed surface modification of ITO slides by contact angle measurements obtained from water droplets on the surface of the ITO slide and characterized the modified ITO slide by cyclic voltammetry and electrical impedance spectroscopy at different points of modification.

After successful modification of the ITO glass slides, several electrochemical experiments were caried out on the uricase modified ITO slide to ensure the viability and the reusability of the biosensing electrode. Figure 48 shows spectra obtained from chronoamperometry experiments on the uricase-modified electrodes over time. Spectra labeled a-f to show the experiment had been repeated several times to illustrate the reusability of the biosensor. After every 100 seconds, an amount of uric acid was added to the solution. With each addition of uric acid to solution, the current response of the ITO slide increases. This increase in current response with increase in uric acid concentration is consistent for each subsequent experiment (b-f).

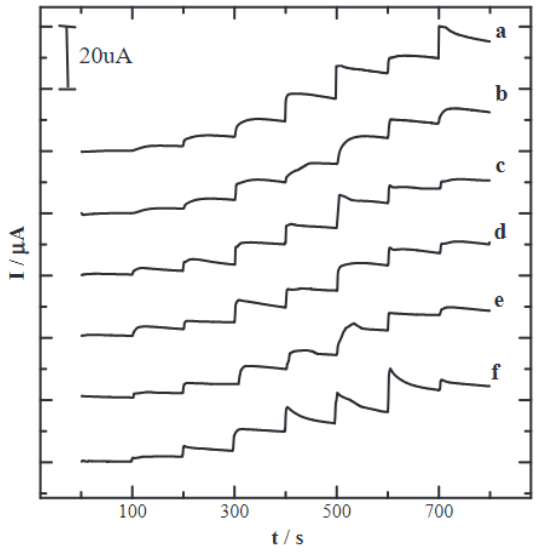

Figure 48: Spectra obtained from chronoamperometry experiments on uricase-modified ITO glass electrodes. As uric acid in solution increases, the current response of the electrode increases. Spectra a-f represent separate chronoamperometry experiments and show the reproducibility of data and reusability of the biosensor. Reprinted from This Solid Films, 519, Tarushee Ahuja, Rajesh, Devendra Kumar, Vinod Kumar Tanwar, Vikash Sharma, Nahar Singh, Ashok M. Biradar, An amperometric uric based biosensor based on Bis[sulfosuccinimidyl] suberate crosslinker /3-aminopropyltriethoxysilane surface modified ITO glass electrode, 1128-1134, Copyright (2010), with permission from Elsevier.[54]

Figure 49 is the calibration curve obtained from the chronoamperometric data comparing concentration of uric acid to current response of the electrode. The response of the modified electrode was found to be linear over the concentration range of 0.05 mM to 0.58 mM and the limit of detection of the device was determined to be 0.037 mM.

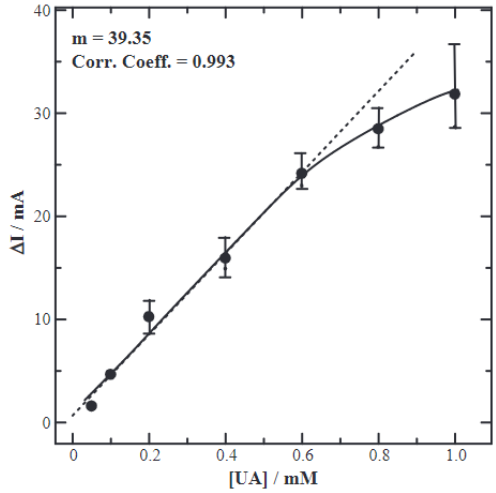

Figure 49: Calibration curve obtained from chronoamperometry spectra (Figure 48). Electrode response is linear for the concentration range of 0.05 mM to 0.58 mM and shows a detection limit of 0.037 mM uric acid. Reprinted from This Solid Films, 519, Tarushee Ahuja, Rajesh, Devendra Kumar, Vinod Kumar Tanwar, Vikash Sharma, Nahar Singh, Ashok M. Biradar, An amperometric uric based biosensor based on Bis[sulfosuccinimidyl] suberate crosslinker /3-aminopropyltriethoxysilane surface modified ITO glass electrode, 1128-1134, Copyright (2010), with permission from Elsevier.[54]

Ahuja *et al* successfully fabricated a uric acid biosensor by chemically attaching uricase enzymes to a modified ITO electrode. The biosensor shows analytical potential with a linear calibration curve for the concentration range of 0.05 mM to 0.58 mM uric acid and shows reusability in practice.

Kim *et al* used APTES modification of ITO slides to fabricate a sandwich type electrochemical immunoassay for the detection of vascular endothelial growth factors (VEGFs).[55] Figure 50 shows the VEGF biosensor fabrication process as well as the biosensing process of the fabricated VEGF biosensor followed by Kim. Kim first modified the ITO coated slides by hydroxylating the surface of the ITO slide. This was done by incubating the ITO slide in an aqueous solution containing H_2O_2 and NH_4OH. After hydroxylation, the slide was rinsed and incubated in a 2% APTES solution. After incubation in the 2% APTES solution, the slide was rinsed with copious amounts of

water. Gold nanoparticles were then immobilized onto the surface of the ITO electrode by incubating the ITO slide in a gold nanoparticle colloid solution (4.32 nM) for 2 hours. The films were then rinsed with water and ethanol several times. 40 μL of a 500 mg/mL solution of VEGF antibodies that had previously been chemically split was placed on the surface of the gold nanoparticle modified ITO slide for one hour, then the electrode was washed with copious amounts of water.

To begin the sensing of VEGF experiments, 50 μL of a solution with varying concentrations of VEGF was placed on the surface of the electrode and allowed to interact for half an hour. After washing the electrode after incubation in a VEGF solution, 50 μL of a ferrocene labeled VEGF antibody containing solution was placed on the surface of the electrode and allowed to interact for one hour. After one hour, the electrode was washed with copious water and DPV experiments were performed to monitor the redox current of the ferrocene attached to the sandwich immunoassay. DPV data were used to quantify VEGF in solution. Control experiments were conducted using ferrocene labeled platelet-derived growth factor (PDGF) antibodies instead of the ferrocene labeled VEGF antibodies, these antibodies are not expected to attach to the modified ITO electrode.

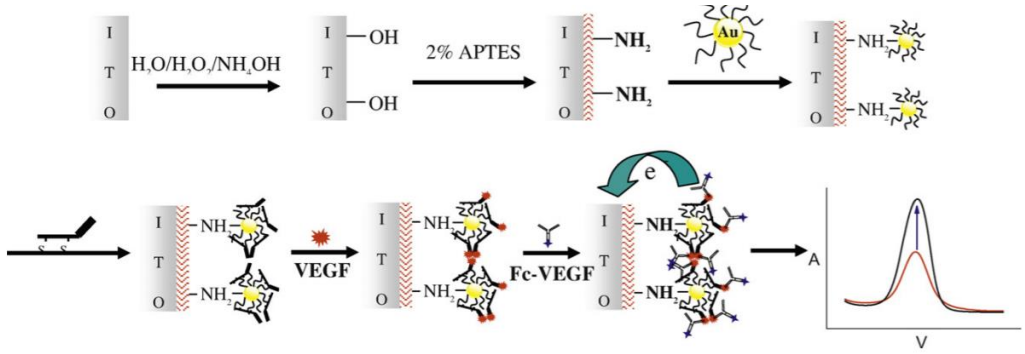

Figure 50: VEGF biosensor fabrication process as well as VEGF sensing process for the VEGF biosensor. Reprinted from Biosensors and Bioelectronics, 25, Gang-Il Kim, Kyung-Woo Kim, Min-Kyu Oh, Yun-Mo Sung, Electrochemical detection of vascular endothelial growth factors (VEGFs) usingVEGF antibody fragments modified Au NPs/ITO electrode, 1717-1722, Copyright (2010), with permission from Elsevier.

Figure 51 shows DVP measurements obtained from the fabricated sandwich immunoassay after being exposed to several concentrations of VEGF. DVP measurements show a linear relationship in which an increase in VEGF concentration results in an increase in current response of the electrode. Kim explains that the oxidation reaction occurring in the DPV measurements is that of the iron in ferrocene oxidizing from Fe (II) to Fe (III). It is inferred that with an increase in the number of ferrocene molecules on the electrode there is an increase in magnitude of the peak current associated with the oxidation of ferrocene. The increase in oxidation current with increasing VEGF concentration can be attributed to a greater presence of VEGF on the electrode when incubated in solutions with higher concentration VEGF, allowing for more ferrocene labeled antibodies that are able to bind to the electrode. This increase in binding ferrocene labeled antibodies resulted in an increase in current response of the electrode.

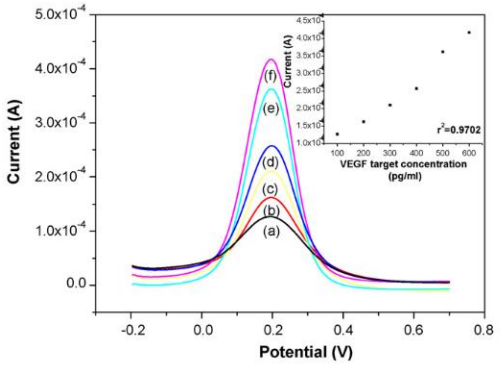

Figure 51: DPV measurements obtained from the sandwich immunoassay after incubation in (a) 100 pg/mL, (b) 200 pg/mL, (c) 300 pg/mL, (d) 400 pg/mL, (e) 500 pg/mL, and (f) 600 pg/mL VEGF solutions. Inset is a plot showing the linear relationship between the concentration of VEGF in solution to current response of the electrode. Reprinted from Biosensors and Bioelectronics, 25, Gang-Il Kim, Kyung-Woo Kim, Min-Kyu Oh, Yun-Mo Sung, Electrochemical detection of vascular endothelial growth factors (VEGFs) usingVEGF antibody fragments modified Au NPs/ITO electrode, 1717-1722, Copyright (2010), with permission from Elsevier.

Kim successfully fabricated a sandwich immunoassay electrode, using APTES modification of an ITO slide, to quantify VEGF proteins in solution. The immunoassay fabricated showed a linear relationship between oxidation current response in DPV measurements and concentration VEGF. The limit of detection of the electrode was calculated to be 100 pg/mL.

Electrochemical polymerization provides more information about an EAP film and presents an opportunity to characterize and perform several different electrochemical experiments on a polymer film adhered to an electrode. The change in oxidation and reduction potentials or current responses of the polymer film can be monitored using electrochemical methods such as CV and DPV. Changes in the anodic and cathodic processes of the polymer film can indicate a change in environment or structure of the EAP. Monitoring the change in the electrochemistry of the polymer film could prove to be an excellent transducing method for the detection of a biomolecule using an EAP based biosensor. In this thesis, electrochemical experiments will be conducted to grow a

conductive polymer film onto an electrode, to characterize the polymer film in several electrolyte solutions, and to provide a transduction method for the sensing of biomolecules using an aptamer functionalized EAP as a biosensor.

3.2 Experimental

3.2.1 Materials

Tetraethylammonium tetrafluoroborate ($TEABF_4$), was purchased from Alfa Aesar and recrystallized by dissolving in hot methanol and precipitating with diethyl ether; it was then collected by vacuum filtration and dried under vacuum overnight. TBAP was purchased from Fluka, recrystallized twice from hot ethanol and recovered by vacuum filtration and dried under vacuum overnight. Anhydrous acetonitrile (ACN) was used as received from Acros Organics. 10X Phosphate buffer saline (PBS) solution was purchased from SeraCare and diluted 10-fold to make a 1X concentration PBS solution (150 mM NaCl, 10 mM sodium phosphate, pH 7.4). Indium tin oxide (ITO) coated glass slides (CG-50IN-CUV (8-12 ohms resistance per square, 7x50x0.7mm)) were purchased from Delta Technologies, Ltd. and cleaned with deionized water, followed by 1M HCl solution, and finally followed by acetone. 1-Ethyl-3-(3-dimethylaminopropyl)-carbodiimide (EDC) and a 98% solution of (3-aminopropyl)triethoxysilane in ethanol were purchased from Alfa Aesar. 2-Thiophenecarboxylic acid (Th-COOH) was purchased from Acros Organics. N-Hydroxysuccinimide (NHS) was purchased from Thermo Scientific. Ethanol (EtOH) was purchased from Pharmco-Aaper. Tris(hydroxymethyl)aminomethane (tris) was purchased from Research Products International. Unless otherwise specified, all reagents were used as received.

3.2.2 Instruments

All CVs were acquired using a Pine WaveNow potentiostat equipped with Aftermath software. All CV experiments were conducted under argon. IR spectra were obtained using a Bruker Tensor II FTIR Spectrometer equipped with an Attenuated Total Reflectance (ATR) attachment. Contact angle measurements were taken using a Ramé-hart model 200-F1 goniometer equipped with DROPimage software.

3.2.3 Electrochemical Procedures

3.2.3.1 Electrochemical Polymerization of ProDOT(CH_2N_3)$_2$ in ACN with TBAP Electrolyte

Electrochemical polymerization of 0.01 M ProDOT(CH_2N_3)$_2$ was carried out in a 0.1 M TBAP solution in ACN to compare the electrochemistry to that found in the literature.[45] A platinum flag was used as the counter electrode, and a Ag/AgCl electrode was used as a reference electrode. The polymer film was grown using a voltage range of -0.3 V to 1.8 V at a scan rate of 100 mV/s. The polymer film was grown over 10 cycles.

The polymer film was rinsed with monomer free electrolyte solution and a cyclic voltammogram was taken of the polymer film in monomer free electrolyte solution to record the oxidation and reduction potentials of the polymer film. The CV was performed over a voltage range of -0.2 V to 0.75 V at a scan rate of 100 mV/s over 10 cycles. The third cycle of the voltammogram was used to record oxidation and reduction values of the polymer film.

An IR spectrum was obtained from the resulting polymer slide using the ATR attachment for the spectrophotometer to ensure the presence of the azide groups on the

polymer film.

3.2.3.2 Electrochemical Polymerization of ProDOT(CH_2N_3)$_2$ in ACN with $TEABF_4$ Electrolyte

Electrochemical polymerization of 0.01M ProDOT(CH_2N_3)$_2$ was carried out in a 0.1 M $TEABF_4$ solution in ACN. A platinum flag was used as the counter electrode, and a Ag/AgCl electrode was used as the reference electrode. The polymer was grown at a voltage range of -0.75 V to 2 V at a scan rate of 100 mV/s over 10 full cycles.

A cyclic voltammogram was then taken of the polymer film in monomer free electrolyte solution to record the oxidation and reduction potentials of the polymer film. The CV was performed over a voltage range of -0.5 V to 1.5 V at a scan rate of 100 mV/s over two cycles. The second cycle of the voltammogram was used to record oxidation and reduction values of the polymer film.

3.2.3.3 Electrochemical Polymerization of ProDOT(CH_2N_3)$_2$ in 1:1 H_2O:ACN with $TEABF_4$ Electrolyte

Electrochemical polymerization of 0.01M ProDOT(CH_2N_3)$_2$ was carried out in a 0.1 M $TEABF_4$ solution in 1:1 H_2O:ACN. A platinum flag was used as the counter electrode, and a Ag/AgCl electrode was used as the reference electrode. The polymer was grown at a voltage range of -0.5 V to 2 V at a scan rate of 100 mV/s over 50 full cycles.

A cyclic voltammogram was then taken of the polymer film in monomer free electrolyte solution to record the oxidation and reduction potentials of the polymer film. The CV was performed over a voltage range of -0.4 V to 1.4 V at a scan rate of 100 mV/s

over 10 cycles. The second cycle of the voltammogram was used to record oxidation and reduction values of the polymer film.

3.2.3.4 Electrochemical Polymerization of ProDOT(CH_2N_3)$_2$ in 1:1 2XPBS:ACN

Electrochemical polymerization of 0.01 M ProDOT(CH_2N_3)$_2$ was carried out in a solution with 1:1 v/v ACN:2XPBS as solvent. A platinum flag was used as the counter electrode and a Ag/AgCl electrode was used as the reference electrode. The attempt at polymer growth was carried out over 2 cycles at a voltage range of -0.5 V to 1.3 V at a scan rate of 100 mV/s.

3.2.3.5 Aqueous Electrochemistry of PProDOT(CH_2N_3)$_2$ Before Aptamer Functionalization with $TEABF_4$ Electrolyte

A polymer film of PProDOT(CH_2N_3)$_2$ that had been polymerized in a solvent system of 1:1 ACN:H_2O was placed in a 0.1M $TEABF_4$ solution in H_2O and cycled 50 times at a voltage range of -0.5 V to 1.8 V at a scan rate of 100 mV/s.

3.2.3.6 Aqueous Electrochemistry of PProDOT(CH_2N_3)$_2$ in PBS Buffer Before Aptamer Attachment

A polymer film of PProDOT(CH_2N_3)$_2$ that had been polymerized in a solvent system of 1:1 ACN:H_2O with 0.1 M $TEABF_4$ as an electrolyte was placed in 1XPBS solution and was cycled 50 times at a voltage range of -0.5 V to 2 V at a scan rate of 100

mV/s.

3.2.3.7 Electrochemistry of PProDOT(CH_2N_3)$_2$ Film when Gradually Changing Aqueous Character of Electrochemical Solvent

A polymer film of PProDOT(CH_2N_3)$_2$ that was grown in a solvent system of 1:1 ACN:H_2O with $TEABF_4$ as an electrolyte was placed in monomer free solution with 1:1 ACN:H_2O as solvent and 0.1 M $TEABF_4$ as electrolyte and cycled 10 times at a voltage range of -0.5 V to 1.4 V using a scan rate of 100 mV/s. After 10 cycles, the polymer film was removed from the solution and 1 mL of 1XPBS was added to the electrochemical solution, increasing the aqueous character of the solution. After thorough mixing of the solution, the polymer film was then reintroduced to the electrochemical solution and cycled 10 times at a voltage range of -0.5 V to 1.4 V at a scan rate of 100 mV/s. This process was repeated 13 times until the film was finally introduced to a solution of just 1XPBS (150 mM NaCl, 10 mM sodium phosphate, pH 7.4) and cycled 10 times at a voltage range of -0.5 V to 1.4 V with a scan rate of 100 mV/s.

3.2.3.8 Surface Modification of ITO-Coated Conductive Glass Slides

Chemical modification of the surface of the ITO-coated glass slides was performed in an attempt to prevent delamination of the polymer films from the slides. First, the aminosilane APTES was used to functionalize the ITO surface with primary amine groups through silanization. Then, the amine-functionalized surface was used as a covalent anchor for Th-COOH via EDC/NHS chemistry. Finally, the anchored Th-COOH

was electrochemically co-polymerized with ProDOT(CH_2N_3)$_2$ to result in immobilized PProDOT(CH_2N_3)$_2$.

Protocols published from Thermo Scientific were modified for the immobilization of APTES onto the ITO-coated glass slides.[56] A 2% APTES solution in EtOH was prepared by diluting 408 µL of 98% APTES in EtOH to a total volume of 20 mL. 100 µL of the 2% APTES solution in EtOH was pipetted onto the surface of the ITO-coated slide and allowed to react for 10 minutes. After 10 minutes, the glass slide was rinsed several times with EtOH and dried under argon flow. For the EDC/NHS coupling reaction, 100 µL of a 0.1 M Th-COOH solution containing 30 mg/mL NHS, 25 mg/mL EDC was pipetted onto the surface of the APTES-modified ITO surface and allowed to react for one hour. After one hour, the slide was rinsed several times with water and dried under argon flow. IR spectra and contact angle measurements of the surface of the ITO-coated slide were taken before and after each surface modification reaction. For contact angle measurements, 5 µL of liquid was pipetted onto the surface of a material, and the angle between the surface of the material and the liquid/vapor interface was measured. This contact angle can be telling of the favorable or unfavorable interactions between the surface of the substrate and the liquid.[57] In this case, water was the liquid used for contact angle measurements and the relative hydrophobicity or hydrophilicity of the surface was determined from these contact angle measurements.

3.2.3.9 Polymerization of ProDOT(CH_2N_3)$_2$ onto the Modified ITO-Coated Slide

Electrochemical polymerization of 0.01 M ProDOT(CH_2N_3)$_2$ was carried out in a solution containing 0.1 M $TEABF_4$ in ACN at a scan rate of 100 mV/s. The polymer film was grown over 5 cycles at a voltage range of 0.5 V to 2 V. A platinum flag was used as the counter electrode, a Ag/AgCl electrode was used as the reference electrode, and the chemically modified ITO coated glass electrode was used as the working electrode.

3.2.3.10 Electrochemistry of the PProDOT(CH_2N_3)$_2$ Film Attached to the Chemically Modified ITO Slide in Various Solvent Systems

SRD dependence experiments were carried out in several solutions on the polymer film obtained from section 3.2.3.9 of this thesis. The polymer film was placed in a 0.1 M $TEABF_4$ solution in ACN and cycled from 0.5 V to 1.2 V for the scan rates of 50 mV/s, 100 mV/s, and 200 mV/s, and then cycled from 0.5 V to 1.3 V for the scan rates of 300 mV/s and 400 mV/s. These SRD experiments were also carried out on the same polymer film in a solution containing 0.1 M $TEABF_4$ in 1:1 ACN:H_2O, and a solution containing 0.1 M $TEABF_4$ in H_2O. The same polymer film was then stored overnight in a 0.1 M tris-HCl solution, and SRD experiments were performed the next day in a 0.1 M tris-HCl solution at a pH of 7.4.

3.3 Results and Discussion

3.3.1 Electrochemical Polymerization of ProDOT(CH_2N_3)$_2$ in ACN with TBAP Electrolyte

Figure 52 shows the polymerization of PProDOT(CH_2N_3)$_2$ in a TBAP electrolyte solution. Godeau *et al.* reported that monomer oxidation occurs at 1.67 V versus a saturated calomel electrode (SCE).[45] An SCE electrode is +0.24 V relative to a standard hydrogen electrode (SHE), and a Ag/AgCl reference electrode is +0.22 V relative to a SHE electrode.[58] The difference between an SCE electrode and a Ag/AgCl electrode is thus calculated to be 0.02 V. With this calculated difference in potential for the different reference electrodes, the expected monomer oxidation value is 1.65 V vs. Ag/AgCl. The actual observed oxidation of the monomer occurred at around 1.45 V vs. Ag/AgCl. Several factors can change the electrochemistry of a polymer, including the surface area of the working electrode, the solvent, and the electrolyte used. Godeau reported the monomer oxidation using gold wafers as the working electrode, while the experiments reported herein utilized a gold button as the working electrode. This difference in working electrode surface area could account for the differences in oxidation potentials of the ProDOT(CH_2N_3)$_2$ monomer and pProDOT(CH_2N_3)$_2$ films.

Figure 93 in the appendix section of this thesis shows the voltammogram obtained from the polymer film in monomer free electrolyte solution at a scan rate of 100 mV/s. The oxidation and reduction potentials of the polymer film taken from Figure 93 are 0.57 V and 0.41 V respectively. These values are recorded in Table 2 of this thesis.

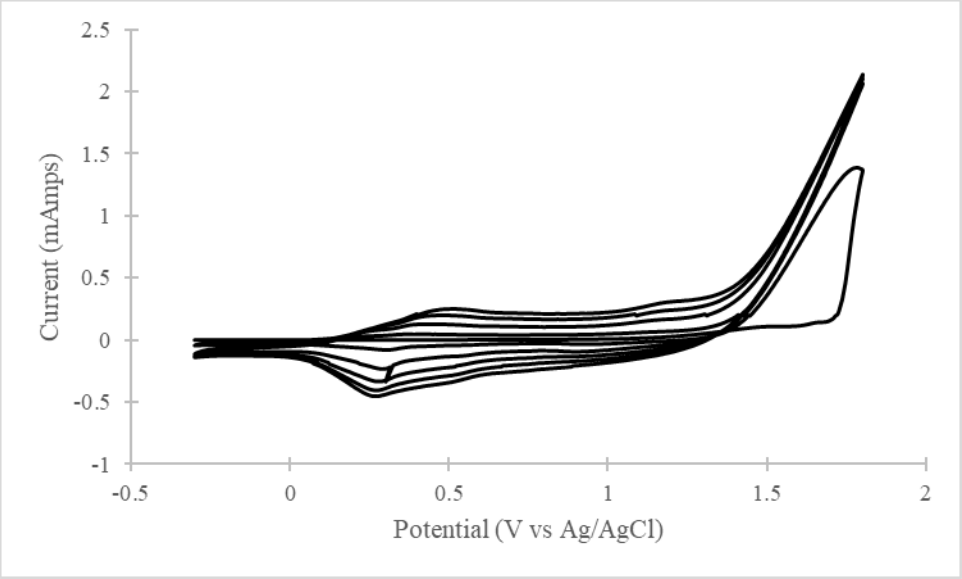

Figure 52: Cyclic voltammogram for the electrochemical polymerization of ProDOT(CH_2N_3)$_2$ in a solution containing 0.01 M ProDOT(CH_2N_3)$_2$ and 0.1 M TBAP in ACN. The polymer film was grown over 10 cycles.

Figure 53 shows the IR spectrum obtained from the pProDOT(CH_2N_3)$_2$ film grown on an ITO-coated glass slide. The peak present at approximately 2100 cm^{-1} indicates the presence of azide groups on the polymer film.

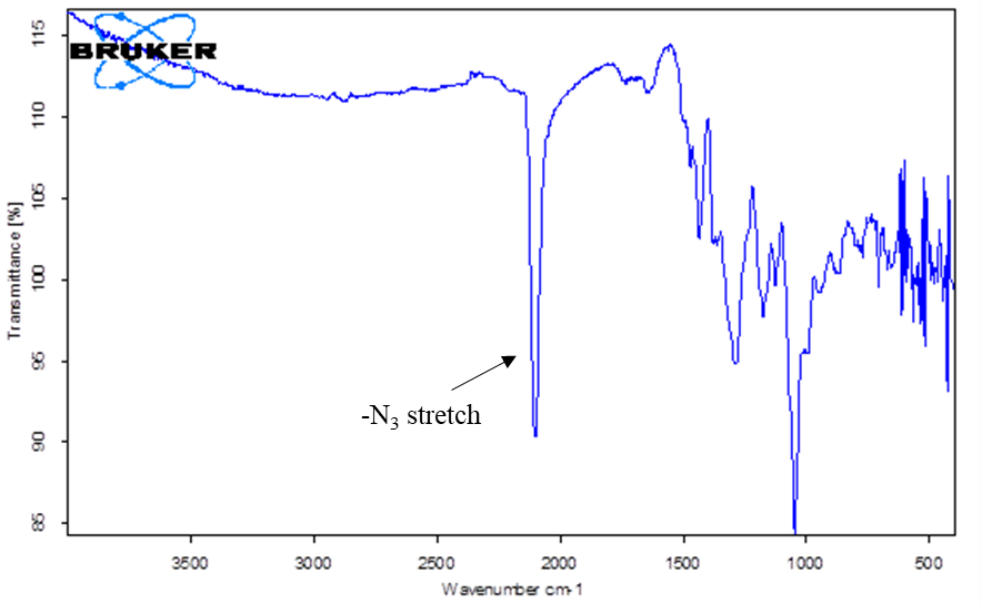

Figure 53: IR spectrum of a PProDOT(CH_2N_3)$_2$ film grown in a solution of 0.01 M ProDOT(CH_2N_3)$_2$ containing 0.1 M TBAP in ACN. The IR shows a peak at ~ 2100 cm^{-1} corresponding to the -N_3 stretch of an azide group.

3.3.2 Electrochemical Polymerization of ProDOT(CH_2N_3)$_2$ in ACN with $TEABF_4$ Electrolyte

Figure 54 shows the voltammogram of the electrochemical polymerization of ProDOT(CH_2N_3)$_2$ in ACN with 0.1M $TEABF_4$ as the electrolyte. Figure A1 in the appendix section of this thesis shows the voltammogram obtained from the polymer film in monomer free electrolyte solution at a scan rate of 100 mV/s. The oxidation and reduction potentials of the polymer film taken from Figure 94 are 1.13 V and 0.28 V respectively. These values are recorded in Table 2 of this thesis.

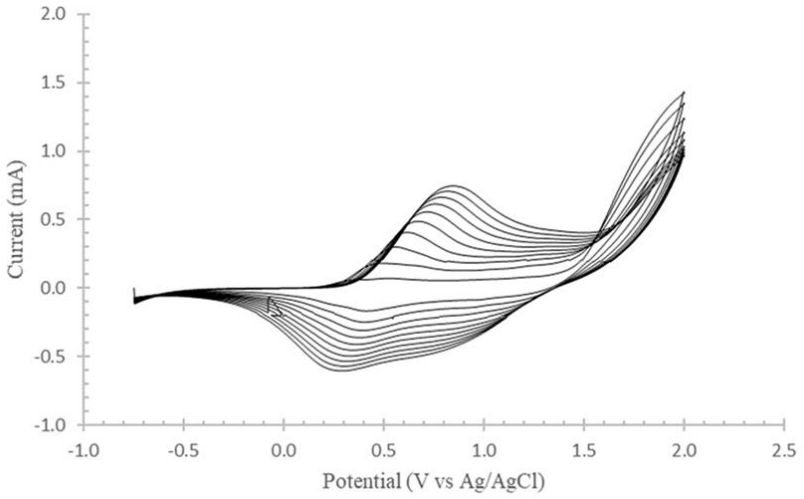

Figure 54: Cyclic voltammogram of the electrochemical polymerization of 0.01 M ProDOT(CH_2N_3)$_2$ in 0.1 M $TEABF_4$ in an ACN solution. PProDOT(CH_2N_3)$_2$ film was grown over 10 cycles.

3.3.3 Electrochemical Polymerization of ProDOT(CH_2N_3)$_2$ in 1:1 ACN:H_2O with $TEABF_4$ Electrolyte

Figure 55 shows the voltammogram obtained during the electrochemical polymerization of ProDOT(CH_2N_3)$_2$ in 1:1 ACN:H_2O with 0.1M $TEABF_4$ as an electrolyte. The electrochemical solvent system was changed because PProDOT(CH_2N_3)$_2$ films grown in ACN partially delaminated from the ITO slide during aqueous CV

experiments. Because of the limited solubility of the monomer and electrolyte in the solvent system of 1:1 ACN:H_2O, it was necessary to grow the polymer over 50 cycles in order to deposit a considerable thickness of the polymer onto the ITO slide.

Figure A2 in the appendix section of this thesis shows the voltammogram obtained from the polymer film in monomer free electrolyte solution at a scan rate of 100 mV/s. The oxidation and reduction potentials of the polymer film taken from Figure A2 are 0.98 V and 0.32 V respectively. These values are recorded in Table 2 of this thesis.

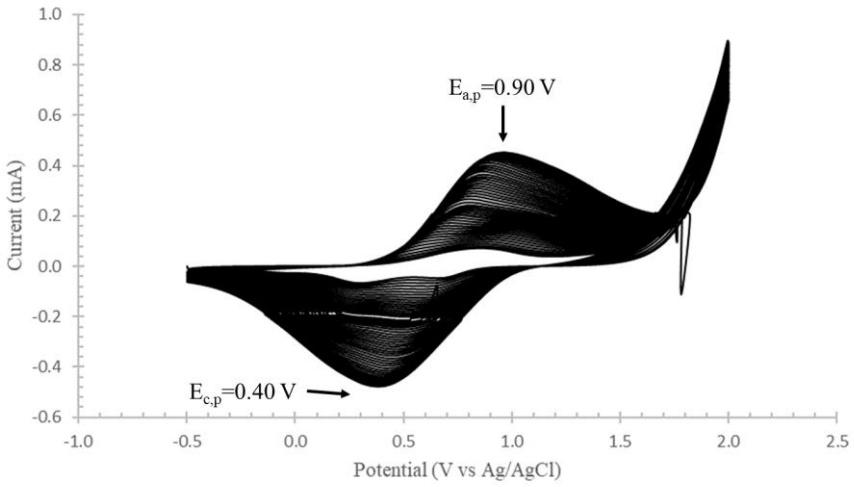

Figure 55: Cyclic voltammogram of the electrochemical polymerization of 0.01 M ProDOT(CH_2N_3)$_2$ in a 0.1 M $TEABF_4$ solution with a solvent system of 1:1 H_2O:ACN. PProDOT(CH_2N_3)$_2$ film was grown over 50 cycles.

3.3.4 Electrochemical Polymerization of ProDOT(CH_2N_3)$_2$ in 1:1 2XPBS:ACN With PBS Electrolyte

Figure 56 shows the voltammograms obtained when the polymerization of ProDOT(CH_2N_3)$_2$ was attempted using the salt components in PBS as electrolyte. No monomer oxidation, polymer oxidation, or polymer reduction can be seen. The attempt to polymerize ProDOT(CH_2N_3)$_2$ using the salts in PBS as an electrolyte was unsuccessful.

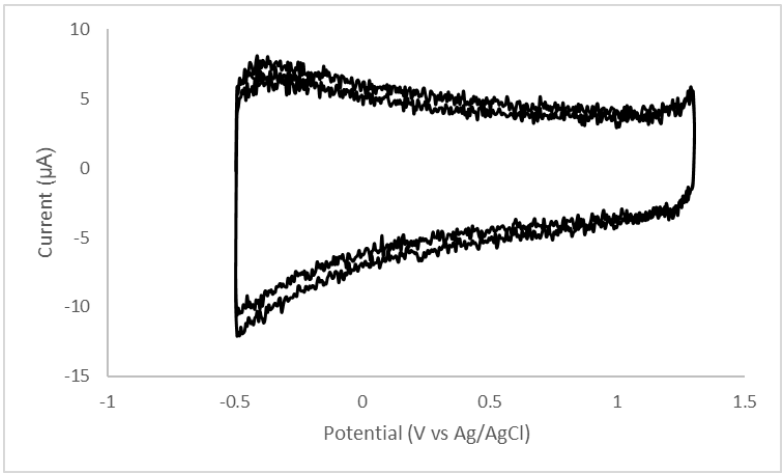

Figure 56: Cyclic voltammogram of the attempt of polymerization of ProDOT(CH_2N_3)$_2$ using a solution of 1:1 2XPBS:ACN containing 0.01 M ProDOT(CH_2N_3)$_2$. No peaks can be seen that attribute to monomer oxidation, polymer oxidation, or polymer reduction.

3.3.5 Aqueous Electrochemistry in H_2O with $TEABF_4$ Electrolyte Before Aptamer Attachment

In order to prevent undesired changes in the configuration of the aptamer during electrochemical target detection, the detection of adenosine must be conducted in an aqueous solution. To understand the aqueous electrochemistry of the aptamer-functionalized EAP before and after the detection of adenosine, it is necessary to understand the aqueous electrochemistry of the polymer before the attachment of the aptamer. Figure 57 shows the voltammogram obtained for the aqueous electrochemistry of a PProDOT(CH_2N_3)$_2$ film grown in 1:1 ACN:H_2O with $TEABF_4$ electrolyte. The current response of the oxidation and reduction of the polymer are dramatically decreased and are not well defined when compared to the current response in the voltammogram obtained during the electrochemical polymerization process (Figure 55). It is believed that the change in solvent system from 1:1 ACN:H_2O to H_2O is responsible for the decrease in current response of the polymer film. The hydrophobic film constricts in an aqueous electrolyte solution, preventing ion movement into and out of the film. In this

case, only the surface of the polymer film is electroactive.

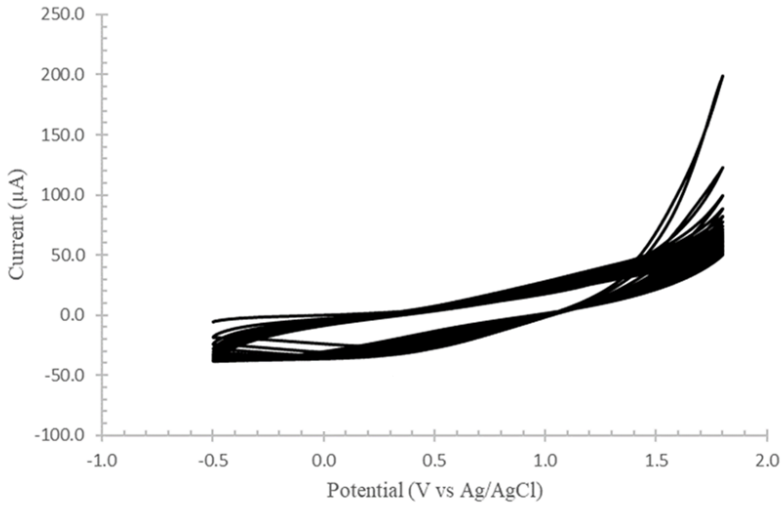

Figure 57:Cyclic voltammogram of the aqueous electrochemistry of a PProDOT(CH_2N_3)$_2$ film (film was grown in a 1:1 ACN:H_2O 0.1 $TEABF_4$ solution) in 0.1M $TEABF_4$ in H_2O.

3.3.6 Aqueous Electrochemistry in PBS Solution Before Aptamer Attachment

Figure 58 shows the voltammogram obtained from the aqueous electrochemistry of a PProDOT(CH_2N_3)$_2$ film (polymerized in 1:1 ACN:H_2O with $TEABF_4$ as the electrolyte) in a 1XPBS solution. PBS is a buffer solution that is compatible with the adenosine-specific aptamer and for the electrochemical detection of adenosine. No polymer oxidation or reduction peaks can be seen in the voltammogram, only oxidation of the PBS solution. Figure 93 shows a cyclic voltammogram of 1XPBS solution and is located in the appendix section of this thesis. It is likely that the change in solvent and electrolyte used between the polymerization solution and the aqueous electrochemistry solution is the reason why no polymer oxidation and reduction peaks can be seen. Hillman *et al.* studied how changing the solvent used during the polymerization process can lead to dramatic changes in film behavior of the same polymer.[59] Both ion transport and ease of movement of the polymer chains depend on the solvation of the polymer film

and the compatibility between the polymer film and the solvent; Hillman has referred to these changes in polymer and ion transport dynamics as "reconfiguration" processes.[60] Positive interactions between a polymer film and solvent will allow the film to swell (thereby increasing its radius of gyration), while negative interactions between the film and solvent will cause the polymer film to constrict. Switching a polymer film made in one solvent to a solvent in which the polymer is much less compatible can cause a dramatic change in electroactivity. When a polymer film is in a highly compatible solvent, ion transport is more "liquid-like" while ion transport for a polymer that is in a much less compatible solvent is more "solid state-like".[59] During the polymerization process, voids are created in the polymer film to accommodate the movement of tetrafluoroborate ions into the film. When the film is switched from a solution in which the polymer is more compatible with the solvent into a solution in which the polymer is less compatible with the solvent, the film becomes more rigid and polymer chains are not as easily moved to create voids for anion intercalation; this is described as more "solid state-like". Because of the change of solvent and in physical properties of the polymer film, the ions cannot freely move from the electrolyte solution into the polymer film. Ion transport into and out of the polymer matrix is crucial for electrochemical polymerization and electroactivity in an EAP film by CV.[61] If ions are not able to transport in and out of the polymer film, the film will not be electroactive. Electrochemical polymerization of ProDOT(CH_2N_3)$_2$ in a more aqueous solvent system (1:1 ACN:H_2O) using NaCl as the electrolyte could solve this problem and result in better data for aqueous electrochemistry of the polymer slide in 1XPBS solution.

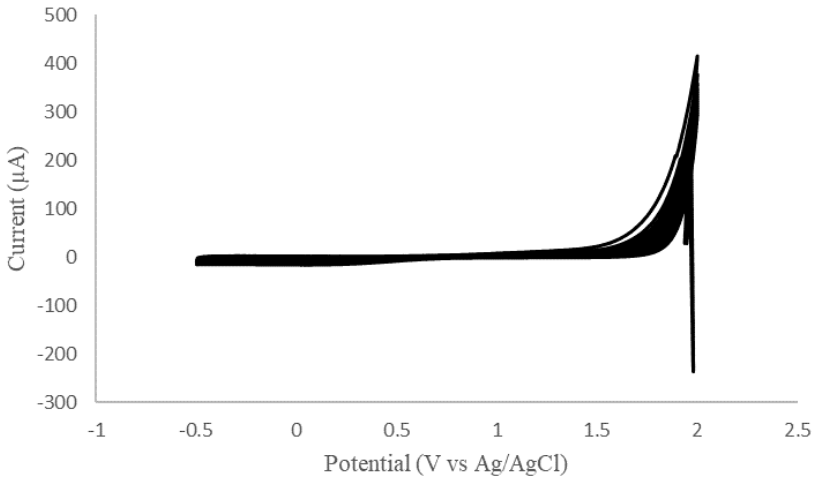

Figure 58: Cyclic voltammogram obtained from the aqueous electrochemistry of a polymer film of PProDOT(CH_2N_3)$_2$ (polymerized in 1:1 ACN:H_2O with $TEABF_4$ as an electrolyte) in 1X PBS solution.

3.3.7 Electrochemistry of PProDOT(CH_2N_3)$_2$ Film when Gradually Changing Aqueous Character of Electrochemical Solvent

Figure 59 shows an overlay of several cyclic voltammograms obtained when increasing the aqueous character of the electrochemical solution. It can be seen that when approximately 11 mL of 1X PBS is added to the electrochemical solution, the oxidation of the polymer film is difficult and almost impossible to see. Therefore, this method of gradually increasing the aqueous character of the electrochemical solution did not improve the polymer film's compatibility with the PBS solution. Table 1 shows the electrolyte concentrations for each solution during this process as well as the aqueous percent.

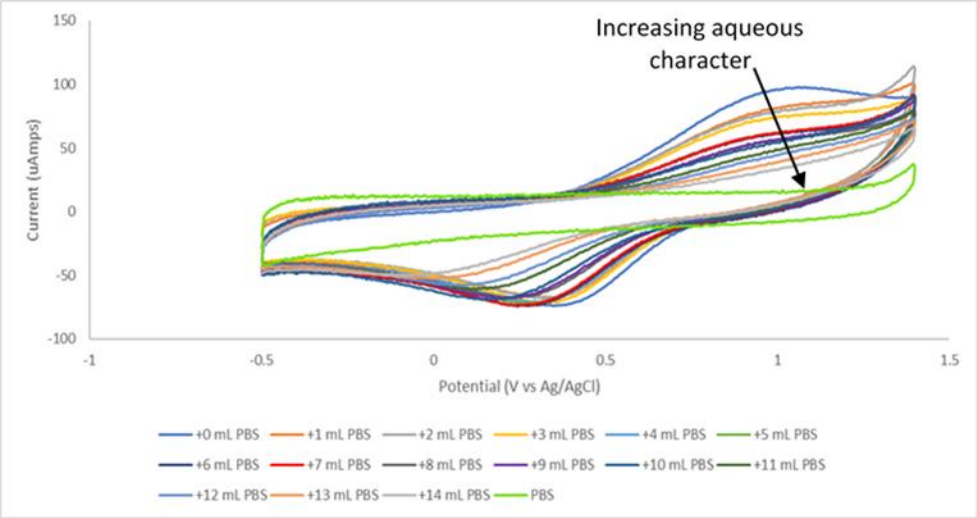

Figure 59: Overlay of cyclic voltammograms obtained from PProDOT(CH_2N_3)$_2$ film (polymerized in 1:1 ACN:H_2O with $TEABF_4$ as an electrolyte) when the aqueous character of the electrochemical solution was gradually increased

Table 1: Electrolyte concentrations and aqueous percent of electrochemical solutions used while increasing the aqueous character of the solution. Refer to figure 59 to see cyclic voltammograms.

Solution	Concentration $TEABF_4$	Concentration NaCl	Aqueous %
+0 mL PBS	0.1 M	0 M	50 %
+1 mL PBS	0.083 M	0.025 M	58.33 %
+2 mL PBS	0.0714 M	0.0428 M	64.29 %
+3 mL PBS	0.0625 M	0.05625 M	68.75 %
+4 mL PBS	0.055 M	0.067 M	72.22 %
+5 mL PBS	0.05 M	0.075 M	75 %
+6 mL PBS	0.045 M	0.0818 M	77.27 %
+7 mL PBS	0.0416 M	0.0875 M	79.16 %
+8 mL PBS	0.0385 M	0.0923 M	80.77 %
+9 mL PBS	0.0357 M	0.0964 M	82.14 %
+10 mL PBS	0.033 M	0.1 M	83.33 %
+11 mL PBS	0.03125 M	0.103 M	84.37 %
+12 mL PBS	0.0294 M	0.1059 M	85.29 %
+13 mL PBS	0.0278 M	0.1083 M	86.11 %
+14 mL PBS	0.026 M	0.1105 M	86.84 %
PBS	0 M	0.15 M	100 %

Gradual increase in aqueous character was not sufficient to enable PProDOT(CH_2N_3)$_2$ films produced in 1:1 ACN:H_2O to be analyzed through aqueous

electrochemistry. To try to resolve this, surface modification of the ITO coated slides was attempted to promote adhesion of the polymer film to the electrode and to obtain aqueous electrochemistry of the polymer slide.

3.3.8 Surface Modification of ITO Coated Conductive Glass Slides

Figure 60 illustrates the approach used for the modification of the surface of the conductive glass slides.

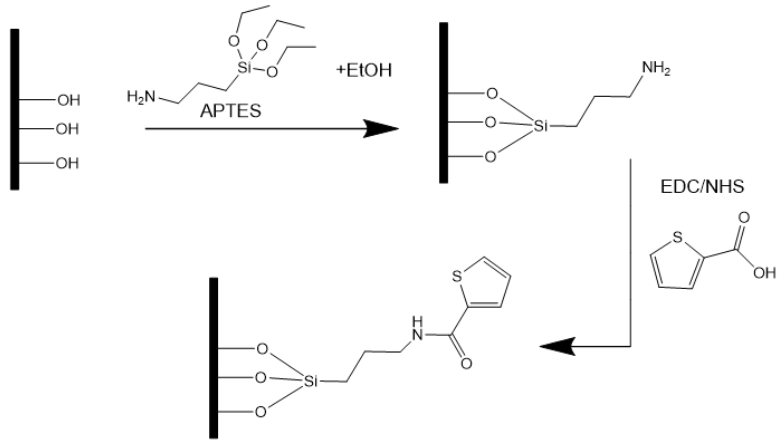

Figure 60: Surface modification of an ITO-coated glass slide

The surface modification of the ITO-coated glass slides was attempted using a two-step synthesis process starting with the immobilization of (3-aminopropyl)triethoxysilane (APTES) onto the surface of the electrode followed by the formation of an amide bond via 1-ethyl-3-(3-dimethylaminopropyl) carbodiimide (EDC) / N-hydroxysuccinimide (NHS) coupling reaction with 2-thiophenecarboxylic acid (Th-COOH). This thienyl amide (ThAm) surface modified ITO slide could then be used as a working electrode during the electrochemical polymerization process of ProDOT(CH_2N_3)$_2$. ProDOT(CH_2N_3)$_2$ monomers were expected to electrochemically

polymerize with the thiophene groups off of the surface modified ITO slide, creating a chemical bond between the polymer film and the ITO-coated glass slide.

Changes in contact angle are often used as evidence of changes in surface chemistry.[62] Figure 61 shows contact angle measurements of water on the conductive surface of the ITO coated slide at different points during the chemical modification process.

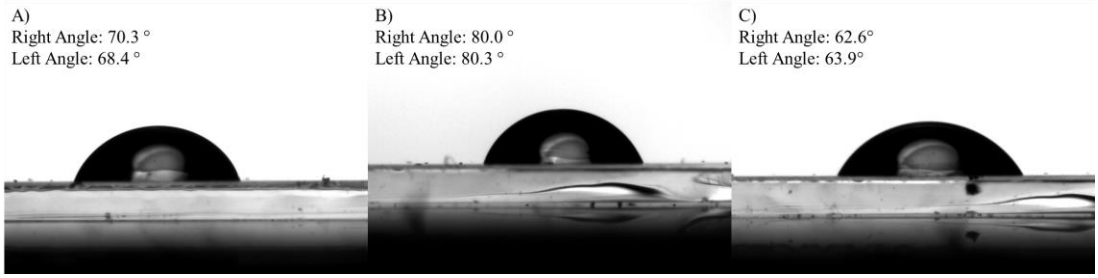

Figure 61: Contact angle measurements obtained from A) unmodified, bare ITO glass, B) after the modification of the ITO surface with APTES, and C) after EDC/NHS coupling with Th-COOH to form an amide linkage.

The larger the contact angle, the less the liquid spreads out and interacts with the surface. When water is used as the liquid, the larger the contact angle, the more hydrophobic the surface. From the modification of the ITO coated slide with APTES, the average contact angle increased from 69.4° to 80.2°, indicating an increase in hydrophobicity of the surface of the glass slide. Modifying the surface of the ITO coated slide with APTES molecules changes the chemical groups on the surface of the slide from hydroxyl groups to amine groups. The hydroxyl group is more polar and hydrophilic than the amine group, causing a greater contact angle on the surface of the glass slide after the modification with APTES. After the EDC/NHS coupling of Th-COOH to the surface of the slide, the average contact angle decreases from 80.2° to 63.3° and there is an increase in hydrophilicity of the surface of the glass slide. With the

EDC/NHS coupling, the functional groups on the surface of the glass slide change from amine groups to organic thiophene group. The thienyl group is an organic substituent and much less polar than the amine group; the contact angle of water on the surface of the ThAm modified ITO slide is expected to increase because of the unfavorable interactions between organic groups like thiophene and water. The unexpected decrease in contact angle could be attributed to the reaction conditions of the EDC/NHS coupling reaction. The coupling reaction takes place in water, and the slide is rinsed with water before taking contact angle measurements of the surface. The water on the slide may not have dried completely and effected the contact angle measurements taken.

Infrared spectroscopy is expected to provide additional insight into chemical changes occurring at the surface of ITO coated slides during surface modification experiments. Figure 62 shows stacked IR spectra obtained during different stages of the surface modification of ITO experiments. The peak intensities in the IR spectra collected is extremely low and crucial absorptions could be skewed by the noise of the spectra because of this. A spectrum with similar intensities to that of the bare ITO slide using the ATR attachment was obtained when using the spectrophotometer in transmittance mode without the ATR attachment. Figure 94 in the appendix section of this thesis compares IR spectra obtained using an ATR attachment of a glass microscope slide, a boroaluminosilicate glass slide, and an ITO-coated glass slide. It can be seen that the intensities of the peaks in the IR spectrum of the ITO coated slide are drastically lower than those of the other glass surfaces. This lack in significant intensities of IR absorption could be due to the fact that only the surface of the ITO slide participates in functionalization. The surface of the slide is just a small fraction of the ITO slide, and as

only a small fraction of the slide participates in modification, it can be difficult to monitor change in the surface chemistry of the slide if only a small fraction of the slide has changed.

For an ATR attachment, good, consistent contact between the ATR crystal and the surface of the ITO slide to obtain significant IR absorption peaks. If the surface of the ITO slide is rough, contact between the ATR crystal and the ITO slide can affect the IR spectrum obtained. This exceptionally low IR absorption peaks may be due to poor contact between the ITO slide and the ATR crystal.

Because of the small peak intensities of the IR spectra obtained, small concentrations of new functional groups on the surface of the ITO slide could not be detected and ITO surface modification could not be confirmed by IR spectroscopy.

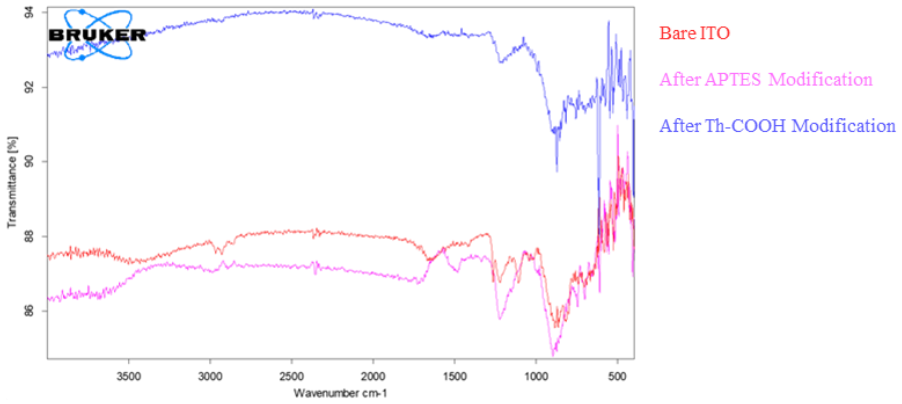

Figure 62: Stacked IR spectra obtained during the modification of the surface of ITO coated conductive glass slides

ThAm modification of ITO slides cannot be confirmed by IR spectroscopy. Given the results from contact angle measurements it can be seen that the surface of the ITO slide is changing with each step of modification. The resulting ThAm modified ITO slide was further used for electrochemical experiments to determine if the surface modification improved the adhesion of PProDOT(CH_2N_3)$_2$ films to ITO coated glass slides.

3.3.9 Polymerization of ProDOT(CH_2N_3)$_2$ onto the ThAm Modified ITO Surface Coated Slide

Figure 63 shows the CV obtained from the polymerization of ProDOT(CH_2N_3)$_2$ onto the ThAm modified ITO coated slide using a solution containing 0.01 M ProDOT(CH_2N_3)$_2$ and 0.1 M $TEABF_4$ in ACN. The polymer film was successfully grown over 5 cycles at a scan rate of 100 mV/s over the voltage range of -0.5 V to 2 V. The onset of monomer oxidation occurs at approximately 1.57 V relative to Ag/AgCl, this is comparable to the onset of monomer oxidation when polymerizing ProDOT(CH_2N_3)$_2$ onto unmodified ITO slides ($E_{on,\ m}$= 1.48 V).

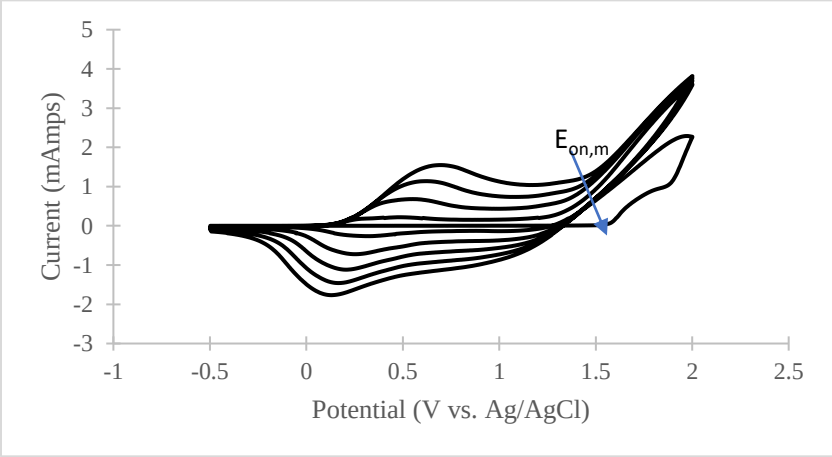

Figure 63: CV obtained from the polymerization of ProDOT(CH_2N_3)$_2$ onto the ThAm -modified ITO slide.

3.3.10 Electrochemistry of the PProDOT(CH_2N_3)$_2$ film Attached to the ThAm Modified ITO Slide in Various Solvent Systems

Figure 64 shows an overlay of the CVs obtained at various scan rates (A)as well as a linear plot of scan rate versus peak current response (B) for the polymer film in a 0.1 M $TEABF_4$ solution in can. The linearity of the plot and the R^2 values suggest that the

polymer film is well adhered to the slide in this solution.

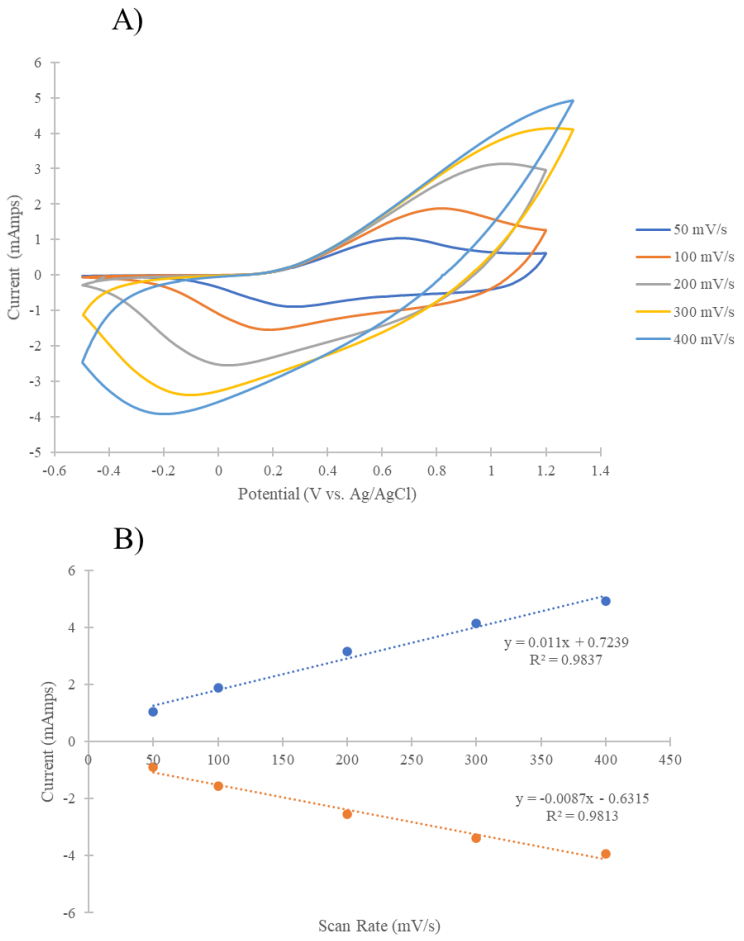

Figure 64: A) CVs obtained from the PProDOT(CH_2N_3)$_2$ film polymerized onto the ThAm-modified ITO slide in 0.1 M TEABF$_4$ in ACN and B) linear plots of scan rate versus peak current response for the oxidation and reduction of the polymer film reveal that the polymer film is well adhered to the surface of the slide.

The same film used to produce the voltammograms in Figure 64 was then transferred to an electrochemical solution containing 0.1 M TEABF$_4$ in 1:1 ACN:H_2O and SRD CV experiments were repeated in this solution. Figure 65 shows an overlay of the CVs obtained at various scan rates (A)as well as a linear plot of scan rate versus peak current response (B) for the polymer film in 0.1 M TEABF$_4$ in 1:1 H_2O:ACN to determine if the polymer film is well adhered to the glass slide. The linearity of the plot

and the R^2 value suggest that the polymer film is well adhered to the slide in this solution.

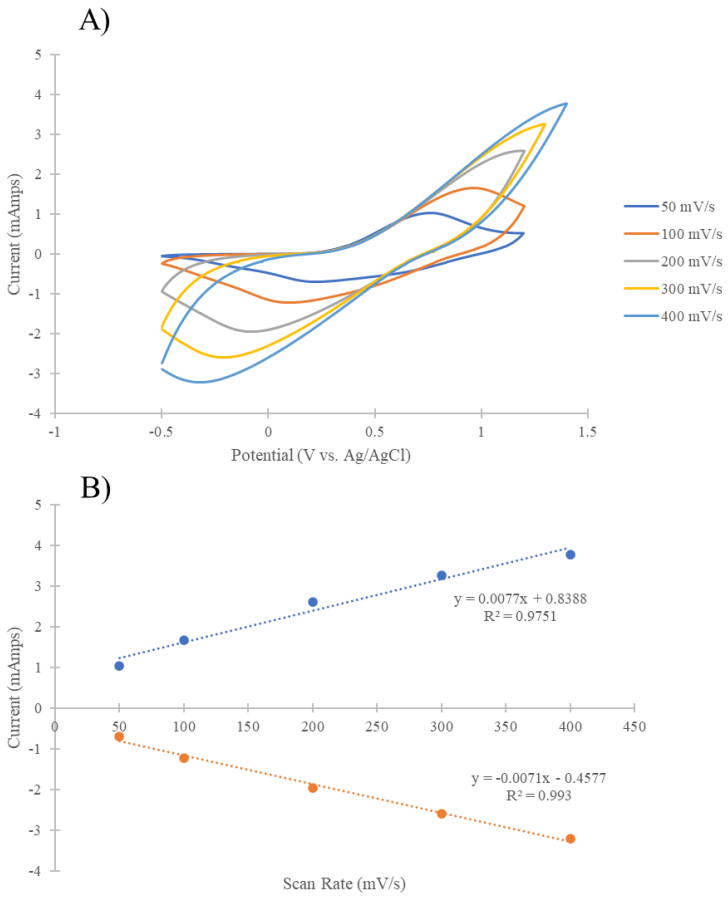

Figure 65: A) CVs obtained from the PProDOT(CH_2N_3)$_2$ film polymerized onto the ThAm -modified ITO slide in 0.1 M $TEABF_4$ in 1:1 H_2O:can and B) linear plot of scan rate versus peak current response for the oxidation and reduction of the polymer film indicates that the polymer film is well adhered to the surface of the slide.

The same film used to produce the voltammograms in Figure 65 was then transferred to an electrochemical solution containing 0.1 M $TEABF_4$ in H_2O and SRD CV experiments were repeated in this solution. Figure 66 shows an overlay of the CVs obtained at various scan rates (A) as well as a linear plot of scan rate versus peak current response (B) for the polymer film in 0.1 M $TEABF_4$ in H_2O. The linearity of the plot and the R^2 value suggest that the polymer film is well adhered to the slide in this solution. Notice that there is not a significant decrease in current response as the aqueous content

of the electrolyte solution is increased from Figure 64 (0% water) to 65 (50% water) to 66 (100% water), in stark contrast to experiments performed without surface pretreatment (Figures 56-59). Before surface modification of ITO slides, polymer films were not viable in aqueous electrochemical solutions and aqueous electrochemistry was impossible to obtain. *This indicates that the surface modification of the ITO was successful in adhering the PProDOT(CH_2N_3)$_2$ film to the working electrodes and enables aqueous electrochemistry of the polymer film.*

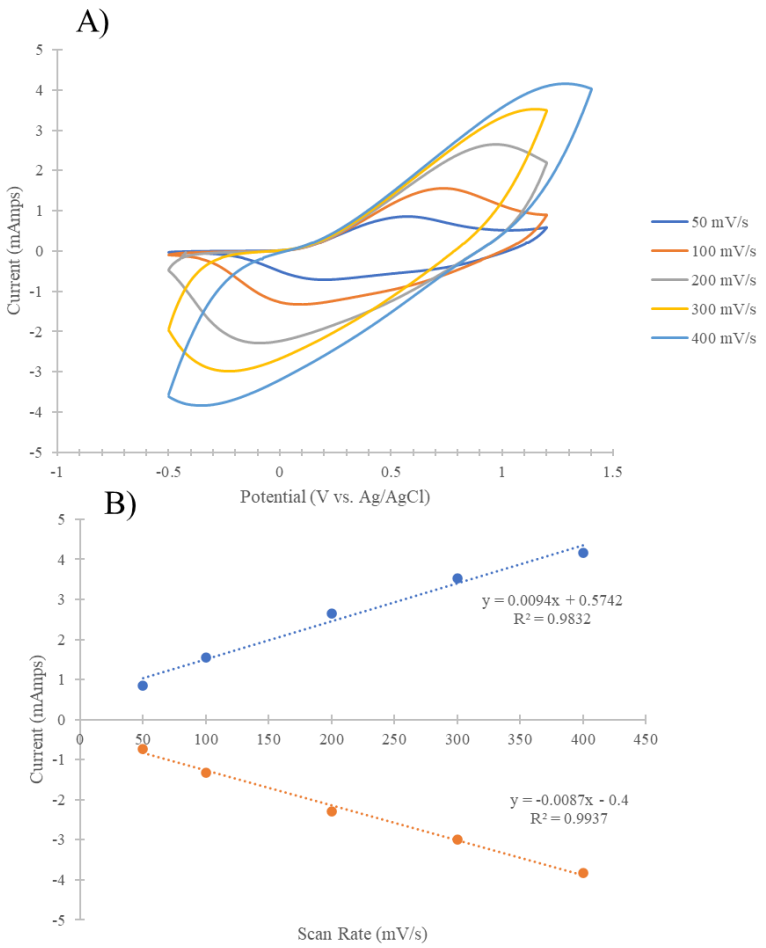

Figure 66: A) stacked CVs obtained from the PProDOT(CH_2N_3)$_2$ film polymerized onto the ThAm modified ITO slide in a 0.1 M $TEABF_4$ in H_2O solution and B) a linear plot of scan rate versus peak current response for the oxidation and reduction of the polymer film to determine if the polymer film is well adhered to the surface of the slide.

Next, the same polymer film was stored overnight in a 0.1 M tris-HCl solution prior to further electrochemistry in order to determine if the films would be stable under conditions appropriate for aptamer testing. Figure 67 shows overlays of the CVs obtained at various scan rates (A) as well as a linear plot of scan rate versus peak current response (B) for the polymer film in a 0.1 M tris-HCl buffer solution to determine if the polymer film is well adhered to the glass slide. The trend of the plot comparing scan rate to peak current response for the oxidation and reduction of the polymer film is less linear than that obtained from all other solutions containing 0.1 M $TEABF_4$. Though the plot is not quite as linear as others obtained, the polymer film did not crack or delaminate from the slide, and peaks in current corresponding to the oxidation and reduction of the polymer film were observed in aqueous solutions. *This indicates that the surface modification of the ITO was successful in adhering the PProDOT(CH_2N_3)$_2$ film to the working electrodes and enables the use of these films for aqueous aptamer sensing.*

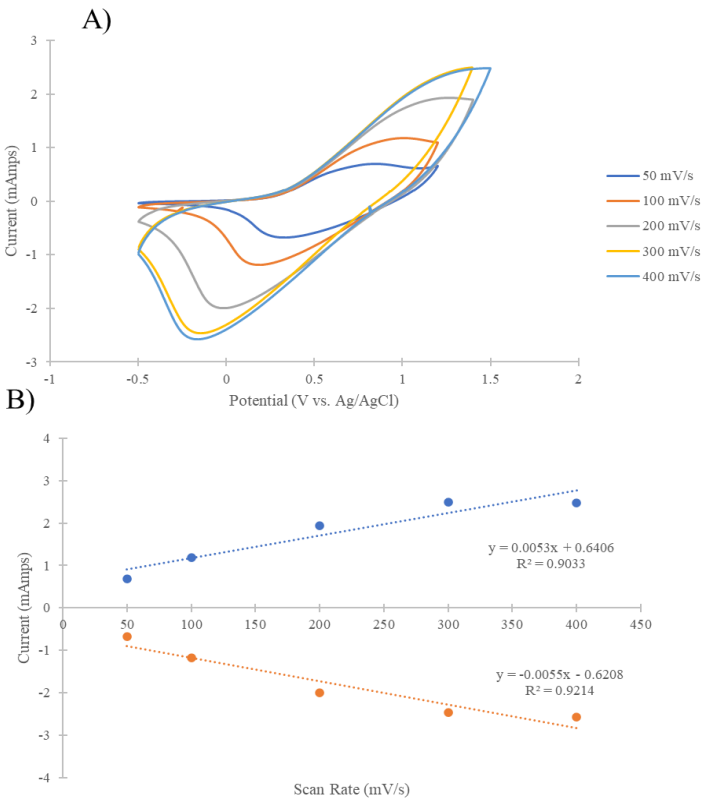

Figure 67: A) stacked CVs obtained from the PProDOT(CH_2N_3)$_2$ film polymerized onto the ThAm - modified ITO slide in 0.1 M tris-HCl after storing the slide in 0.1 M tris-HCl overnight and B) linear plot of scan rate versus peak current response for the oxidation and reduction of the polymer film shows that the polymer film is well adhered to the surface of the slide.

Figure 68 shows two pictures of PProDOT(CH_2N_3)$_2$ films that were grown on differently treated ITO slides after conducting aqueous electrochemical experiments on the films. The picture on the left shows two PProDOT(CH_2N_3)$_2$ films that were grown on unmodified ITO coated glass after aqueous electrochemical experiments, and the picture on the right shows a PProDOT(CH_2N_3)$_2$ film grown on ThAm modified ITO coated slides after aqueous electrochemical experiments. The films on the left are severely cracked, and some of the film has delaminated from the slides. The film on the right has not cracked or delaminated from the slide and was able to undergo polymer oxidation and reduction chemistry in aqueous solutions. *Chemically modifying the surface of ITO*

coated conductive glass slides to form a chemical bond between the polymer film and the glass slide drastically improved the films' mechanical integrity in water as well as the electrochemical data obtained from PProDOT(CH_2N_3)$_2$ films in aqueous solutions.

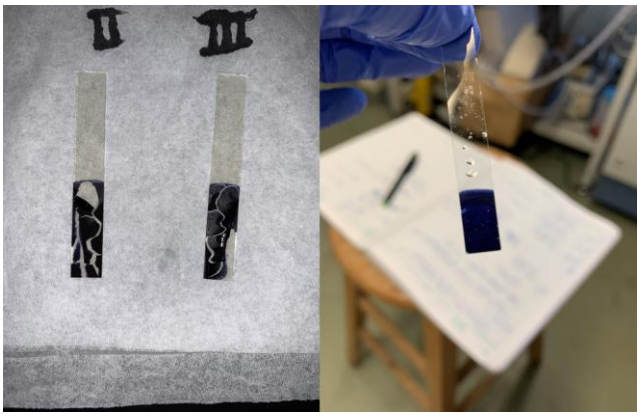

Figure 68: (Left): Two PProDOT(CH_2N_3)$_2$ film that were grown on unmodified ITO slides after conducting aqueous electrochemical experiments on the films and (Right): A PProDOT(CH_2N_3)$_2$ film grown on ThAm modified ITO slides after conducting aqueous electrochemical experiments on the film.

Figure 69 compares the CVs obtained from the PProDOT(CH_2N_3)$_2$ slide polymerized onto the modified ITO slide in several electrochemical solutions, each at a scan rate of 100 mV/s. The polymer film was grown in a 0.01 M ProDOT(CH_2N_3)$_2$ solution containing 0.1 M $TEABF_4$ in ACN. The film was then switched to monomer-free electrolyte solutions for SRD experiments in the following order of solvents systems: 1) ACN, 2) 1:1 ACN:H_2O, 3) H_2O. The polymer film was then stored in a 0.1 M tris-HCl buffer solution overnight and SRD experiments in 0.1 M tris-HCl were conducted the next day. As the electrochemical solution becomes more aqueous, the current response of the polymer film decreases. This decrease in electroactivity is due to the change in solvent from ACN, which the polymer film was grown in, to an aqueous solution. The PProDOT(CH_2N_3)$_2$ film is hydrophobic, creating unfavorable interactions and a decrease in electroactivity in more aqueous solutions. As the solutions change from $TEABF_4$

electrolyte containing solutions to a tris-HCl buffer solution, the peak for the oxidation of the polymer film broadens. This peak broadening is due to the change in electrolyte from $TEABF_4$ to tris-HCl. During the polymerization process, holes in the polymer film form to accommodate intercalation of ions into the polymer film. These holes are most compatible with the ions present during polymerization. With a change in electrolyte and ions in solution, intercalation of the different ions into the holes of the polymer film take more time and energy (if possible), thus broadening the current peak obtained for polymer oxidation.

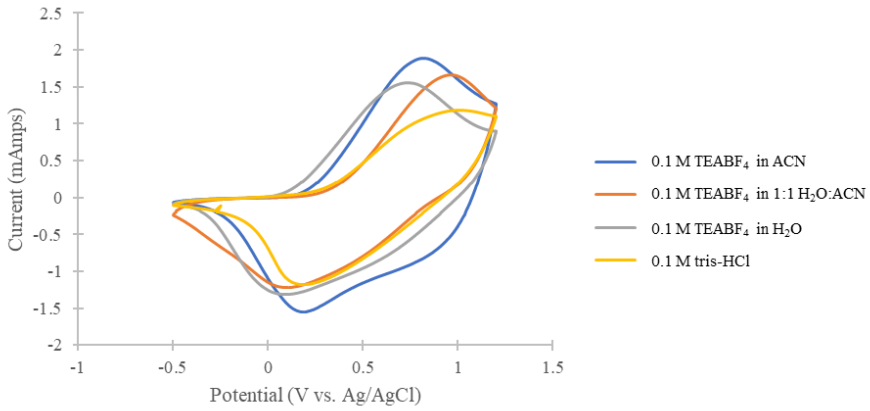

Figure 69: Stacked CVs comparing the electrochemistry of the PProDOT(CH_2N_3)$_2$ film polymerized onto the ThAm modified ITO slide in different electrochemical solutions.

Table 2 below compares the oxidation and reduction values of PProDOT(CH_2N_3)$_2$ films in different electrochemical solutions.

Table 2: Polymer oxidation and reduction values for PProDOT(CH_2N_3)$_2$ film in various electrochemical solutions.

Electrochemical Solution	Polymer Oxidation, $E_{a,p}$ (V vs. Ag/AgCl)	Polymer Reduction, $E_{c,p}$ (V vs. Ag/AgCl)
0.1 M TBAP in ACN	0.57 V	0.41 V
0.1 M $TEABF_4$ in ACN	1.13 V	0.28 V
0.1 M $TEABF_4$ in 1:1 H_2O:ACN	0.98 V	0.32 V
0.1 M $TEABF_4$ in H_2O	--	--

PBS Solution (Polymerized in 0.1 $TEABF_4$ Solution)	--	--
0.1 M $TEABF_4$ in ACN (Polymerized onto Th-COOH modified ITO slide)	0.81 V	0.18 V
0.1 M $TEABF_4$ in 1:1 ACN:H_2O (Polymerized onto Th-COOH modified ITO slide)	0.97 V	0.10 V
0.1 M $TEABF_4$ in H_2O (Polymerized onto Th-COOH modified ITO slide)	0.73 V	0.09 V
0.1 M tris-HCl in H_2O (Polymerized onto Th-CCOH modified ITO slide)	1.01 V	0.19V

ProDOT$(CH_2N_3)_2$ was successfully polymerized in several solutions, including a solution with considerable aqueous character (1:1 ACN:H_2O). Challenges arose when aqueous electrochemical experiments damaged polymer films and resulted in delamination of the polymer films from the ITO slides. The viability of the polymer film in aqueous solutions is vital when fabricating a biosensor. ThAm surface modification of ITO coated slides promoted adhesion of the polymer film to the ITO slide, allowing for the ability to perform aqueous electrochemical experiments without damaging the polymer film. Now that a method has been established for the modification of ITO slides that helps maintain the character of PProDOT$(CH_2N_3)_2$ films in aqueous conditions, fabrication of a biosensor in aqueous click chemistry conditions as well as sensing a biochemical analyte in an aqueous solution is now possible.

4. DEVELOPMENT OF APTAMER BIOSENSOR

4.1 Introduction to the Development of an Aptamer-Based Biosensor

In 1995, Huizenga *et al.* reported the isolation and characterization of an aptamer that selectively binds to adenosine triphosphate (ATP) and adenosine.[63] Huizenga *et al.* used methods similar to the SELEX process described in Chapter 2 to identify an ATP/adenosine aptamer by using affinity chromatography with an ATP agarose column. ATP was bonded to the agarose matrix using a linker. A pool of random sequences of DNA was fed through the affinity chromatography column. DNA that did not bind to the ATP/agarose column matrix was flushed out of the column with buffer solution. DNA that was bound to the ATP/agarose matrix was flushed out of the column with buffer solution containing ATP. The DNA-ATP complex would be replaced by the ATP in the buffer solution. Bound DNA was then concentrated and amplified using polymerase chain reaction (PCR). The aptamer sequence with the strongest affinity for ATP was found to be 5'CCTGGGGGAGTATTGCGGAGGAAGG-3'.[63] This aptamer binds similarly to ATP, adenosine monophosphate (AMP), and adenosine, suggesting that the phosphate groups do not interact with or affect the selectivity of the aptamer.

In 1997, Lin and Patel used Nuclear Overhauser Effect Spectroscopy (NOESY) NMR to determine the structure and folding of an AMP-DNA complex.[64] NOESY is a type of NMR experiment which correlates protons that are close to each other in space (4.5 Å or less).[65] Through their NMR studies, Lin and Patel were able to determine that two adenosine molecules bind to the aptamer in its guanine-rich centers. Figure 70 shows how an adenosine specific aptamer is expected to bind to adenosine.

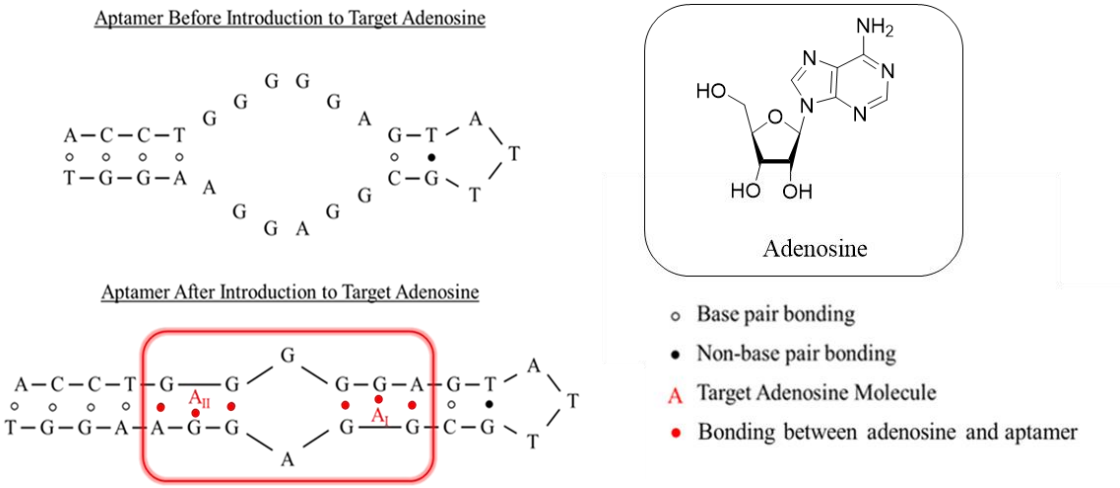

Figure 70: Illustration of how adenosine interacts with guanine-rich centers in our adenosine specific aptamer. AI and AII represent the two nonequivalent bonding sites and the stoichiometry of the two molecules of adenosine per aptamer. The red dots in this figure represent interaction sites between adenosine and the aptamer. Adapted with permission from Lin, C. H.; Patei, D. J. Structural Basis of DNA Folding and Recognition in an AMP-DNA Aptamer Complex: Distinct Architectures but Common Recognition Motifs for DNA and RNA Aptamers Complexed to AMP. Chem. Biol. 1997, 4 (11), 817–832. Copyright (1997) American Chemical Society. [64]

4.2 "Click Chemistry" Review

Huisgen *et al.* first published catalyst-free 1,3-dipolar cycloaddition reactions involving organic alkynes and azides in 1967.[66] Huisgen 1,3-dipolar cycloaddition reactions have since been termed "click chemistry" reactions because of the efficiency of the reaction. In 2001, Tornøe *et al.* studied how the use of a Cu(I) catalyst greatly improved the yield and regiospecificity of these Huisgen 1,3-dipolar cycloaddition reactions, creating a new name for these reactions: Cu(I)-catalyzed alkyne-azide cycloaddition (CuAAC) reactions.[67] Worrell *et al.* conducted isotopic labeling and kinetic studies in an attempt to better understand the catalytic cycle that takes place during CuAAC reactions.[68] They found that two copper atoms are necessary during the catalytic cycle to form the desired triazole ring. Figure 71 illustrates this catalytic cycle.

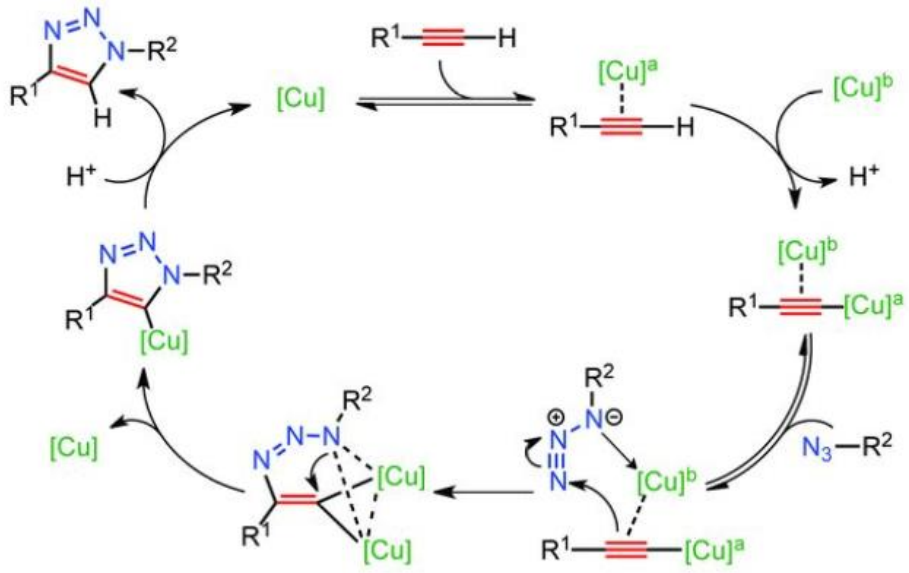

Figure 71: Catalytic cycle involving two copper atoms for CuAAC reactions. From Worrell, B. T.; Malik, J. A.; Fokin, V. V. Direct Evidence of a Dinuclear Copper Intermediate in Cu(I)-Catalyzed Azide-Alkyne Cycloadditions. *Science (457-460)*. 2013. Reprinted with permission from AAAS.[68]

Aqueous conditions are needed during CuAAC attachment reactions when using a molecule that is not soluble in organic solvents, like an aptamer, or when the compound is labile in organic solvents, like proteins. Aqueous click chemistry conditions that are most commonly used were first published by Rostovtsev *et al.* in 2002.[69] Because of the poor solubility of Cu(I) salts in water, Cu(II) salts and a reducing agent are typically used in aqueous click chemistry reactions.

For the fabricated EAP-based biosensor, an adenosine-specific aptamer was attached to an EAP film through click chemistry as a proof of concept for other, more complex aptamer sequences. The aptamer[63] used in this research for adenosine detection is functionalized with an alkynyl substituent, which is expected to form a triazole ring with PProDOT$(CH_2N_3)_2$ under aqueous click chemistry conditions. In future work, aptamers specific to more complex molecules could be attached to the EAP film through click chemistry to fabricate a biosensor.

4.3 Experimental

4.3.1 Materials

ProDOT(CH_2N_3)$_2$ was prepared using synthesis and purification methods described a in section 2.5 of this thesis and polymerized following the methods in section 3.2.2 of this thesis. 10XPBS was purchased from SeraCare (10 mM sodium phosphate, 150 mM NaCl, pH 7.4). $CuSO_4 \cdot 5H_2O$, sodium ascorbate, diisopropylethylamine (DIPEA), and *tert*-butylalcohol (*t*-BuOH) were purchased from Sigma-Aldrich and used as received. Glycerol was purchased from Sigma and used as received. Copper iodide (CuI) was purchased from Alfa Aesar and used as received. Ascorbic acid was purchased from VWR. Adenosine was purchased from Calbiochem. A solution of 10 mM copper(II)-tris[(1-benzyl-1H-1,2,3-triazol-4-yl)methyl]amine (TBTA) complex in 55% DMSO was purchased from Lumiprobe®. Triethylammonium acetate buffer was made by mixing 2.78 mL triethylamine with 1.14 mL glacial acetic acid and diluting the solution to a total volume of 10 mL with water. Triethylamine was purchased form Alfa Aesar and glacial acetic acid was purchased from EMD Millipore. Tris-base was purchased from Research Products International and used to make a 50 mM tris solution that was adjusted to a pH of 7.4 using concentrated HCl to make a 50 mM tris-HCl solution. Dimethylsulfoxide (DMSO) and hydrochloric acid (HCl) were purchased from Fisher Scientific and used as received. An aptamer with a sequence of 5'-/5Hexynyl/-AAA AAC ACT GAC CTG GGG GAG TAT TGC GGA GGA AGG T-/36-FAM/-3' was purchased from Integrated DNA Technologies and diluted in autoclaved water to make a 100 μM and a 800 μM aptamer solution. The aptamer solution as purchased has a molecular weight of 12,306.1 Da, an extinction coefficient of 399,500 L/(mol·cm),

contains 37 oligo bases, has a hexynyl modification on the 5' end of the oligonucleotide and has a 6-FAM modification on the 3' end of the oligonucleotide. There is an addition of five units of adenosine on the 5' end of the aptamer that act as a spacer between the binding site of the aptamer to the polymer film and the active site of the aptamer that will bind to adenosine. This distance should prevent steric hindrance for the binding interaction of adenosine and the aptamer. The hexynyl modification of the aptamer participates in an aqueous CuAAC reaction with the azide functionalized EAP. The FAM tag (fluorescein amidite) was used to determine efficiency of aptamer attachment reactions via fluorescence imaging. Figure 72 shows and explains fragments of the aptamer sequence used.

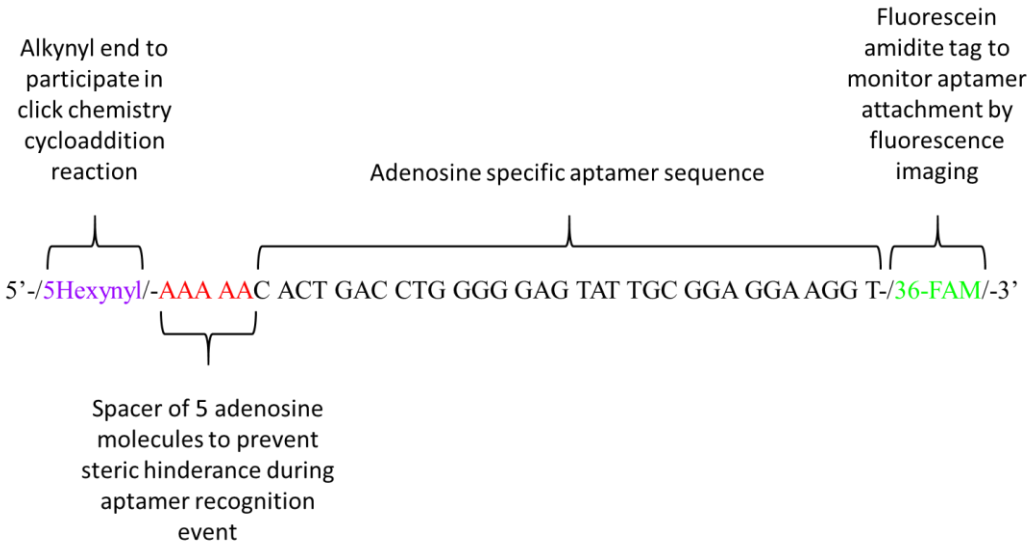

Figure 72: Sequence of aptamer used along with description and of aptamer fragments.

Fluorescein absorbs light at a wavelength of 494 nm and emits light at a wavelength of 512 nm. The 100 µM aptamer solution was stored in a freezer at -25°C. Figure 73 and 74 are the UV-Vis and fluorescence emission spectra, respectively, of the aptamer solution at a concentration of 1 µM.

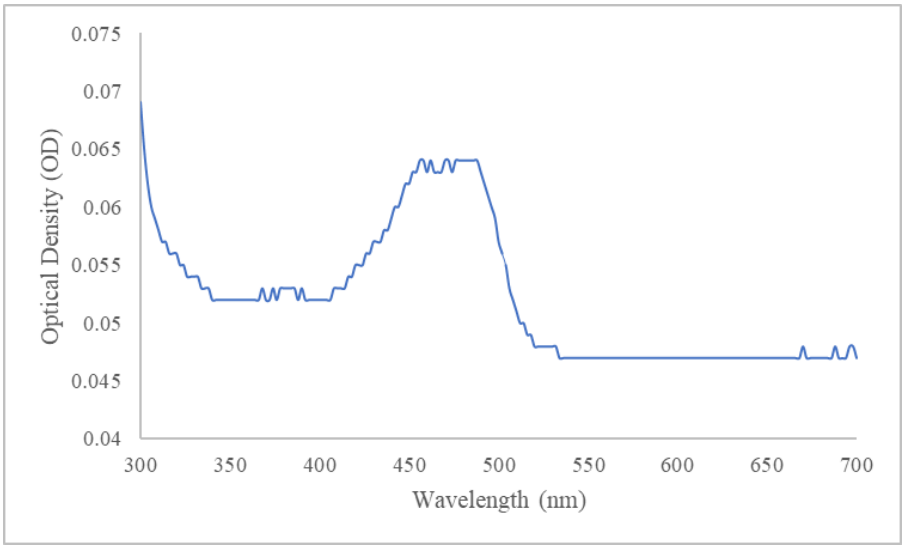

Figure 73: UV-Vis absorption spectrum of 1 µM aptamer solution.

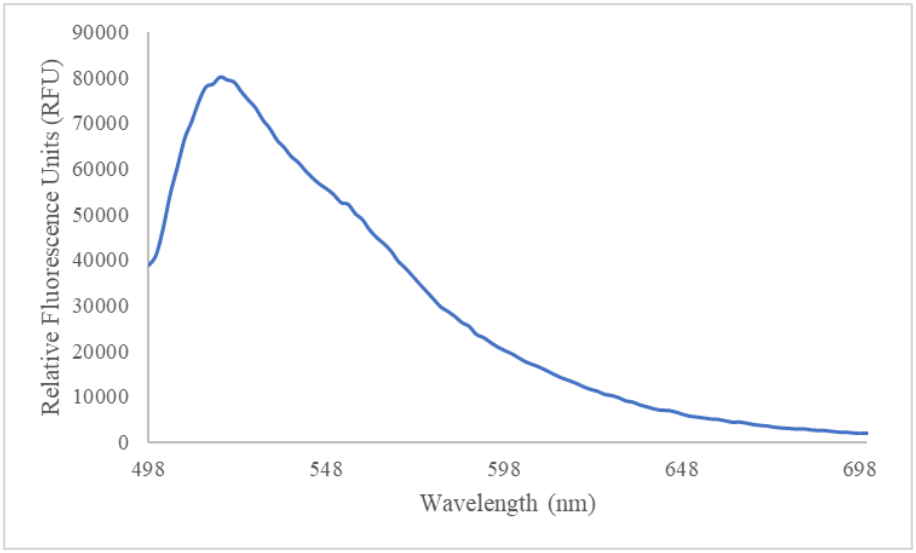

Figure 74: Fluorescence spectrum of 1 µM aptamer solution.

4.3.2 Instruments

All fluorescence images were taken using an AMG EVOS FL microscope equipped with an EVOS^{TM} Green Fluorescent Protein (GFP) filter cube. The excitation and emission wavelengths of the filter cube are 470/22 nm and 525/50 nm, respectively.

The numbers before the dash represent the median value of the pass-band while the numbers after the slash represent the width of the pass-band. For excitation, the pass-band ranges from 459 nm to 481 nm. For emission, the pass-band ranges from 500 nm to 550 nm. UV-Vis spectra were obtained using a Biotek Synergy H4 hybrid microplate reader.

4.3.3 "Click Chemistry" Aptamer Functionalization of PProDOT(CH_2N_3)$_2$

4.3.3.1 First Failed Attempt of Aptamer Attachment Through "Click Chemistry" Reaction

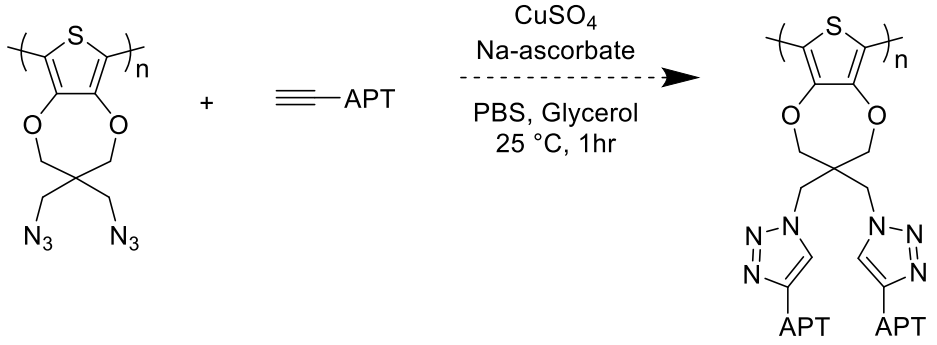

Figure 75: First failed attempt of functionalizing ProDOT(CH_2N_3)$_2$ with an aptamer through click chemistry reaction.

The procedures of Ratajczak *et al.* were followed.[70] A solution of 4 μM aptamer was made by diluting 1 μL of 100 μM aptamer solution in 24 μL of 1X PBS buffer. A solution of 0.1 M $CuSO_4 \cdot 5H_2O$ in PBS was prepared by dissolving 62.4 mg $CuSO_4$ in 2.5 mL 1X PBS, and a solution of 0.1 M sodium ascorbate in PBS was prepared by dissolving 23.8 mg sodium ascorbate in 1.2 mL 1X PBS. 1 μL of 4 μM aptamer solution, 250 μL of 0.1 M $CuSO_4$ solution, 120 μL of 0.1 M sodium ascorbate solution, and 50 μL of glycerol were pipetted separately on top of the polymer film in that order. Solutions

were not mixed together prior to being pipetted onto the polymer slide. Glycerol was used to mitigate the evaporation of the water from the polymer slides. The reaction mixture was left in a humidity chamber at 70% humidity and allowed to react over one hour at room temperature. After one hour, the slides were rinsed with 1XPBS and analyzed under a fluorescence microscope.

4.3.3.2 Second Failed Attempt of Aptamer Attachment Through "Click Chemistry" Reaction

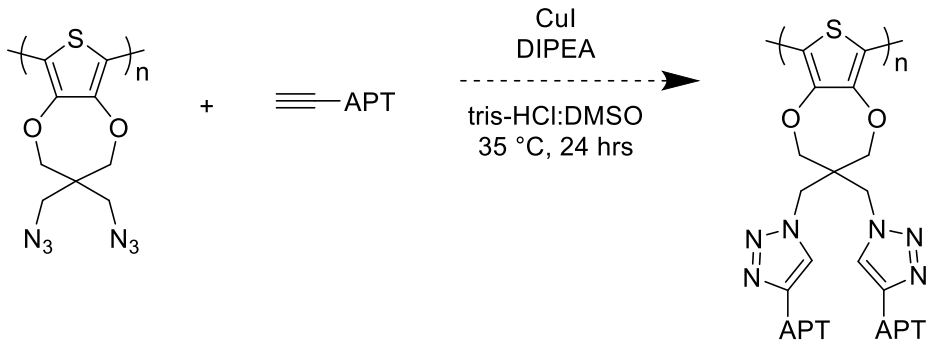

Figure 76: Second failed attempt of functionalizing PProDOT(CH_2N_3)$_2$ with an aptamer through click chemistry reaction.

The procedures of Galán et al.[25] were followed. 2.5 µL of 100 µM stock aptamer solution (2.5 nmol) was dissolved in a 50 mM tris-HCl solution creating a total volume of 250 µL. A 120 molar equivalent of diisopropylethylamine (DIPEA) (300 nmol) and a 100 molar equivalent of CuI (250 nmol) were dissolved in 250 µL DMSO. The tris-HCl and DMSO solutions were combined in a vial and an ITO slide with a film of PProDOT(CH_2N_3)$_2$ was placed in the reaction mixture for 24 hours at a temperature of 35°C, under argon, on a shaker table. After 24 hours, the slide was removed from solution and rinsed with water. The rinsed slide was examined under a fluorescence

imaging microscope and with a UV-Vis spectrophotometer.

4.3.3.3 Third Failed Attempt of Aptamer Attachment Through "Click Chemistry" Reaction

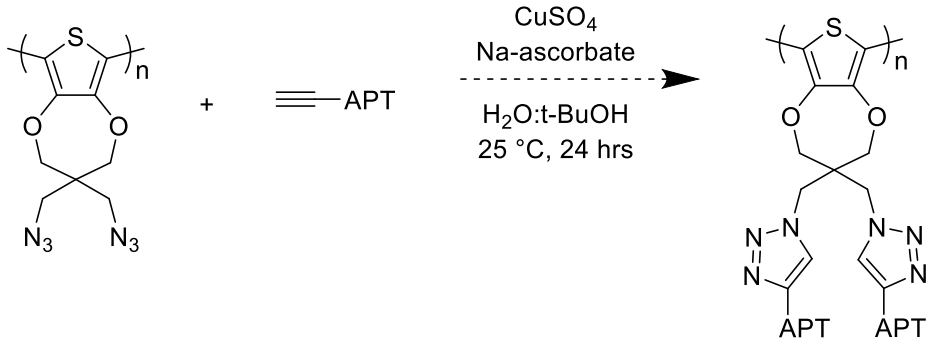

Figure 77: Third failed attempt of functionalizing PProDOT(CH_2N_3)$_2$ with an alkyne functionalized aptamer through click chemistry reaction.

Three polymer films were used to study the different variables during this attachment attempt (Slides I, II, and III). The procedures of Kuijpers *et al.* were followed.[71] 10 µL of 100 µM aptamer solution, a 0.2 molar equivalent of $CuSO_4$ (2 µL of a stock solution of 100 µM $CuSO_4$•$5H_2O$ in H_2O) , and a 0.4 molar equivalent of sodium ascorbate (4 µL of a stock solution of 100 µM sodium ascorbate in H_2O) were pipetted separately onto slide I, the main sample. 10 µL of 100 µM aptamer solution was pipetted onto slide II as a control for non-specific aptamer adsorption. A 0.2 molar equivalent of $CuSO_4$•$5H_2O$ and a 0.4 molar equivalent of sodium ascorbate were pipetted separately onto slide III as a control for the effect of click chemistry reagents on the polymer film. Appropriate volumes of t-BuOH and water were added to each slide to make a solvent system of 1:1 H_2O:t-BuOH and to make a total reaction volume of 100 µL for each slide. The slides were left in a humidity chamber with a humidity of 70% at room temperature

to react overnight. After 12 hours the solvent had evaporated. The slides were rinsed with water several times and analyzed using fluorescence microscopy imaging.

4.3.3.4 Aptamer Attachment Through "Click Chemistry" Reaction, Following Lumiprobe® Protocols

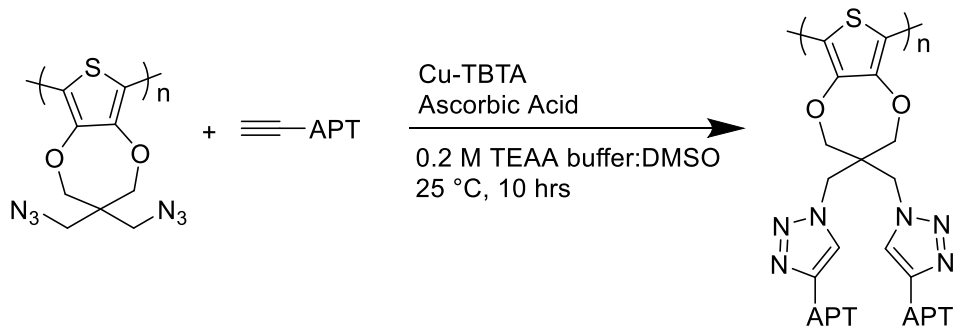

Figure 78: Click chemistry reaction scheme described in Lumiprobe®'s click chemistry on DNA protocol.

Several click chemistry reactions and control experiments were performed following Lumiprobe®'s protocol for click chemistry on DNA (twelve polymer films used, labeled A-L.[72] four polymer films used for each experiment (one set of click reactions and two sets of control reactions)). For the click chemistry reactions, 6.25 µL of an 800 µM aptamer solution, 5 µL of 2 M TEAA buffer, 25 µL of DMSO, and 5 µL of 5 mM ascorbic acid solution in water was combined in a microcentrifuge tube. The solution was degassed with argon for 30 seconds, then 2.5 µL of 10 mM Cu-TBTA in 55 vol % DMSO was added to the solution. The solution was then mixed by pipetting several times. Once mixed, the click chemistry reaction solution was pipetted onto a polymer film and left in a cuvette overnight under argon to react.

For one set of control experiments (control I experiments), the aptamer solution

was absent from the overall reaction solution. For another set of control experiments (control II experiments), the source of copper (Cu-TBTA complex solution) and the reducing agent for the copper (ascorbic acid) were absent from the overall reaction solution (control for non-specific aptamer adsorption). The same procedures for the click chemistry reaction were also followed for the control reactions.

Fluorescent microscope images were obtained from all twelve films after being exposed to their respective click chem or control reaction. Cyclic voltammograms were performed on the polymer slides before and after the polymer films were exposed to their respective control or click chemistry reaction. The CV experiments were carried out in 0.1 M tris-HCl buffer solution over the range of -0.5 V to 1.4 V at a scan rate of 100 mV/s for 10 cycles.

4.4 Results and Discussion

4.4.1 First Failed Attempt of Aptamer Attachment Through "Click Chemistry" Reaction

Figure 79 shows the image obtained from the polymer film slide using a fluorescence imaging microscope. Fluorescence microscopy imaging showed no detectable fluorescence after the attempted attachment reaction. It is possible that the aptamer did not successfully bond to the polymer film. This could be attributed to the use of a 4 µM aptamer solution instead of a 40 µM aptamer solution described in the procedures of Ratajczak *et al.*[70] Solutions were also not properly mixed together before being pipetted onto the polymer slide, which could result in the failure of this aptamer

attachment reaction. It is also possible that the polymer film was imaged on the wrong side of the ITO electrode, making it impossible to see any fluorescence on the surface of the polymer film. The polymer film may not have been wet enough for the fluorescein tag to show fluorescence in solution. Fluorescence may not have been seen if the polymer film was dry; the fluorescein tag is much less fluorescent when dry than when in solution and may not have been visible using the fluorescence microscope if the film was too dry.

Figure 79: Fluorescence microscopy image of the polymer film after first aptamer attachment attempt. No fluorescence is visible.

4.4.2 Second Failed Attempt of Aptamer Attachment Through "Click Chemistry" Reaction

Figure 80 is the image obtained of the polymer film after the click chemistry was performed on the film obtained from fluorescent microscope imaging. No fluorescence was detected on the slide by the fluorescence imaging microscope or by the UV-Vis spectrophotometer. It is possible that the aptamer did not chemically bond to the polymer film, or it is possible that fluorescence was not observed for one of the reasons described above.

Figure 80: Fluorescence microscopy image of polymer film after second aptamer attachment attempt. No fluorescence was visible.

4.4.3 Third Failed Attempt of Aptamer Attachment Through "Click Chemistry" Reaction

Figures 81, 82, and 83 are images of polymer films after click chemistry and control experiments were performed obtained from fluorescence microscope imaging. Slides I (Figure 81) and III (Figure 83) showed inconsistent spots of fluorescence throughout the polymer film, which is not what is expected from a successful aptamer attachment reaction. Slide III is not expected to show any fluorescence as it had not been exposed to any aptamer solution. The fluorescence seen on slide III could have only come from some outside contaminant as the other solutions used during the click chemistry reaction did not fluoresce. Slide II (Figure 82) showed no significant fluorescence. This lack of fluorescence is expected when no click chemistry reagents are present to initiate the cycloaddition reaction and the unattached aptamer is washed away with water. Aptamer attachment through click chemistry following these procedures was unsuccessful.

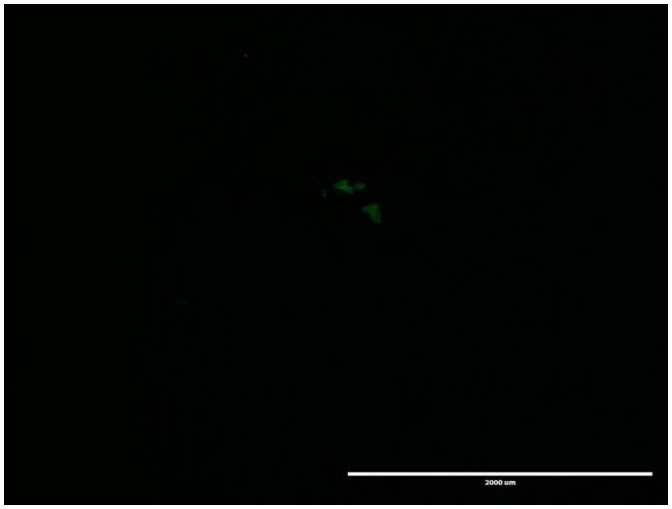

Figure 81: Fluorescence microscopy image of Slide I. Small, inconsistent spots of fluorescence could be seen in several areas on the polymer slide.

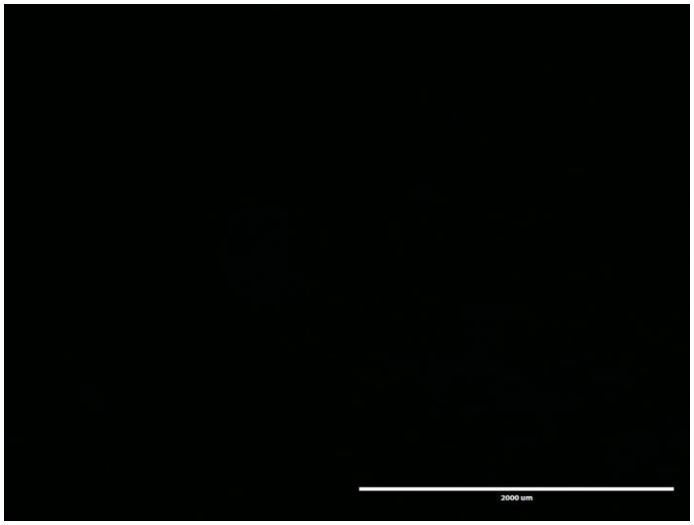

Figure 82: Fluorescence microscopy image of control slide II. No areas of fluorescence could be seen on slide II. Slide II was exposed to the aptamer solution but was not exposed to any copper catalyst or reducing agent from the click chemistry reaction.

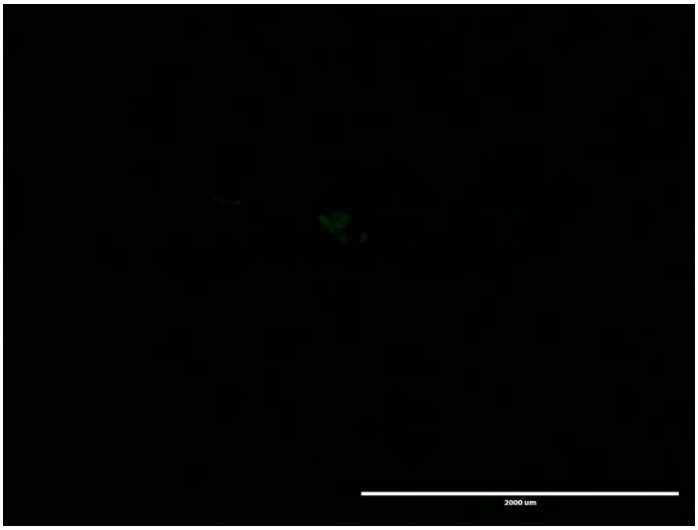

Figure 83: Fluorescence microscopy image of control slide III. Similar to slide I, slide III showed several small spots of fluorescence throughout the polymer slide. Slide III was exposed to the copper catalyst and the copper reducing reagents for the click chemistry reaction but was not exposed to the aptamer.

4.4.4 Aptamer Attachment Through "Click Chemistry" Reaction, Following Lumiprobe® Protocols

Figure 84 shows fluorescent images obtained from four separate polymer films (labeled as slide A, slide J, slide K, and slide L) that were reacted with the aptamer through click chemistry utilizing the conditions recommended by Lumiprobe® protocol for click chemistry reactions involving DNA. Significant fluorescent spots can be seen throughout the entirety of all four polymer films.

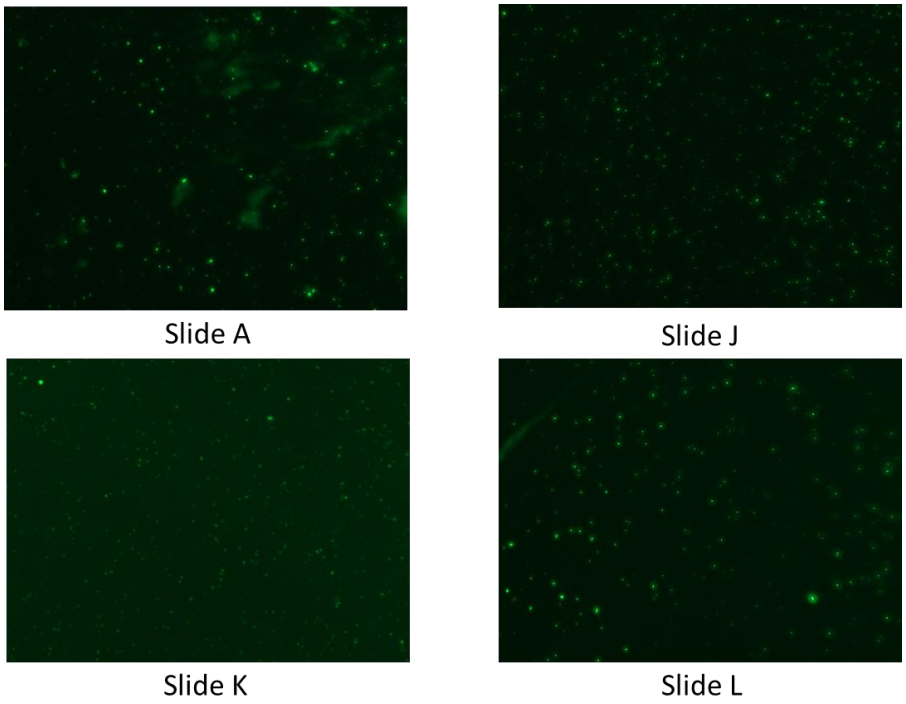

Figure 84: Fluorescence microscopy images from four polymer films (slide A, slide J, slide K, and slide L) that were exposed to Lumiprobe®'s click chemistry protocols. Significant and consistent fluorescent spots can be seen throughout all polymer films.

Figure 85 shows cyclic voltammograms obtained from polymer films on slides A, J, K, and L before and after aptamer attachment via click chemistry. In all slides, a slight decrease of electroactivity is observed after aptamer functionalization. This decrease in electroactivity is attributed to the attachment of electrically insulating, non-conjugated DNA strands to the surface of the polymer film.[25]

It can be seen that for voltammograms obtained before and after aptamer attachment to the polymer film on slide J, the voltammograms seem to be skewed and tilted relative to each other, this illustrates that there is a significant decrease in current response and electroactivity of the polymer film. This loss in electroactivity could be attributed to the functionalization of the polymer film with electrically insulating, non-conjugated DNA strands. It is also possible that the dramatic loss in electroactivity seen

for the polymer film on slide J is due to loss of polymer film on the electrode from the film slightly delaminating or by accidental scrapping off of the polymer film while conducting CV experiments. Further experiments need to be conducted to determine the reproducibility of obtaining electrochemistry of PProDOT(CH_2N_3)$_2$ films in a tris-HCl solution before and after aptamer attachment.

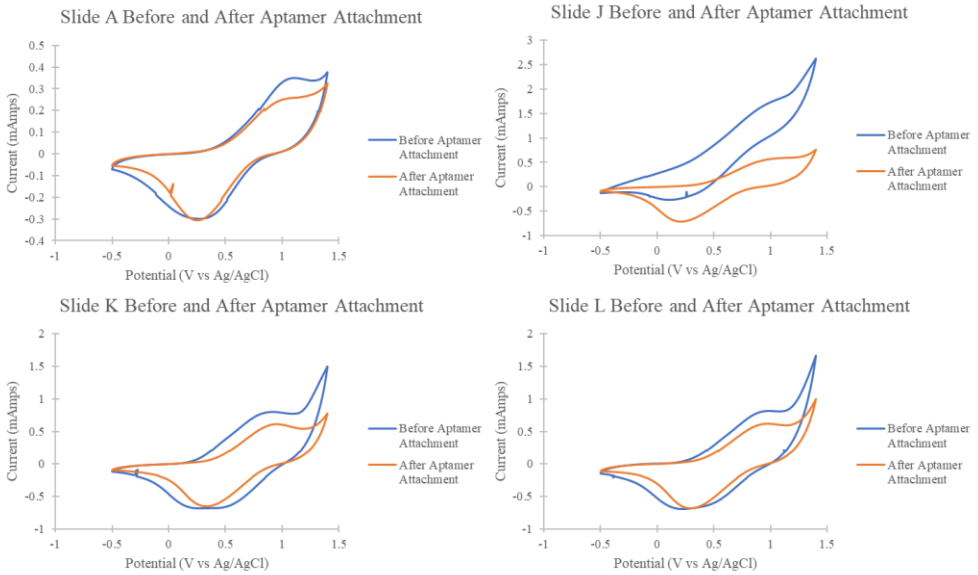

Figure 85: Cyclic voltammograms obtained from polymer films on slides A, J, K, and L before and after aptamer attachment via click chemistry.

Figure 86 shows images obtained from four separate polymer films (labeled as slide F, slide G, slide H, and slide I) that were used for control experiments in which the slides were exposed to all "click chemistry" reagents, but in the absence of the aptamer. None of the polymer films show any significant fluorescence, which is expected in the absence of aptamer.

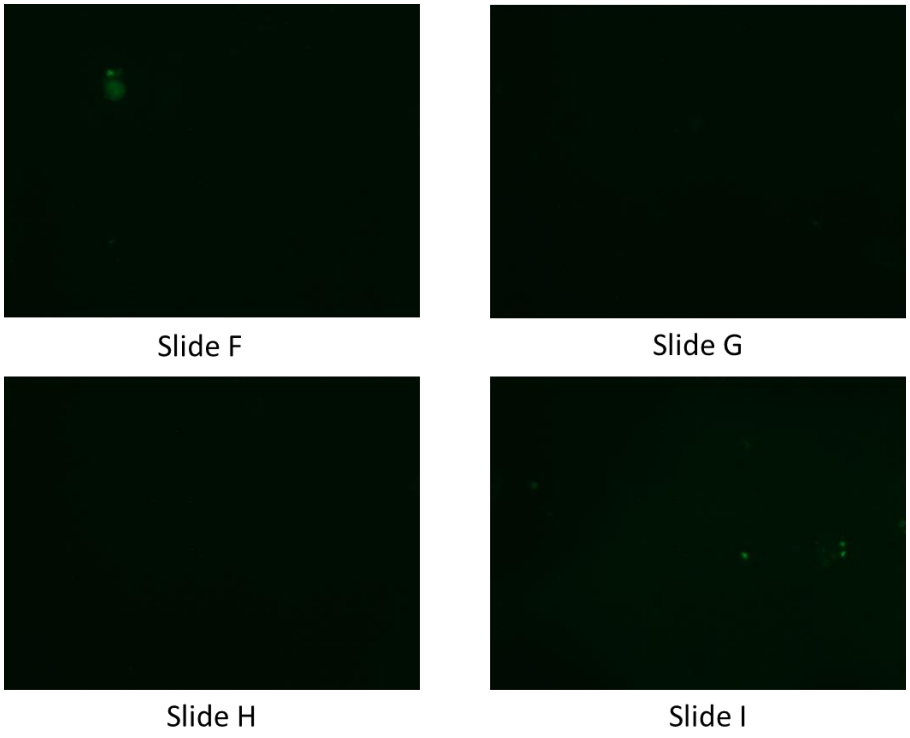

Figure 86: Fluorescence microscopy images from four polymer films (slide F, slide G, slide H, and slide I) that were used during control experiments that were exposed to Lumiprobe®'s click chemistry protocols in the absence of aptamer.

Figure 87 shows cyclic voltammograms obtained from polymer films on slides F, G, H, and I before and after control I experiment conditions (no aptamer in solution). There is a trend of a slight decrease in electroactivity of the polymer films. The voltammograms obtained from polymer films on slides H and I are skewed similar to voltammograms obtained from slide J in figure 85. This dramatic decrease in electroactivity of the polymer film may be due to undesirable side reactions occurring between the reagents used in click chemistry reactions and the polymer film. It can be inferred that incubating the PProDOT(CH_2N_3)$_2$ films in the reagents used for the click chemistry aptamer attachment reaction (copper catalyst and reducing agent for the copper in solution) results in a loss of electroactivity of the polymer films.

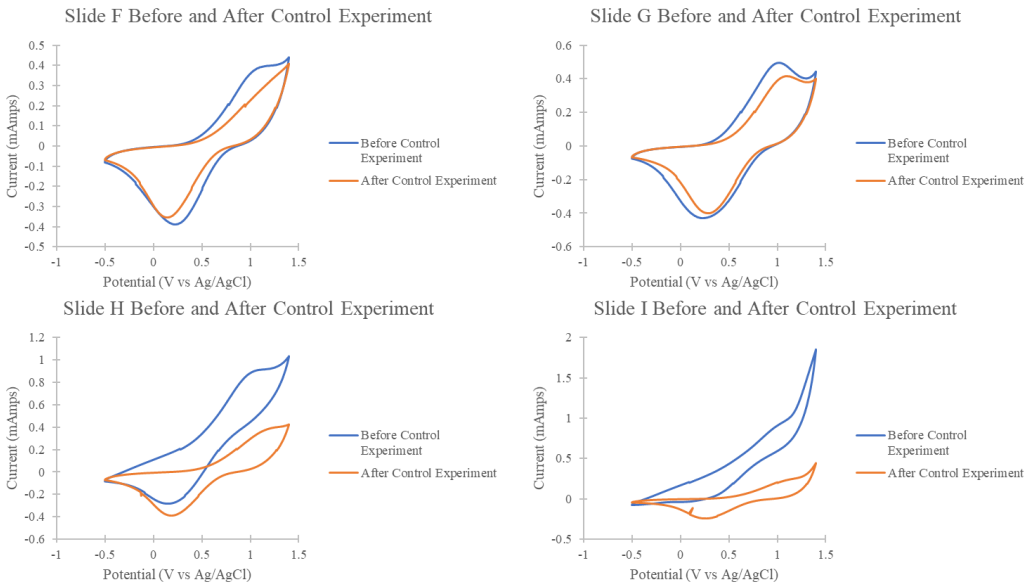

Figure 87: Cyclic voltammograms obtained from polymer films on slides F, G, H, and I before and after being exposed to control I experiments (no aptamer in solution).

Figure 88 shows images obtained from four different polymer films (slide B, slide C, slide D, slide E) that were used for control experiments in which the slides were exposed to the aptamer but in the absence of copper catalyst and reducing agent for the copper catalyst. This control tests for non-specific adsorption of the aptamer to the polymer surface. The slides show some fluorescence from aptamer that has adhered to the surface of the polymer films, though there are fewer and less consistent fluorescent spots than that of the polymer films that were reacted with the aptamer via click chemistry (refer to Figure 84).

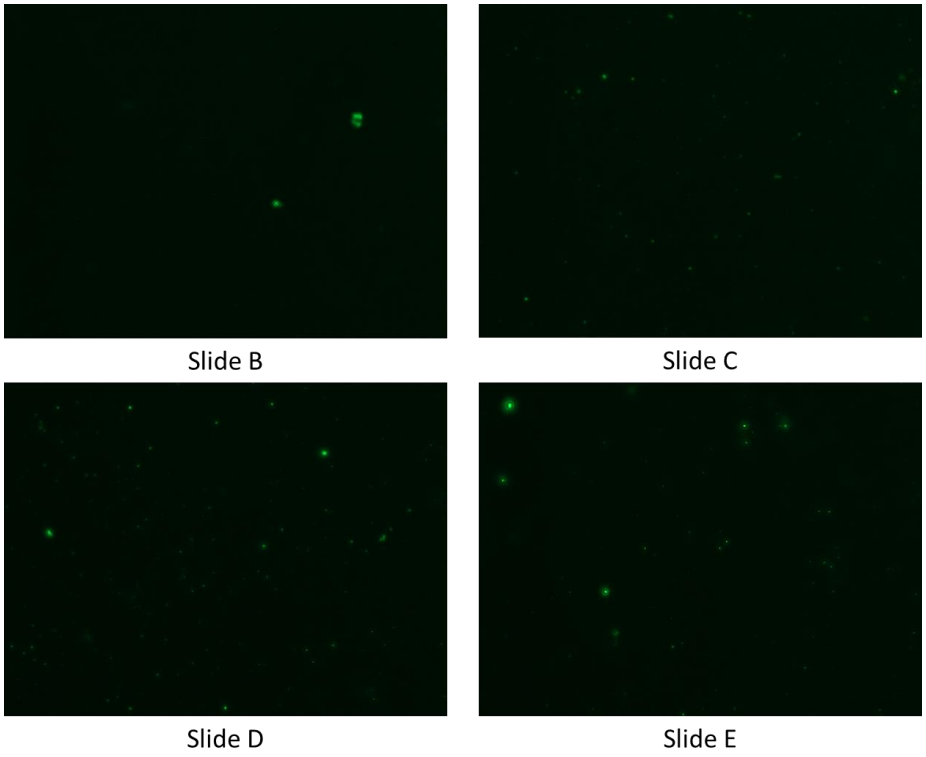

Figure 88: Fluorescence microscopy images from four polymer films (slide B, slide C, slide D, and slide E) that were used during control experiments that utilized the aptamer but lacked copper catalyst and reducing agent for copper in solution.

Figure 89 shows cyclic voltammograms obtained from polymer films on slides B, C, D, and E before and after exposure to control II experiments (no copper catalyst or copper reducing agents in solution). The changes in electrochemistry of the polymer films before and after control II experiments are inconsistent among the four films tested. For slides B and D, there was a slight decrease in electroactivity after control II experiments, while the electroactivity of slide C increases after control II experiments. The electroactivity of slide E seems unchanged after exposure to control II experimental conditions. There is no electrochemical trend to be seen between slides B, C, D, and E after conducting control II experiments. Several factors can contribute to the inconsistency in electrochemical change of polymer films seen here. If polymer films are

not treated and grown exactly the same throughout experimentation, major differences in the electroactivity and inconsistencies between polymer films can be seen. In the future, care must be taken to ensure that all polymer films are treated the same for during all experimentation to obtain consistent results. Further experiments need to be conducted to determine the reproducibility of obtaining aqueous electrochemistry from polymer films grown on ThAm modified ITO slides.

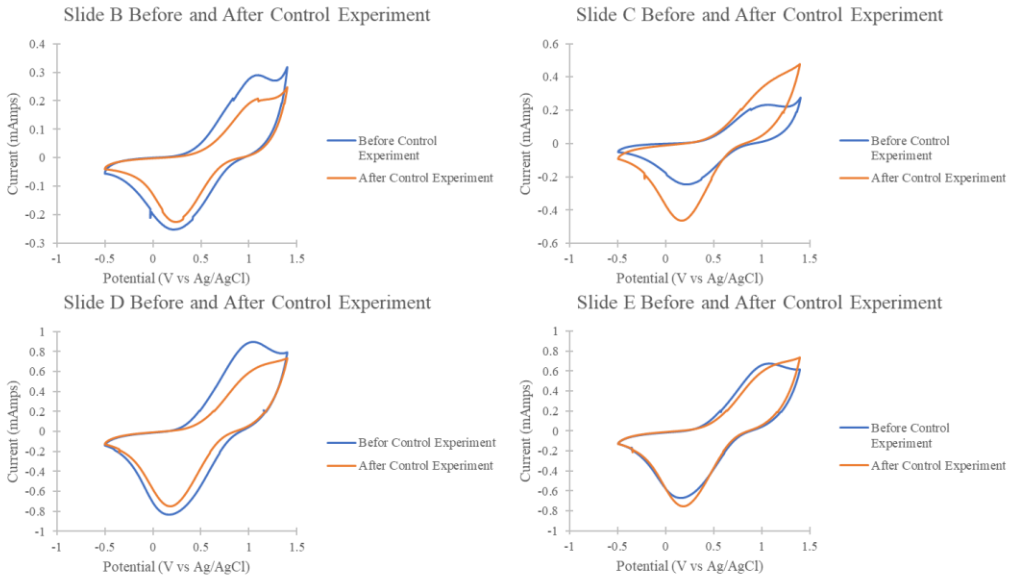

Figure 89: Cyclic voltammograms obtained from polymer films on slides B, C, D, and E before and after being exposed to control II experiments (no copper catalyst and no reducing agent for copper in solution).

In summary, only polymer films that were exposed to the click chemistry environment described in Lumiprobe®'s protocol showed consistent fluorescence throughout the slide that was characteristic of a fluorescent molecule chemically attached to the surface of the polymer film and showed electrochemistry consistent with aptamer functionalization. Aptamer functionalization of PProDOT(CH_2N_3)$_2$ films following Lumiprobe®'s click chemistry protocol was successful.

4.5 Detection of Target Molecule with Aptamer Biosensor

4.5.1 Experimental

An initial experiment was conducted in which four separate aptamer-functionalized slides were utilized to sense one concentration of adenosine each. Specifically, slides A, J, K, and L described in section 4.4.4 of this thesis were incubated in solutions of 3.32 mM, 0.415 mM, 0.83 mM, and1.66 mM adenosine in 0.1 M tris-HCl buffer, respectively, for two hours. After two hours, the polymer films were taken out of their respective incubation solution and placed in a 0.1 M tris-HCl solution, CV experiments were then carried out in the 0.1 M tris-HCl solution on each slide over the voltage range of -0.5 V to 1.4 V at a scan rate of 100 mV/s for 10 cycles. These voltammograms were then compared to voltammograms obtained before adenosine incubation and after aptamer functionalization. Voltammograms from all four slides were compared to evaluate the analytical ability of the fabricated biosensor to sense different concentrations of adenosine.

Slide L was regenerated by incubating in 0.05 M tris-HCl buffer overnight to allow the aptamer to release the bound adenosine. After this regeneration process, slide L was incubated in a solution of 0.417 mM adenosine in 0.1 M tris-HCl for 2 hours. After two hours, CV experiments were carried out on slide L at a voltage range of -0.5 V to 1.25 V at a scan rate of 100 mV/s for 10 cycles. After obtaining the voltammogram from the incubation of slide L in a 0.417 mM adenosine solution, the slide was incubated in a 0.83 mM adenosine solution and the CV experiments repeated. This procedure was also repeated for a 1.67 mM and a 3.33 mM adenosine solution. Voltammograms were then plotted and compared to determine the analytical ability of the fabricated biosensor.

4.5.2 Results and Discussion

Figure 90 shows cyclic voltammograms of polymer films on slide A, J, K, and L after incubation in adenosine solutions. Slide A was incubated in a 3.32 mM adenosine solution, slide J was incubated in a 0.415 mM adenosine solution, slide K was incubated in a 0.83 mM adenosine solution, and slide L was incubated in a 1.66 mM adenosine solution. The current response of each slide decreased after adenosine incubation. There is a consistent decrease in electroactivity seen in all polymer films; this decrease is due to the binding of insulating adenosine molecules to the aptamer-functionalized EAP biosensor, and the conformation change of the aptamer of the biosensor. Several studies claim that a decrease in electroactivity of an electrochemical biosensor is indicative of the transducing event of the biosensor.[25,73,74] Roncali *et al.* reports that alkyl substituents containing 10 or more carbons on polythiophene had the ability to drastically change the electroactivity of the polythiophene based films.[75] It can be inferred that the binding event between the aptamer and adenosine, a molecule larger and more polar than a C_{10} carbon chain (refer to Figure 70 for the structure of adenosine), is what causes this decrease in electroactivity seen among all the biosensing electrodes tested.

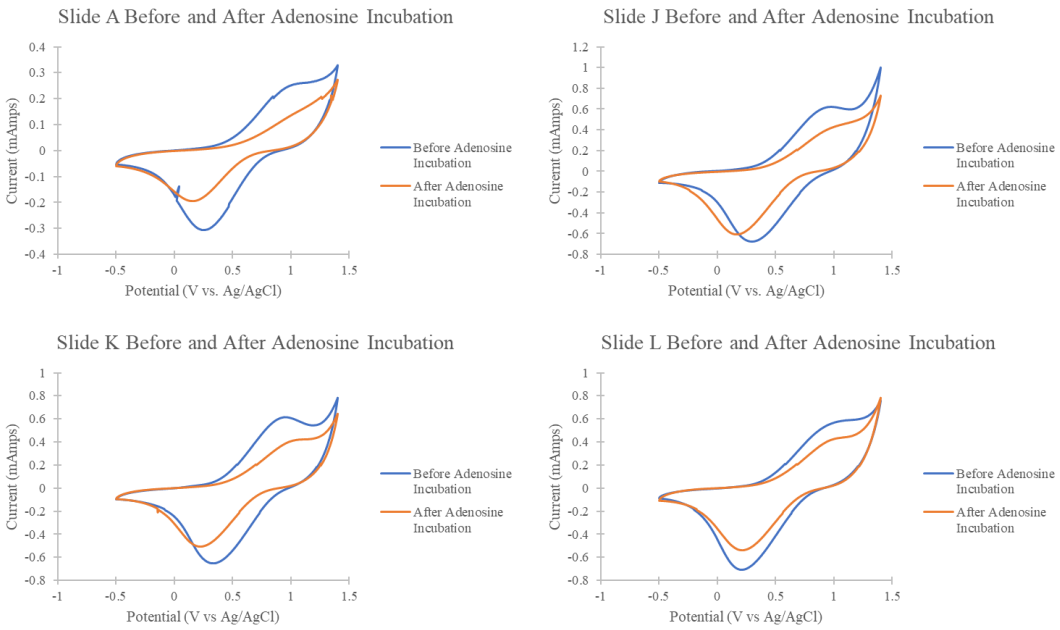

Figure 90: Cyclic voltammograms obtained from polymer films on slides A, J, K, and L before and after incubation in adenosine solutions with different concentrations. Slide A was incubated in a 3.32 mM adenosine solution, slide J was incubated in a 0.415 mM adenosine solution, slide K was incubated in a 0.83 mM adenosine solution, and slide L was incubated in a 1.66 mM adenosine solution.

Figure 91A shows cyclic voltammograms obtained from polymer films on slides A, J, K, and L after incubation in adenosine solutions of different concentrations, while Figure 91B shows a plot comparing current response of the polymer films versus the concentration of adenosine in the incubation solution. The plot comparing current response of the polymer film to adenosine concentration shows a slight linear relationship that could improve with optimization of adenosine sensing experiments.

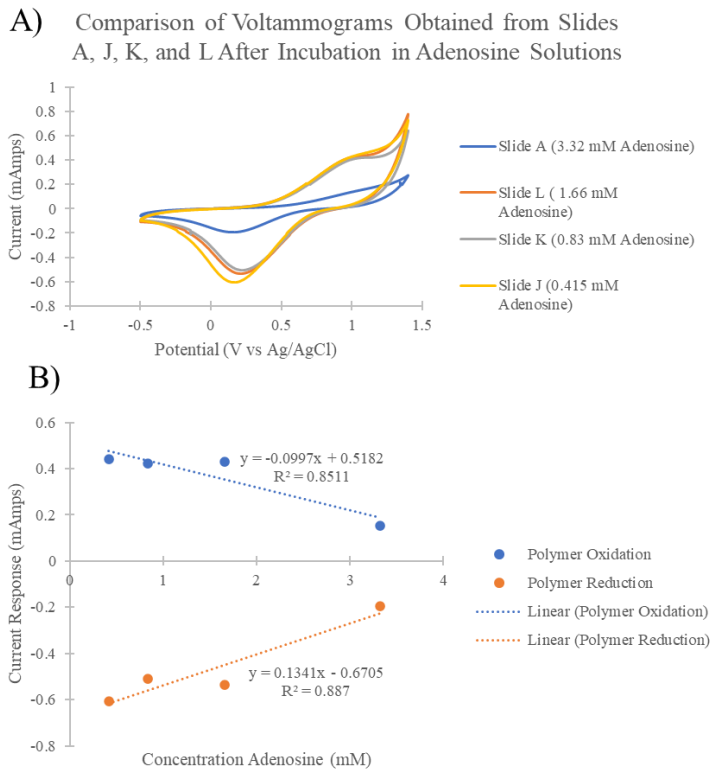

Figure 91: A): A comparison of cyclic voltammograms obtained from polymer films on slides A, J, K, and L after incubation in their respective adenosine solution and B): a plot comparing the adenosine concentration in the incubation solution to the current response of the corresponding polymer film.

Figure 92 shows a plot of concentration of adenosine versus normalized current response of the polymer film (current after adenosine incubation/ current before adenosine incubation). There is not a linear relationship between the concentration of adenosine the polymer films are exposed to and the change in current response of the polymer films. With the use of multiple, non-identical polymer films for the analytical sensing of adenosine experiments, more variables (thickness of polymer film, the difference in degree of adherence of polymer films to electrode, relative current responses/changes, etc.) are introduced that could affect the data and outcome of the experiment. A more appropriate test of the analytical ability of the fabricated biosensor would be to incubate a single polymer film in several solutions of differing adenosine

concentrations and monitor the electrochemistry of the slide before and after incubation by CV.

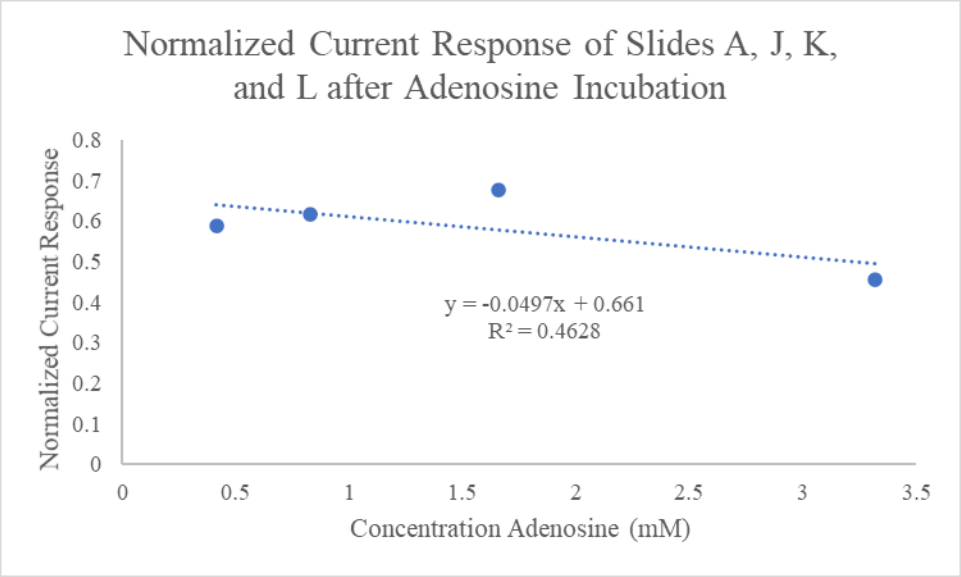

Figure 92: Plot of concentration of adenosine in incubation solution versus normalized current response of the polymer film.

Figure 92A shows stacked cyclic voltammograms obtained from the polymer film on slide L before and after incubation in several adenosine solutions of different concentrations, while Figure 92B shows a plot comparing of the current response of the polymer film on slide L as a function of adenosine concentration. As the concentration of adenosine in solution increases, the current response of the polymer film decreases. This decrease in current response is expected when insulating adenosine molecules bind to the aptamers on the surface of the electrochemical biosensor. The decrease in current response with increase in adenosine concentration shows a relatively linear relationship. The fabricated biosensor shows promise for the analytical sensing of adenosine, though additional sensing experiments need to be performed and optimized before a significant linear relationship between adenosine concentration and current response of the polymer

film can be confirmed.

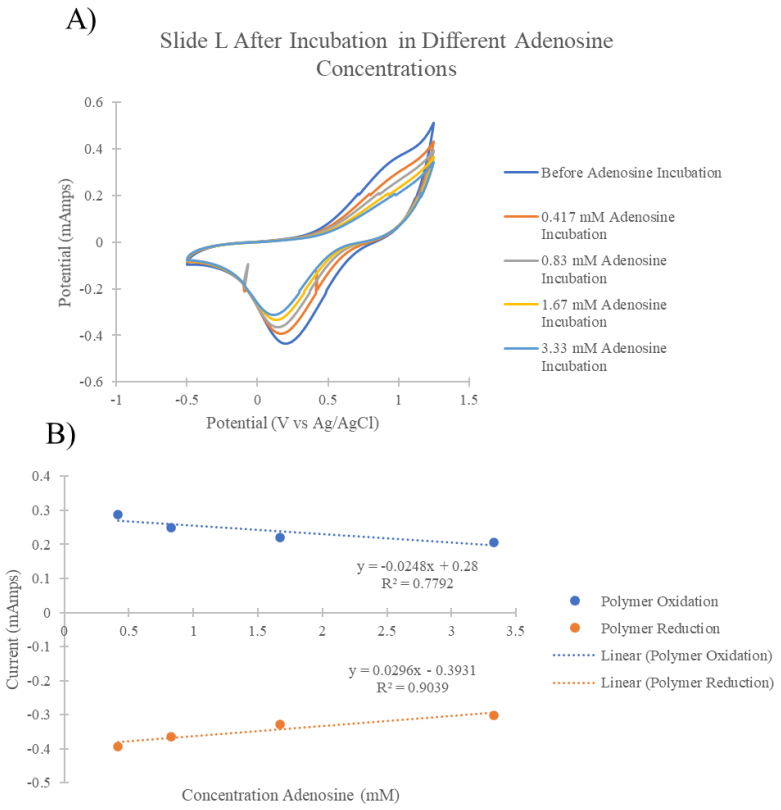

Figure 93: A): Cyclic voltammograms obtained from the polymer film on slide L before and after incubation in adenosine solutions at concentrations of 3.33 mM, 1.67 mM, 0.83 mM, and 0.417 mM adenosine and B): a plot comparing the relationship between current response of the polymer film and adenosine concentration.

5. CONCLUSIONS

5.1 Monomer Synthesis

Synthesis of ProDOT($CH_2CCH)_2$ proved challenging. Attempted synthesis of ProDOT($CH_2CCH)_2$ using S_N2 and protecting group chemistry reactions was unsuccessful. ^1H NMR spectra of crude and purified products from S_N2 reactions suggested that acetylide ions in solution were possibly participating in the opening of the seven-membered ring on the ProDOT structure by nucleophilic attack. ^1H NMR spectra of crude products from the attempted S_N2 reactions performed on protected starting material suggested that acetylide ions were deprotecting the molecule by nucleophilic attack. Synthesis of ProDOT(CH_2CCH) was unsuccessful. On the other hand, ProDOT($CH_2N_3)_2$ was successfully synthesized by S_N2 reaction between ProDOT($CH_2Br)_2$ and NaN_3. ProDOT($CH_2N_3)_2$ was further used to electrochemically polymerize a PProDOT($CH_2N_3)_2$ film for biosensor fabrication.

5.2 Electrochemistry

PProDOT($CH_2N_3)_2$ polymer films were successfully grown in several solutions using different electrolyte/solvent combinations, including a solution with considerable aqueous character (50% H_2O). Problems arose when the hydrophobic polymer films would crack and delaminate from the electrode when performing electrochemical experiments in an aqueous solvent. Chemical modification of the surface of the ITO electrode with ThAm proved to promote attachment of the polymer films to the ITO slides. Not only did polymer films grown on ThAm -modified ITO slides retain their

integrity during aqueous electrochemical experiments, polymer oxidation and reduction peaks could be observed in voltammograms obtained in aqueous solutions. The successful modification of ITO slides proved crucial in obtaining aqueous electrochemistry of the polymer films and to ensure that films retained their integrity during the biosensor fabrication and biosensing processes.

5.3 Development of Aptamer Biosensor

Functionalization of PProDOT(CH_2N_3)$_2$ films with an adenosine-specific aptamer through click chemistry presented challenges. Several attempts at click chemistry between PProDOT(CH_2N_3)$_2$ films and the adenosine specific aptamer were performed. Several factors were different between each reaction including solvent system, type of copper salt used as a source for copper catalyst, and presence of reducing agent for the copper in solution. After several failures of aptamer functionalization (possibly due to error in analysis techniques), a successful click chemistry aptamer attachment reaction was performed following protocols published by Lumiprobe®.

Several aptamer functionalized PProDOT(CH_2N_3)$_2$ films were used to conduct adenosine sensing experiments and to evaluate the analytical potential of the fabricated biosensor. All polymer films showed an expected reduction in electroactivity when incubated in adenosine-containing solutions. A relatively linear relationship exists between the current response of the polymer film and the concentration of adenosine in solution. Further tests are needed to confirm a significant relationship between the current response of the polymer film and adenosine concentration. Fabrication of an adenosine specific electrochemical biosensor and adenosine detection using said biosensor was

promising.

5.4 Future Work

Future work should explore the difference in PProDOT(CH_2N_3)$_2$ films grown on ThAm modified and unmodified ITO slides. The viability of PProDOT(CH_2N_3)$_2$ films grown on ThAm modified ITO slides over extended periods of time compared to that of films grown on unmodified ITO slides should be studied. Conducting studies to determine if polymerizing ProDOT(CH_2N_3)$_2$ onto ThAm modified ITO slides changes the band gap of the polymer film could prove to be interesting.

Experiments to evaluate the selectivity of the fabricated biosensor should be conducted. To test the selectivity of the biosensor, aptamer functionalized polymer films should be incubated in a solution with comparable concentrations of non-specific binding molecules to see if a change in electrochemistry can be seen. If the fabricated biosensor is selective, there should not be a change in electrochemistry similar to the change in electrochemistry obtained when incubated in adenosine containing solutions.

Several experiments should be conducted incubating aptamer functionalized polymer films in solutions of varying adenosine concentrations to determine the analytical capabilities of the fabricated biosensor. Enough studies should be conducted to confidently determine the limit of detection, limit of quantification, and limit of linearity of the fabricated biosensor.

Future work for this project would include functionalizing EAP films with aptamers specific to disease biomarkers, making a biosensing device for early detection of serious illnesses.

APPENDIX SECTION

Figure **Page**

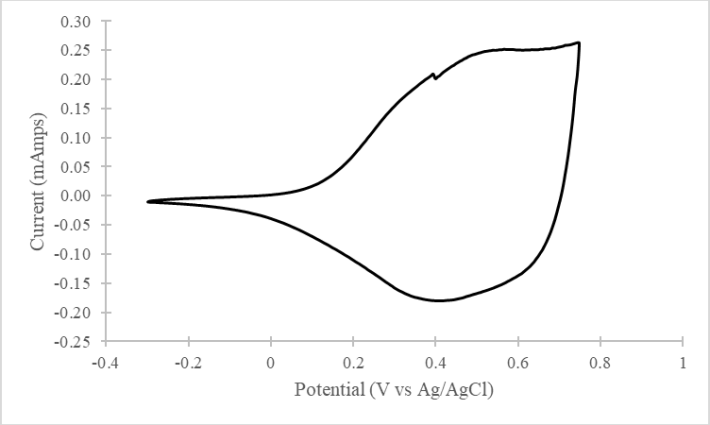

Figure A 1: Voltammogram Obtained from PProDOT(CH_2N_3)$_2$ film grown from a 0.01 M ProDOT(CH_2N_3)$_2$, 0.1 M TBAP solution in ACN over the voltage range of -0.3 V to 0.75 V at a scan rate of 100 mV/s.

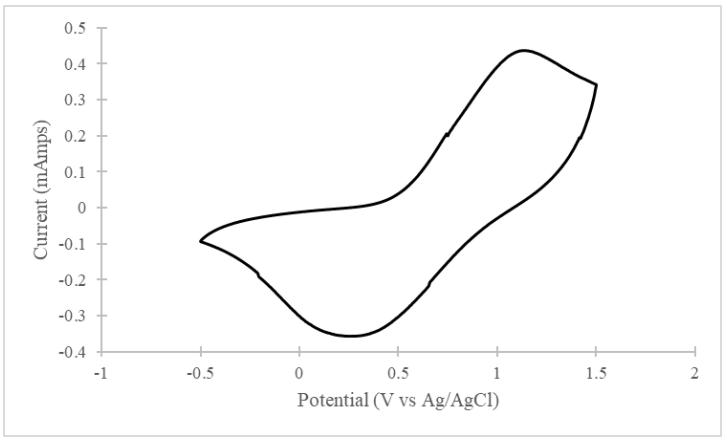

Figure A 2: Voltammogram obtained from PProDOT(CH_2N_3)$_2$ film grown from a 0.01 M ProDOT(CH_2N_3)$_2$, 0.1 M $TEABF_4$ solution in ACN over the voltage range of -0.5 V to 1.5 V at a scan rate of 100 mV/s.

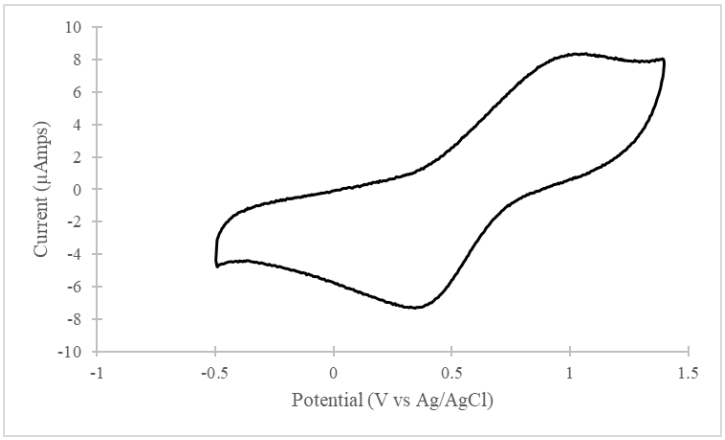

Figure A 3: Voltammogram obtained from PProDOT(CH_2N_3)$_2$ film grown from a 0.01 ProDOT(CH_2N_3)$_2$, 0.1 M $TEABF_4$ solution in 1:1 H_2O:ACN over the voltage range of -0.5 V to 1.5 V at a scan rate of 100 mV/s.

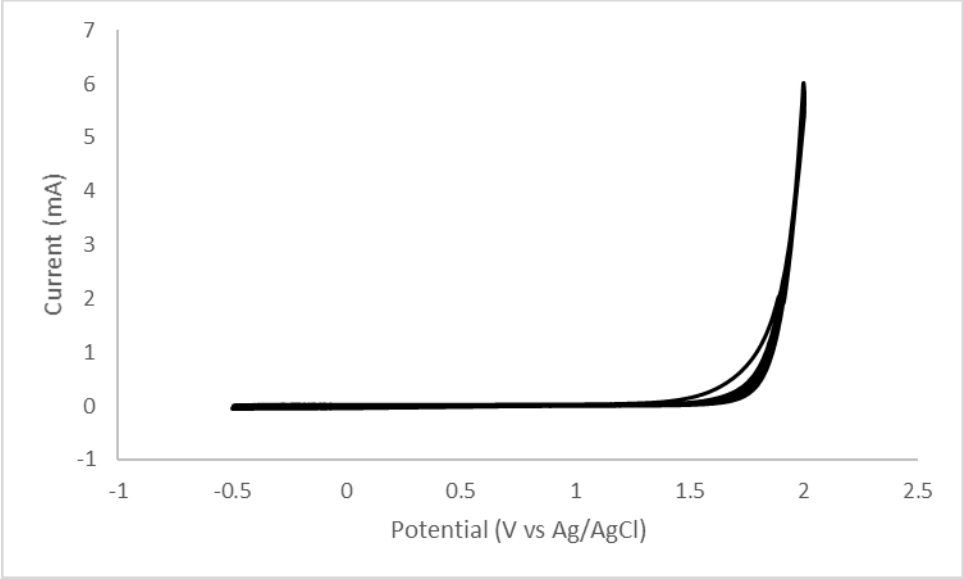

Figure A 4: Voltammogram of a 1XPBS solution against an Ag/AgCl reference electrode.

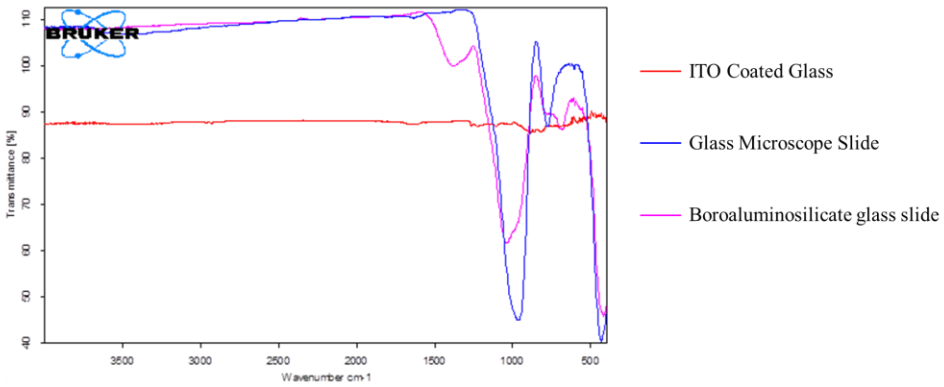

Figure A 5: Stacked IR spectra obtained from different glass surfaces.

LITERATURE CITED

(1) M. Beaujuge, P.; R. Reynolds, J. Color Control in π-Conjugated Organic Polymers for Use in Electrochromic Devices. *Chem. Rev.* **2010**, *110* (1), 268–320. https://doi.org/10.1021/cr900129a.

(2) Stassen, I.; Sloboda, T.; Hambitzer, G. Membrane with Controllable Permeability for Drugs. *Synth. Met.* **1995**, *71* (1–3), 2243–2244. https://doi.org/10.1016/0379-6779(94)03241-W.

(3) Bar-Cohen, Y. Electroactive Polymers as Artificial Muscles: A Review. *J. Spacecr. Rockets* **2002**, *39* (6), 822–827. https://doi.org/10.2514/2.3902.

(4) Wallace, G. G.; Spinks, G. M.; Kane-Maguire, L. A. P.; Teasdale, P. R. *Conductive Electroactive Polymers: Intelligent Materials Systems, Second Edition*; Taylor & Francis, 2002.

(5) Zhang, Y.; Feng, H.; Wu, X.; Wang, L.; Zhang, A.; Xia, T.; Dong, H.; Li, X.; Zhang, L. Progress of Electrochemical Capacitor Electrode Materials: A Review. *International Journal of Hydrogen Energy*. Pergamon June 1, 2009, pp 4889–4899. https://doi.org/10.1016/j.ijhydene.2009.04.005.

(6) Mortimer, R. J. Organic Electrochromic Materials. *Electrochim. Acta* **1999**, *44* (18), 2971–2981. https://doi.org/10.1016/S0013-4686(99)00046-8.

(7) Wallace, G. G.; Smyth, M.; Zhao, H. Conducting Electroactive Polymer-Based Biosensors. *TrAC - Trends Anal. Chem.* **1999**, *18* (4), 245–251. https://doi.org/10.1016/S0165-9936(98)00113-7.

(8) Carpi, F.; Smela, E. *Biomedical Applications of Electroactive Polymer Actuators*; John Wiley and Sons, 2009. https://doi.org/10.1002/9780470744697.

(9) Shirakawa, H.; Louis, E. J.; MacDiarmid, A. G.; Chiang, C. K.; Heeger, A. J. Synthesis of Electrically Conducting Organic Polymers: Halogen Derivatives of Polyacetylene, (CH)X. *J. Chem. Soc. Chem. Commun.* **1977**, No. 16. https://doi.org/10.1039/C39770000578.

(10) Heeger, A.; MacDiarmid, A. G.; Shirakawa, H. The Nobel Prize in Chemistry, 2000: Conductive Polymers. *Stock. Sweden R. Swedish Acad. Sci.* **2000**, 1–16. https://doi.org/http://www.nobelprize.org/nobel_prizes/chemistry/laureates/2000/advanced-chemistryprize2000.pdf.

(11) Guo, B.; Finne-Wistrand, A.; Albertsson, A. C. Degradable and Electroactive Hydrogels with Tunable Electrical Conductivity and Swelling Behavior. *Chem. Mater.* **2011**, *23* (5), 1254–1262. https://doi.org/10.1021/cm103498s.

(12) Guarino, V.; Zuppolini, S.; Borriello, A.; Ambrosio, L. Electro-Active Polymers (EAPs): A Promising Route to Design Bio-Organic/Bioinspired Platforms with on Demand Functionalities. *Polymers*. 2016. https://doi.org/10.3390/polym8050185.

(13) Roncali, J. Conjugated Poly(Thiophenes): Synthesis, Functionalization, and Applications. *Chem. Rev.* **1992**, *92* (4), 711–738. https://doi.org/10.1021/cr00012a009.

(14) Irvin, David J; Dudis, D. S.; Reynolds, J. R. . *Polym. Prepr.* **1997**, *38*, 318.

(15) Zarras, P.; Irvin, J. Electrically Active Polymers. In *Encyclopedia of Polymer Science and Technology*; Wiley Interscience, 2004. https://doi.org/10.1002/0471440264.pst107.

(16) Bundgaard, E.; Krebs, F. C. Low Band Gap Polymers for Organic Photovoltaics. *Sol. Energy Mater. Sol. Cells* **2007**, *91* (11), 954–985. https://doi.org/10.1016/J.SOLMAT.2007.01.015.

(17) Ma, J.; Li, S.; Jiang, Y. A Time-Dependent DFT Study on Band Gaps and Effective Conjugation Lengths of Polyacetylene, Polyphenylene, Polypentafulvene, Polycyclopentadiene, Polypyrrole, Polyfuran, Polysilole, Polyphosphole, and Polythiophene. *Macromolecules* **2001**, *35* (3), 1109–1115. https://doi.org/10.1021/ma011279m.

(18) Mooney, J.; Kambhampati, P. Get the Basics Right: Jacobian Conversion of Wavelength and Energy Scales for Quantitative Analysis of Emission Spectra. *J. Phys. Chem. Lett.* **2013**, *4* (19), 3316–3318. https://doi.org/10.1021/jz401508t.

(19) Le, T. H.; Kim, Y.; Yoon, H. Electrical and Electrochemical Properties of Conducting Polymers. *Polymers*. 2017. https://doi.org/10.3390/polym9040150.

(20) Thévenot, D. R.; Toth, K.; Durst, R. A.; Wilson, G. S. Electrochemical Biosensors: Recommended Definitions and Classification. *Biosens. Bioelectron.* **2001**, *16* (1–2), 121–131. https://doi.org/10.1016/S0956-5663(01)00115-4.

(21) Runsewe, D.; Betancourt, T.; Irvin, J. A. Biomedical Application of Electroactive Polymers in Electrochemical Sensors: A Review. *Materials*. August 18, 2019, p 2629. https://doi.org/10.3390/ma12162629.

(22) Aydemir, N.; Malmström, J.; Travas-Sejdic, J. Conducting Polymer Based Electrochemical Biosensors. *Physical Chemistry Chemical Physics*. 2016, pp 8264–8277. https://doi.org/10.1039/c5cp06830d.

(23) Mahbubur Rahman, M.; Li, X. B.; Lopa, N. S.; Ahn, S. J.; Lee, J. J. Electrochemical DNA Hybridization Sensors Based on Conducting Polymers. *Sensors (Switzerland)*. 2015, pp 3801–3829. https://doi.org/10.3390/s150203801.

(24) Peng, H.; Zhang, L.; Soeller, C.; Travas-Sejdic, J. Conducting Polymers for Electrochemical DNA Sensing. *Biomaterials*. 2009, pp 2132–2148. https://doi.org/10.1016/j.biomaterials.2008.12.065.

(25) Galán, T.; Prieto-Simón, B.; Alvira, M.; Eritja, R.; Götz, G.; Bäuerle, P.; Samitier, J. Label-Free Electrochemical DNA Sensor Using "Click"-Functionalized PEDOT Electrodes. *Biosens. Bioelectron.* **2015**, *74*, 751–756. https://doi.org/10.1016/j.bios.2015.07.037.

(26) Adachi, T.; Nakamura, Y. Aptamers: A Review of Their Chemical Properties and Modifications for Therapeutic Application. *Molecules*. 2019, p 4229. https://doi.org/10.3390/molecules24234229.

(27) Tuerk, C.; Gold, L. Systematic Evolution of Ligands by Exponential Enrichment: RNA Ligands to Bacteriophage T4 DNA Polymerase. *Science (80-.).* **1990**, *249* (4968), 505–510. https://doi.org/10.1126/science.2200121.

(28) Ellington, A. D.; Szostak, J. W. In Vitro Selection of RNA Molecules That Bind Specific Ligands. *Nature* **1990**, *346* (6287), 818–822. https://doi.org/10.1038/346818a0.

(29) Baryeh, K.; Takalkar, S.; Lund, M.; Liu, G. Introduction to Medical Biosensors for Point of Care Applications. In *Medical Biosensors for Point of Care (POC) Applications*; Elsevier Inc., 2017; pp 3–25. https://doi.org/10.1016/B978-0-08-100072-4.00001-0.

(30) Sheng, W.; Chen, T.; Kamath, R.; Xiong, X.; Tan, W.; Fan, Z. H. Aptamer-Enabled Efficient Isolation of Cancer Cells from Whole Blood Using a Microfluidic Device. *Anal. Chem.* **2012**, *84* (9), 4199–4206. https://doi.org/10.1021/ac3005633.

(31) Lu, W.; Ranjini Arumugam, S.; Senapati, D.; K. Singh, A.; Arbneshi, T.; Afrin Khan, S.; Yu, H.; Chandra Ray, P. Multifunctional Oval-Shaped Gold-Nanoparticle-Based Selective Detection of Breast Cancer Cells Using Simple Colorimetric and Highly Sensitive Two-Photon Scattering Assay. *ACS Nano* **2010**, *4* (3), 1739–1749. https://doi.org/10.1021/nn901742q.

(32) Li, S.; Chen, N.; Zhang, Z.; Wang, Y. Endonuclease-Responsive Aptamer-Functionalized Hydrogel Coating for Sequential Catch and Release of Cancer Cells. *Biomaterials* **2013**, *34* (2), 460–469. https://doi.org/10.1016/j.biomaterials.2012.09.040.

(33) Dickey, D. D.; Giangrande, P. H. Oligonucleotide Aptamers: A next-Generation Technology for the Capture and Detection of Circulating Tumor Cells. *Methods* **2016**, *97*, 94–103. https://doi.org/10.1016/J.YMETH.2015.11.020.

(34) Le Floch, F.; Ho, H. A.; Leclerc, M. Label-Free Electrochemical Detection of Protein Based on a Ferrocene-Bearing Cationic Polythiophene and Aptamer. *Anal. Chem.* **2006**, *78* (13), 4727–4731. https://doi.org/10.1021/ac0521955.

(35) Taleat, Z.; Cristea, C.; Marrazza, G.; Mazloum-Ardakani, M.; Săndulescu, R. Electrochemical Immunoassay Based on Aptamer-Protein Interaction and Functionalized Polymer for Cancer Biomarker Detection. *J. Electroanal. Chem.* **2014**, *717–718*, 119–124. https://doi.org/10.1016/j.jelechem.2014.01.015.

(36) Shafaat, A.; Faridbod, F.; Ganjali, M. R. Label-Free Detection of Cytochrome: C by a Conducting Polymer-Based Impedimetric Screen-Printed Aptasensor. *New J. Chem.* **2018**, *42* (8), 6034–6039. https://doi.org/10.1039/c7nj03844e.

(37) Dietrich, M.; Heinze, J.; Heywang, G.; Jonas, F. Electrochemical and Spectroscopic Characterization of Polyalkylenedioxythiophenes. *J. Electroanal. Chem.* **1994**, *369* (1–2), 87–92. https://doi.org/10.1016/0022-0728(94)87085-3.

(38) Park, H.; Ma, B. S.; Kim, J. S.; Kim, Y.; Kim, H. J.; Kim, D.; Yun, H.; Han, J.; Kim, F. S.; Kim, T. S.; et al. Regioregular- Block-Regiorandom Poly(3-Hexylthiophene) Copolymers for Mechanically Robust and High-Performance Thin-Film Transistors. *Macromolecules* **2019**, *52* (20), 7721–7730. https://doi.org/10.1021/acs.macromol.9b01540.

(39) Kim, J. S.; Kim, J. H.; Lee, W.; Yu, H.; Kim, H. J.; Song, I.; Shin, M.; Oh, J. H.; Jeong, U.; Kim, T. S.; et al. Tuning Mechanical and Optoelectrical Properties of Poly(3-Hexylthiophene) through Systematic Regioregularity Control. *Macromolecules* **2015**, *48* (13), 4339–4346. https://doi.org/10.1021/acs.macromol.5b00524.

(40) D. Reeves, B.; R. G. Grenier, C.; A. Argun, A.; Cirpan, A.; D. McCarley, T.; R. Reynolds, J. Spray Coatable Electrochromic Dioxythiophene Polymers with High Coloration Efficiencies. *Macromolecules* **2004**, *37* (20), 7559–7569. https://doi.org/10.1021/ma049222y.

(41) Kolb, H. C.; Finn, M. G.; Sharpless, K. B. Click Chemistry: Diverse Chemical Function from a Few Good Reactions. *Angewandte Chemie - International Edition*. 2001, pp 2004–2021. https://doi.org/10.1002/1521-3773(20010601)40:11<2004::AID-ANIE2004>3.0.CO;2-5.

(42) Rutledge, T. F. Sodium Acetylide. II. Reactions of Sodium Acetylide in Organic Diluents. Preparation of Monoalkyl Acetylenes. *J. Org. Chem.* **1959**, *24* (6), 840–842. https://doi.org/10.1021/jo01088a029.

(43) Sunazuka, T.; Hirose, T.; Harigaya, Y.; Takamatsu, S.; Hayashi, M.; Komiyama, K.; Ōmura, S.; A. Sprengeler, P.; B. Smith, A. Relative and Absolute Stereochemistries and Total Synthesis of (+)-Macrosphelides A and B, Potent, Orally Bioavailable Inhibitors of Cell−Cell Adhesion. *J. Am. Chem. Soc.* **1997**, *119* (42), 10247–10248. https://doi.org/10.1021/ja971657w.

(44) Chaudhary, S. K.; Hernandez, O. 4-Dimethylaminopyridine: An Efficient and Selective Catalyst for the Silylation of Alcohols. *Tetrahedron Lett.* **1979**, *20* (2), 99–102. https://doi.org/10.1016/S0040-4039(01)85893-7.

(45) Godeau, G.; N'Na, J.; Darmanin, T.; Guittard, F. Poly(3,4-Propylenedioxythiophene) Mono-Azide and Di-Azide as Platforms for Surface Post-Functionalization. *Eur. Polym. J.* **2016**, *78*, 38–45. https://doi.org/10.1016/j.eurpolymj.2016.02.027.

(46) J. Corey, E.; Venkateswarlu, A. Protection of Hydroxyl Groups as Tert-Butyldimethylsilyl Derivatives. *J. Am. Chem. Soc.* **2002**, *94* (17), 6190–6191. https://doi.org/10.1021/ja00772a043.

(47) Tanaka, K.; Shichiri, T.; Wang, S.; Yamabe, T. A Study of the Electropolymerization of Thiophene. *Synth. Met.* **1988**, *24* (3), 203–215. https://doi.org/10.1016/0379-6779(88)90258-5.

(48) Shoog, D. A.; West, D. M. Fundamentals of Analytical Chemistry. **1976**. https://doi.org/10.1201/9781420056716.ch25.

(49) Frazer, J. B. *IMPACT OF PROCESSING PARAMETERS ON CONDUCTIVE POLYMER ELECTROACTIVITY*; San Marcos, 2018.

(50) Elgrishi, N.; J. Rountree, K.; D. McCarthy, B.; S. Rountree, E.; T. Eisenhart, T.; L. Dempsey, J. A Practical Beginner's Guide to Cyclic Voltammetry. *J. Chem. Educ.* **2017**, *95* (2), 197–206. https://doi.org/10.1021/acs.jchemed.7b00361.

(51) Sawyer, D. T. T. A. M. U.; Roberts, J. L. J. U. O. R. ELECTROCHEMISTRY FOR CHEMISTS Second Edition. *JOHN WILEY SONS INC* **1994**, 133.

(52) Scholz, F. *Electroanalytical Methods: Guide to Experiments and Applications*; 2010. https://doi.org/10.1007/978-3-642-02915-8.

(53) Bioanalytical Systems, I. Pulse Voltammetric Techniques https://www.basinc.com/manuals/EC_epsilon/Techniques/Pulse/pulse (accessed Jan 21, 2020).

(54) Ahuja, T.; Rajesh; Kumar, D.; Tanwar, V. K.; Sharma, V.; Singh, N.; Biradar, A. M. An Amperometric Uric Acid Biosensor Based on Bis[Sulfosuccinimidyl] Suberate Crosslinker/3-Aminopropyltriethoxysilane Surface Modified ITO Glass Electrode. In *Thin Solid Films*; 2010; Vol. 519, pp 1128–1134. https://doi.org/10.1016/j.tsf.2010.08.056.

(55) Kim, G. Il; Kim, K. W.; Oh, M. K.; Sung, Y. M. Electrochemical Detection of Vascular Endothelial Growth Factors (VEGFs) Using VEGF Antibody Fragments Modified Au NPs/ITO Electrode. *Biosens. Bioelectron.* **2010**, *25* (7), 1717–1722. https://doi.org/10.1016/j.bios.2009.12.015.

(56) Tip, T. Attach an Antibody onto Glass, Silica or Quartz Surface. *Thermo.Com* **2015**, *0747* (815).

(57) Decker, E. L.; Frank, B.; Suo, Y.; Garoff, S. Physics of Contact Angle Measurement. *Colloids Surfaces A Physicochem. Eng. Asp.* **1999**, *156* (1–3). https://doi.org/10.1016/S0927-7757(99)00069-2.

(58) Skoog, D. A.; Holler, F. J.; Crouch, S. R. *Principles of Instrumental Analysis Sixth Edition*; 2007. https://doi.org/10.1017/CBO9781107415324.004.

(59) Robert Hillman, A.; Daisley, S. J.; Bruckenstein, S. Solvent Effects on the Electrochemical P-Doping of PEDOT. *Phys. Chem. Chem. Phys.* **2007**, *9* (19), 2379–2388. https://doi.org/10.1039/b618786b.

(60) Hillman, A. R.; Bruckenstein, S. Role of Film History and Observational Timescale on Redox Switching Kinetics of Electroactive Films. Part 1. - A New Model for Permselective Films with Polymer Relaxation Processes. *J. Chem. Soc. Faraday Trans.* **1993**, *89* (2), 339–348. https://doi.org/10.1039/FT9938900339.

(61) Cosnier, S.; Karyakin, A. *Electropolymerization: Concepts, Materials and Applications*; 2010. https://doi.org/10.1002/9783527630592.

(62) Bruel, C.; Queffeulou, S.; Darlow, T.; Virgilio, N.; Tavares, J. R.; Patience, G. S. Experimental Methods in Chemical Engineering: Contact Angles. *Can. J. Chem. Eng.* **2019**, *97* (4), 832–842. https://doi.org/10.1002/cjce.23408.

(63) Huizenga, D. E.; Szostak, J. W. A DNA Aptamer That Binds Adenosine and ATP. *Biochemistry* **1995**, *34* (2), 656–665. https://doi.org/10.1021/bi00002a033.

(64) Lin, C. H.; Patei, D. J. Structural Basis of DNA Folding and Recognition in an AMP-DNA Aptamer Complex: Distinct Architectures but Common Recognition Motifs for DNA and RNA Aptamers Complexed to AMP. *Chem. Biol.* **1997**, *4* (11), 817–832. https://doi.org/10.1016/S1074-5521(97)90115-0.

(65) Silverstein, RM. Webster X. F., K. J. D. *Spectrometric Identification of Organic Compounds 7th Edition*; 2005.

(66) Huisgen, R.; Szeimies, G.; Möbius, L. 1.3-Dipolare Cycloadditionen, XXXII. Kinetik Der Additionen Organischer Azide an CC-Mehrfachbindungen. *Chem. Ber.* **1967**, *100* (8), 2494–2507. https://doi.org/10.1002/cber.19671000806.

(67) Tornøe, C. W.; Christensen, C.; Meldal, M. Peptidotriazoles on Solid Phase: [1,2,3]-Triazoles by Regiospecific Copper(I)-Catalyzed 1,3-Dipolar Cycloadditions of Terminal Alkynes to Azides. *J. Org. Chem.* **2002**, *67* (9), 3057–3064. https://doi.org/10.1021/jo011148j.

(68) Worrell, B. T.; Malik, J. A.; Fokin, V. V. Direct Evidence of a Dinuclear Copper Intermediate in Cu(I)-Catalyzed Azide-Alkyne Cycloadditions. *Science (80-.).* **2013**, *340* (6131), 457–460. https://doi.org/10.1126/science.1229506.

(69) Rostovtsev, V. V.; Green, L. G.; Fokin, V. V.; Sharpless, K. B. A Stepwise Huisgen Cycloaddition Process: Copper(I)-Catalyzed Regioselective "Ligation" of Azides and Terminal Alkynes. *Angew. Chemie - Int. Ed.* **2002**, *41* (14), 2596–2599. https://doi.org/10.1002/1521-3773(20020715)41:14<2596::AID-ANIE2596>3.0.CO;2-4.

(70) Ratajczak, T.; Uszczyńska, B.; Frydrych-Tomczak, E.; Chmielewski, M. K. The "Clickable" Method for Oligonucleotide Immobilization onto Azide-Functionalized Microarrays. In *Methods in Molecular Biology*; 2016; Vol. 1368, pp 25–36. https://doi.org/10.1007/978-1-4939-3136-1_3.

(71) Kuijpers, B. H. M.; Groothuys, S.; Keereweer, A. R.; Quaedflieg, P. J. L. M.; Blaauw, R. H.; Van Delft, F. L.; Rutjes, F. P. J. T. Expedient Synthesis of Triazole-Linked Glycosyl Amino Acids and Peptides. *Org. Lett.* **2004**, *6* (18), 3123–3126. https://doi.org/10.1021/ol048841o.

(72) Lumiprobe corporation. Protocol : Click-Chemistry Labeling of Oligonucleotides and DNA. *Lumiprobe* **2013**, 1–3.

(73) Aydemir, N.; Chan, E.; Baek, P.; Barker, D.; Williams, D. E.; Travas-Sejdic, J. New Immobilisation Method for Oligonucleotides on Electrodes Enables Highly-Sensitive, Electrochemical Label-Free Gene Sensing. *Biosens. Bioelectron.* **2017**, *97*, 128–135. https://doi.org/10.1016/j.bios.2017.05.049.

(74) Xu, T.; Song, Y.; Gao, W.; Wu, T.; Xu, L. P.; Zhang, X.; Wang, S. Superwettable Electrochemical Biosensor toward Detection of Cancer Biomarkers. *ACS Sensors* **2018**, *3* (1), 72–78. https://doi.org/10.1021/acssensors.7b00868.

(75) Roncali, J.; Garreau, R.; Yassar, A.; Marque, P.; Garnier, F.; Lemaire, M. Effects of Steric Factors on the Electrosynthesis and Properties of Conducting Poly(3-Alkylthiophenes). *J. Phys. Chem.* **1987**, *91* (27), 6706–6714. https://doi.org/10.1021/j100311a030.